



**Michigan
Technological
University**

Michigan Technological University
Digital Commons @ Michigan Tech

Dissertations, Master's Theses and Master's Reports

2023

STRUCTURAL ANALYSIS AND INTERPRETATION OF DEFORMATION ALONG THE KEWEENAW FAULT SYSTEM FROM LAKE LINDEN TO MOHAWK, MICHIGAN

Nolan G. Gamet
Michigan Technological University, ngamet@mtu.edu

Copyright 2023 Nolan G. Gamet

Recommended Citation

Gamet, Nolan G., "STRUCTURAL ANALYSIS AND INTERPRETATION OF DEFORMATION ALONG THE KEWEENAW FAULT SYSTEM FROM LAKE LINDEN TO MOHAWK, MICHIGAN", Open Access Master's Thesis, Michigan Technological University, 2023.
<https://doi.org/10.37099/mtu.dc.etr/1620>

Follow this and additional works at: <https://digitalcommons.mtu.edu/etr>



Part of the [Geographic Information Sciences Commons](#), [Geology Commons](#), [Stratigraphy Commons](#), and the [Tectonics and Structure Commons](#)

STRUCTURAL ANALYSIS AND INTERPRETATION OF DEFORMATION ALONG
THE KEWEENAW FAULT SYSTEM FROM LAKE LINDEN TO MOHAWK,
MICHIGAN

By

Nolan Gamet

A THESIS

Submitted in partial fulfillment of the requirements for the degree of

MASTER OF SCIENCE

In Geology

MICHIGAN TECHNOLOGICAL UNIVERSITY

2023

© 2023 Nolan G. Gamet

This thesis has been approved in partial fulfillment of the requirements for the Degree of MASTER OF SCIENCE in Geology.

Department of Geological and Mining Engineering and Sciences

Thesis Advisor: *James M. DeGraff*

Committee Member: *Chad D. Deering*

Committee Member: *Jeremy M. Shannon*

Committee Member: *William I. Rose*

Department Chair: *Aleksey V. Smirnov*

Table of Contents

List of Figures	v
List of Tables	viii
Acknowledgements	ix
List of Abbreviations	x
Abstract	xii
1 Introduction	1
2 Geologic Background and Setting	6
2.1 The Midcontinent Rift System	7
2.2 Post-rift Compression and Crustal Shortening	15
2.3 The Keweenaw Fault	17
3 Methods, Equipment, and Materials	20
3.1 Field Operations	21
3.2 Data Management and Analysis	25
3.3 Sample Preparation and Analysis	28
4 Results and Findings	29
4.1 Overview of EdMap Project Results	29
4.2 Houghton-Douglass Falls and St. Louis Ravine	34
4.3 Natural Wall Ravine and Mayflower Fault Block	41
4.4 Copper City Rhyolite and Allouez Gap Fault	47
5 Structural Analysis and Interpretation	58
5.1 Stratal Deformation and Fold Analysis	59
5.2 Fault-Slip Characterization and Kinematic Analysis	68
5.3 Cross-Section Construction and Interpretation	75
6 Discussion of Results and Significance	92
7 Conclusion	101
8 Reference List	103
A Diamond Drill Holes	109
A.1 Mayflower Diamond Drill Holes	109
A.2 Old Colony Diamond Drill Holes	112
A.3 St. Louis Diamond Drill Holes	116

B	Refined Bedrock Geology Maps.....	119
C	New Cross-Section Models.....	121
D	Copywrite Documentation.....	122

List of Figures

Figure 1: Mesoproterozoic Keweenawan Supergroup rocks of the Midcontinent Rift System in the Lake Superior region.....	1
Figure 2: Cross section of the Keweenaw Peninsula north of Portage Lake.....	3
Figure 3: Generalized bedrock geology of the Keweenaw Peninsula showing three completed EdMap project areas.....	3
Figure 4: Extent of the Midcontinent Rift System relative to the Superior Craton and geographic position of the Grenville Front.	7
Figure 5: Timeline of the stages of the Midcontinent Rift System evolution.....	8
Figure 6: Stratigraphic column of the western Upper Peninsula of Michigan.	10
Figure 7: Main PLV basalt textural varieties observed in the map area.....	11
Figure 8: Idealized cartoon of a cross section through an inflated pahoehoe lava lobe....	12
Figure 9: Regional cross section spanning the entire width of the MRS.....	15
Figure 10: Local cross section across the Keweenaw fault near Dover Creek.....	18
Figure 11: Workflow for data transfer from recording media, processing, analysis, and geospatial data interpretation and visualization.....	26
Figure 12: Legacy bedrock geology map of the Keweenaw Peninsula north of Portage Lake with the 2021-2022 EdMap project is outlined in yellow.....	32
Figure 13: Updated bedrock geology map of the 2021-2022 EdMap project area.....	33
Figure 14: New bedrock geology map showing Houghton-Douglass Falls and St. Louis ravine.....	35
Figure 15: New bedrock geology map showing the Mayflower fault block.....	42
Figure 16: New bedrock geology map showing the Copper City rhyolite complex.....	48
Figure 17: Copper City rhyolite complex with interbedded conglomerate layers.....	52
Figure 18: Copper City rhyolite near boundary of the 2020 and 2022 EdMap projects...53	
Figure 19: Transmitted light microscope images at 4x showing rhyolite features.....	55
Figure 20: Equal area stereonet plots and analysis of footwall JS stratal orientations From Houghton-Douglass Falls.....	60
Figure 21: Equal area stereonet plot and analysis of hanging-wall PLV stratal Orientations at Houghton-Douglass Falls.....	61

Figure 22: Equal area stereonet plot and analysis of all JS stratal orientations from the Natural Wall.....	62
Figure 23: Equal area stereonet plot and analysis of grouped JS stratal orientations located at Natural Wall.....	63
Figure 24: Equal area stereonet plot and analysis of all JS stratal orientations Between Old Colony Road and Mayflower Road.....	64
Figure 25: Equal area stereonet plot and analysis of grouped JS footwall stratal orientations between Old Colony Road and Mayflower Road.....	65
Figure 26: Equal area stereonet plot and analysis of grouped PLV hanging wall stratal orientations between Old Colony Road and Mayflower Road.....	66
Figure 27: Equal area stereonet plot and analysis of PLV Copper City rhyolite orientations.....	67
Figure 28: Fault surface lineations parallel to the slip vector.....	69
Figure 29: Relationship between slip sense and asymmetry of steps formed by synkinematic mineralization.....	69
Figure 30: Lineations on a planar surface are specified either using rake or Plunge and plunge direction, along with strike and dip of the surface.....	69
Figure 31: Radial histogram of all site-averaged rakes of fault-slip lineations.....	71
Figure 32: Radial histograms of fault-slip lineations divided into two groups.....	71
Figure 33: Linked Bingham, fault-plane solution.....	73
Figure 34: Tabulation of slip components and sense for fully determined fault surfaces.....	74
Figure 35: Updated bedrock geology for this thesis with cross section locations.....	77
Figure 36: Geologic cross-section A-A' at Houghton-Douglass Falls.....	80
Figure 37: Geologic cross-section B-B' at St. Louis Ravine.....	83
Figure 38: Geologic cross-section C-C' at the Mayflower fault block.....	88
Figure 39: Geologic cross-section D-D' at the main Copper City rhyolite body.....	91
Figure 40: Comparison of radial rake histograms for the three EdMap projects.....	96
Figure 41: Comparison of fault-slip inversion plots for the three EdMap projects.....	98

Figure A: Diamond Drill Holes.....	109
Figure A.1.1: MAY-7.5 DDH Core Log.....	109
Figure A.1.2: MAY-39 DDH Core Log.....	110
Figure A.1.3: MAY-41 DDH Core Log.....	111
Figure A.2.1: OC-15 DDH Core Log.....	112
Figure A.2.2: OC-21 DDH Core Log.....	113
Figure A.2.3: OC-22 DDH Core Log.....	114
Figure A.2.4: OC-28 DDH Core Log.....	115
Figure A.3.1: St. Louis-11 DDH Core Log.....	116
Figure A.3.1: St. Louis-37 DDH Core Log.....	117
Figure B: Refined Bedrock Geology Maps.....	119
Figure C: New Cross-Section Models.....	121

List of Tables

Table 1: Data types recorded in field book.....	22
Table 2: Geochemical data for bulk rock samples.....	57
Table 3: Fault-slip inversion results with fault-plane solutions.....	72

Acknowledgements

I would like to thank my advisor Jim DeGraff for his support and guidance throughout this project, and Chad Deering, Jeremy Shannon, and Bill Rose for their support as committee members. I would like to thank Katherine Langfield for her collaboration throughout the project and especially with final map submission to the U.S. Geological Survey, and Daniel Lizzadro-McPherson for sharing his ArcGIS expertise and assistance with constructing final maps and cross sections. I greatly appreciate the help from field assistants Jack Hawes, Braxton Murphy, Ian Gannon, Breanne Heusdens, and Gabriel Ahrendt for their diligent fieldwork and sample preparation. This work was made possible by external funding from the U.S. Geological Survey's EdMap program and by matching support from the Department of Geological and Mining Engineering and Sciences at Michigan Technological University. My friends from inside and outside the Geological and Mining Engineering and Sciences department also provided ample help and support. Most importantly, I would like to thank my parents for their constant support and encouragement to do well throughout my educational journey and the exciting, yet sometimes stressful process along the way.

List of Abbreviations

AGF	Allouez Gap fault
DEM	Digital elevation model
DGPS	Differential Global Positioning System
EdMap	Educational Mapping Program (of the U.S Geological Survey)
ESE	East-southeast
FMC	FieldMOVE Clino
FW	Footwall
Ga	Billion years
HW	Hanging wall
JS	Jacobsville Sandstone
KF	Keweenaw fault
KFS	Keweenaw fault system
MAY	Mayflower Mining Company drill hole prefix
Ma	Million years
MF	Mayflower fault
MFB	Mayflower fault block
MRS	Midcontinent Rift System
NE	Northeast
NNE	North-northeast
NNW	North-northwest
NW	Northwest
OC	Old Colony Mining Company drill hole prefix
PLV	Portage Lake Volcanics
Ppm	Parts per million
S/D	Strike and dip
SE	Southeast
SSE	South-southeast
SSW	South-southwest

SW	Southwest
T/P	Trend and plunge
USGS	United States Geological Survey

Abstract

The Keweenaw fault is likely the most significant and most studied fault associated with the Midcontinent Rift System. The fault roughly bisects the Keweenaw Peninsula and places Portage Lake Volcanics (~1.1 Ga) over much younger Jacobsville Sandstone (~1.0 Ga). Published bedrock geology maps with cross sections from the 1950s show the fault as a single continuous trace that is locally associated with smaller cross faults and splays. The accompanying cross-sections show hanging-wall volcanic strata having a well-defined, listric geometry with dip decreasing away from the fault to the northwest.

This M.S. thesis presents a structural analysis and interpretation of the Keweenaw fault system between Lake Linden and Mohawk, MI, which includes the well-known localities of Houghton-Douglass Falls, the St. Louis ravine, the Natural Wall ravine, and the anomalous rhyolite body near Copper City. Objectives of the study were to better define the geometry, movement, and slip kinematics of the Keweenaw fault while also characterizing the fold patterns associated with the fault system. Field observations and data were used to revise existing bedrock geology maps, construct new cross-sections, and analyze fold geometry and fault slip behavior to infer aspects of the tectonic regime that caused the deformation.

New field mapping has refined the trace geometry of the Keweenaw fault and smaller associated faults, revised intersections between several splay faults and the main fault, and suggested the existence of several footwall splays not previously recognized. These map changes better define the Keweenaw fault system in this area as consisting of: 1)

major NNE-trending segments that define the fault system's overall trend and probably have mostly reverse slip; 2) NE-trending segments that branch off the major fault segments and define wedge-shaped fault blocks that widen to the northeast in the footwall; and 3) NNW-trending segments that connect faults of the first two types. At a point southwest of Copper City, the main fault surface abruptly changes strike from N16°E to N58°E traveling in a northeasterly direction and it shifts ~650 m deeper stratigraphically within the Portage Lake Volcanics. This abrupt change in trend and stratigraphic level of the main fault occurs at a complex junction of the Allouez Gap fault with two major segments of the Keweenaw fault at the northeast end of the Mayflower fault block.

Orientation analysis of Jacobsville Sandstone strata in the footwall of the fault system defines fold axes subparallel to nearby faults and with plunge directions that change from southwest to northeast moving in the same direction. Fault-slip analysis reveals both strike slip and dip slip along the fault system rather than only reverse movement as in the generally accepted model. Measured slip directions collectively define a 0.84:1 ratio of strike-to-dip slip for the fault system, and a fault-slip inversion analysis computes a nearly north-south maximum shortening direction of 2°-182°. Fold axis trends in the current area indicate shortening along an ESE-trending line, whereas fault-slip inversion analysis indicates a north-south shortening direction.

1 Introduction

The Keweenaw fault (KF) is one of several major faults that generally trends parallel to the margins of the Midcontinent Rift System (MRS) and is arguably the most significant fault associated with the MRS (Fig. 1). The fault roughly bisects the Keweenaw Peninsula and extends from the northeast-most tip for 250 kilometers southwesterly to northern Wisconsin. Published bedrock geology maps and associated cross sections from the 1950s show the fault as a single continuous trace that is locally associated with smaller cross faults and splays. Reverse slip on the fault, estimated to be on the order of 10 km (Cannon and Nicholson, 2001; DeGraff and Carter, 2023), has juxtaposed Portage Lake Volcanics (PLV, ~1.1 Ga) against much younger Jacobsville Sandstone (JS, ~1.0 Ga).

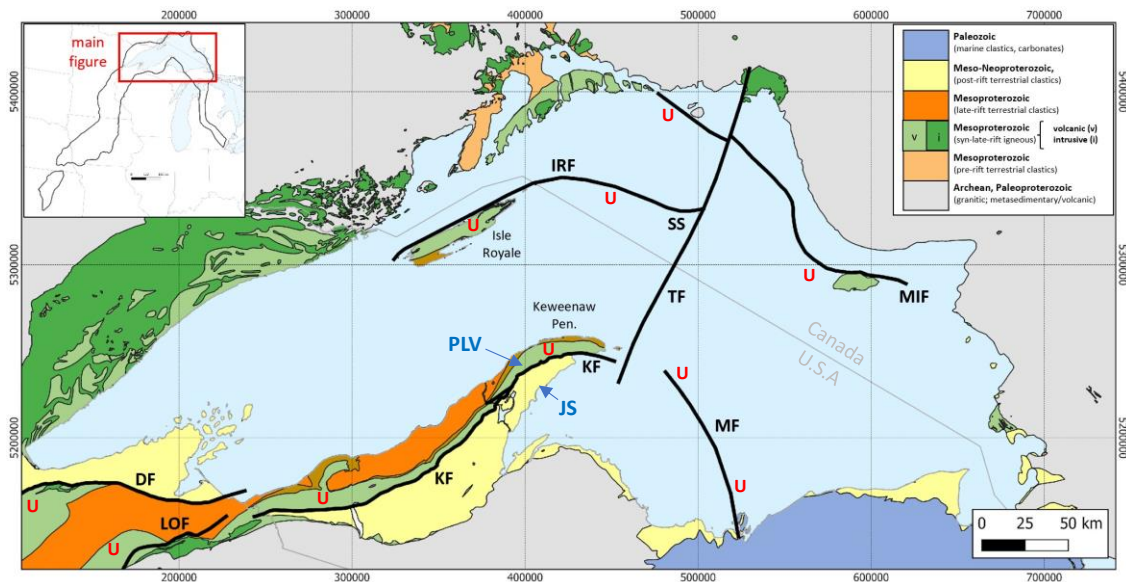


Figure 1: Mesoproterozoic Keweenawan Supergroup rocks of the Midcontinent Rift System (black outline of inset; red box is area of main figure) in the Lake Superior region. Main rock units of interest: PLV—Portage Lake Volcanics; JS—Jacobsville sandstone. Main fault of interest: KF—Keweenaw fault. Other letter codes: DF—Douglass fault; LOF—Lake Owen fault; IRF—Isle Royale fault; TF—Thiel fault; MIF—Michipicoten Island fault; MF—Munising fault; SS—Superior Shoal. Red “U” indicates upthrown sides of faults. Keweenaw Pen. —Keweenaw Peninsula. (modified from DeGraff and Carter, 2023).

The U. S. Geological Survey (USGS) mapped the bedrock geology of the Keweenaw Peninsula in the 1950s because of its important historic copper mining history and remaining mining potential. Native copper was mined along the Keweenaw Peninsula from the 1840s to the 1960s, and Michigan's Copper County was the nation's leading producer of copper from 1845 to 1887 (Stevens, 1909). An analysis of the distribution of mine workings and drilling in the Keweenaw Peninsula (Bodwell, 1972) showed that large volumes of potentially mineralized rock remain untested by drilling, including within the intensely mined portions. These copper deposits are interpreted to be the result of mineralizing hydrothermal fluids likely derived from the rift-filling volcanic rocks that migrated upwards following the active rifting (Bornhorst and Barron, 2011). Some have postulated that the Keweenaw fault and, presumably, lesser faults and fractures acted as conduits for copper-rich hydrothermal solutions to follow and ultimately to deposit these large volumes of native copper (Brown, 2008; Rose, 2020).

Government and copper industry geologists have mapped the position of the Keweenaw fault by finding contacts between the PLV and JS and by interpreting relatively primitive aeromagnetic surveys from the 1950s (Fig.2; Irving and Chamberlin, 1885; Butler and Burbank, 1929; White et al., 1953; Davidson et al., 1955). While state of the art for the time, methods to locate geological features and to create paper maps during the 1950s were somewhat primitive by today's standards of satellite-based positioning and computer-aided digital map production, which made the earlier geologic mapping more difficult, time consuming, and less accurate. Also, during that time, much less was known about fault systems and surface features that indicate slip direction and sense, and so measurements of slip lineations typically were not made. This made characterizing fault

movement and inferring principal strain directions somewhat speculative. Mapping of the Keweenaw fault system since 2017 using modern mapping methods, however, has started to resolve its geometric details and slip kinematics in a way that permits a better interpretation of its origin (DeGraff et al., 2018; 2020).

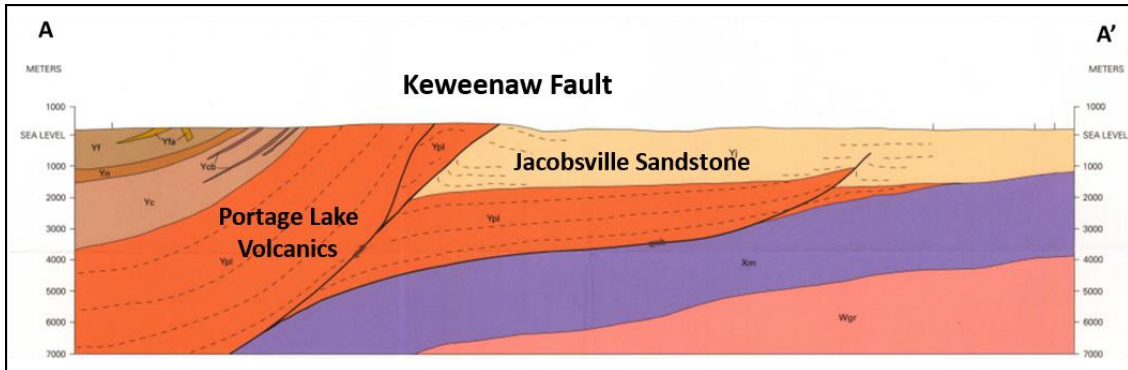


Figure 2: Cross-section of the Keweenaw Peninsula north of Portage Lake (see Figure 2). No vertical exaggeration (Cannon and Nicholson, 2001).

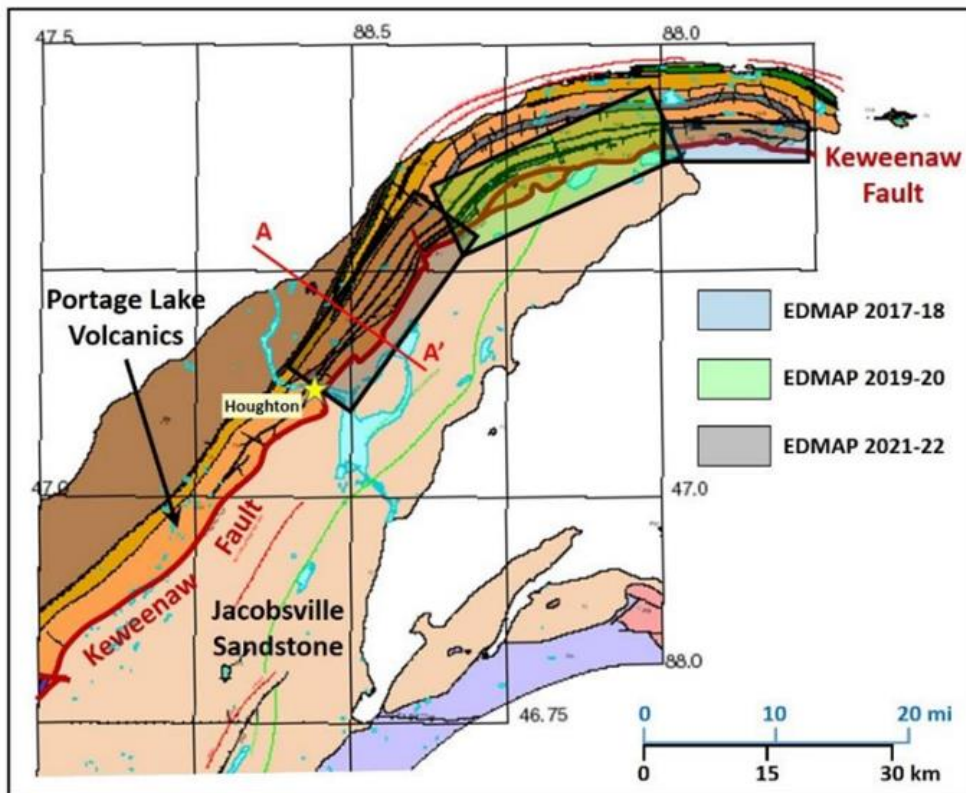


Figure 3: Generalized bedrock geology of the Keweenaw Peninsula showing three completed EdMap project areas; base map from Cannon and Nicholson (2001).

Field-based research by graduate students at Michigan Technological University, supported by USGS Educational Mapping Program (EdMap) grants for 2017-2018 and 2019-2020 (Fig. 3), has enhanced understanding of the Keweenaw fault system (KFS) by improving resolution of fault segment geometry using satellite-based location and by defining fault slip characteristics using fault-surface features. The first EdMap project eastward from Bête Grise Bay revealed the Keweenaw fault to be a complex fault system of ESE-trending, left-stepping faults connected by ENE-trending faults (DeGraff et al., 2018; Tyrrell, 2019), rather than being a single sinuous fault as portrayed on older maps. Measured fault-slip indicators showed that collective slip along the fault system was mostly right-lateral with a lesser, north-side-up, reverse component. The second EdMap project between Mohawk, MI, and Bête Grise Bay recognized three categories of faults within the KFS: 1) ENE-trending segments subparallel to the overall fault trend; 2) ESE-trending segments with a left-stepping echelon pattern; and 3) NNE-trending segments that connect members of the other two fault sets (Mueller, 2021; Lizzadro-McPherson, 2023). Again, this fault segment geometry and fault-slip observations indicate a mostly right-lateral strike-slip system with lesser north-side-up reverse movement.

A third EdMap Project in 2021-2022 (Fig. 3) focused on the Keweenaw fault system between Hancock and Mohawk, MI, where it trends more northerly in contrast with previously investigated parts of the system that trend more easterly (DeGraff et al., 2022). The goal was to test whether previous findings regarding fault geometries, slip kinematics, and related deformation would apply to the more northerly trending part of the Keweenaw fault system (KFS) and to identify any differences and explain their significance for fault slip behavior. Abundant structural data collected during two field

seasons have been analyzed and interpreted to explain fault and fold patterns regarding deformation along the fault trace in the new area. By comparing previous and current analyses, fault-slip kinematics and fold geometries have been re-evaluated with regard to how they change along the Keweenaw Peninsula and what they imply about principal strain directions.

The third EdMap project forms the basis for this thesis, which focuses on fault geometry, fold geometry, and slip kinematics of the Keweenaw fault system between Lake Linden and Mohawk, MI, i.e., the northeast half of the EdMap project area (Fig. 3). The project results reported here provide an improved representation of bedrock geology along the KFS, an updated interpretation of the fault system's slip kinematics, and new insights on deformation patterns in the hanging wall and especially the footwall of the fault system. One potential societal impact of this research is an improved ability to drill successful water wells because of more precise knowledge about fault position and the influence of fault-related deformation on hydrogeologic architecture. Project results also have important scientific implications for fault-system evolution and its tectonic drivers such as the Grenville Orogeny, as well as economic implications about possible fault system control on the location of native copper deposits.

2 Geologic Background and Setting

The Keweenaw Peninsula near the center of Lake Superior's southern shoreline generally follows the arcuate shape of the Lake Superior portion of the Midcontinent Rift System (MRS) and its margins (Fig. 4). The bedrock geology of the peninsula is dominated by Mesoproterozoic rocks related to the rifting and basin subsidence phases of the MRS. Strata associated with active rifting include great volumes of basaltic lavas with minor interflow sedimentary layers, whereas strata associated with basin subsidence are largely sedimentary basin fill. During or after basin subsidence, reverse faulting occurred along the Keweenaw Peninsula during one or more compressional tectonic events probably related to the Grenville Orogeny. Thus, the northwest dipping Keweenaw fault juxtaposes Mesoproterozoic volcanic strata of the Portage Lake Volcanics in the hanging wall against younger Meso- to Neoproterozoic sedimentary strata of the Jacobsville Sandstone in the footwall.

The origin, timing, and nature of the fault have been debated since the late 1800s. The consensus over the last few decades is that the fault began as a rift-related normal fault and was later reactivated as a reverse fault by a subsequent compressional event or events (Cannon et al., 1989; Hinze et al., 1990; Cannon, 1994). More recently, a detached model has been proposed for the Keweenaw and related faults which suggests that they initiated during the Grenville Orogeny and did not exist during the earlier rifting event (DeGraff and Carter, 2023). Additional details about the Midcontinent Rift System, Grenville

Orogeny, and Keweenaw fault are presented below to provide context for the new structural observations being documented along the Keweenaw Peninsula.

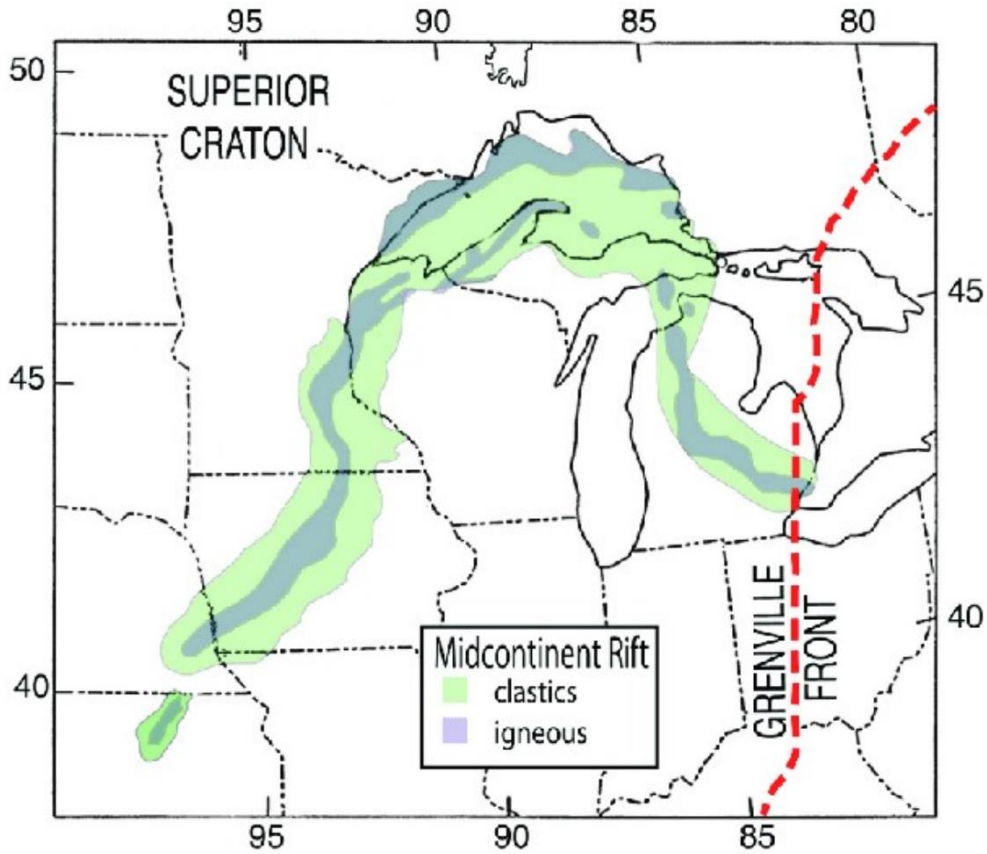


Figure 4: Extent of the Midcontinent Rift System relative to the Superior Craton and position of the Grenville Front (Stein et al., 2011).

2.1 The Midcontinent Rift System

The Midcontinent Rift System (MRS), formed by crustal extension of Laurentia ~1.1 Ga ago, extends ~1,100 km from Kansas northeast to the Lake Superior basin (Fig. 4), and then turns southeast and continues ~800 km beneath the Michigan basin (Woodruff et al.,

2020). The extent of the MRS is defined mostly by large gravity and magnetic anomalies resulting from great volumes of mafic volcanic rocks and intrusions associated with the rift, which are covered by Phanerozoic sedimentary strata except in the Lake Superior region. Evolution of the MRS has been described in terms of an active period of magmatism and crustal extension, followed by a waning period with thermal subsidence, and culminating with a compressional period that caused crustal shortening (Fig. 5; Woodruff et al., 2020). The compressional period is considered to be unrelated to rifting processes and so is discussed separately below. Ignoring the compressional period for now, the active magmatic and extensional period of rifting and the waning period of magmatism with thermal subsidence can be further subdivided into four stages as follows: 1) Plateau Stage (~1112 to 1105 Ma); 2) Rift Stage (~1102 to 1090 Ma); 3) Late-Rift Stage (~1090 to 1083 Ma); and 4) Post-Rift Stage (~1081 to 1060 Ma).

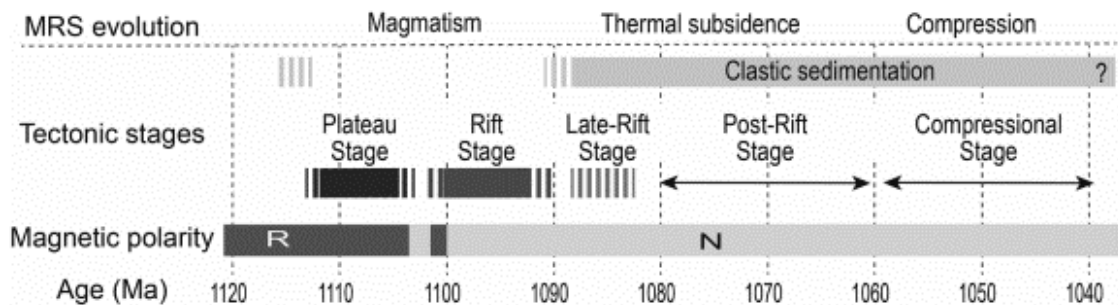


Figure 5: Timeline of the stages of Midcontinent Rift System evolution. Time intervals for magnetic polarity are shown as ‘R’ (reversed) and ‘N’ (normal) (from Woodruff et al., 2020).

The Plateau Stage of rifting produced reversely magnetized basalt flows (Powder Mill Group) that formed a ≤ 10 -kilometer-thick volcanic plateau in the Lake Superior region (Green, 1989; Woodruff et al., 2020). Volcanic strata of this stage crop out at Silver Mountain south of the Keweenaw fault and ~17 kilometers west of Baraga, Michigan,

where they dip 15° to the northeast (Kulakov, 2013). The main Rift Stage produced normally magnetized basalt flows (Bergland Group), which includes the PLV that crops out along the Keweenaw Peninsula. This group is estimated to be up to 14 kilometers thick in some parts of the western Lake Superior basin (Stewart et al., 2018).

Sedimentary interflow units make up 2-3% of the PLV section and become more abundant in the upper PLV, indicating a gradual transition from magmatism to sedimentation (White, 1972b). The Late-Rift Stage marks the end of intense magmatic activity and the beginning of subsidence dominated by clastic sedimentation. During this stage, alluvial fan conglomerates and fluvial lithic sandstones were deposited along with locally extruded basaltic lavas dated at 1087.2 ± 1.6 Ma to 1085.57 ± 0.25 Ma (Davis and Paces, 1990). Subsidence and sedimentation continued during the Post-Rift Stage, first as a sequence of green-gray-brown shale, siltstone, and sandstone (Nonesuch Formation), followed by red-brown lithic arkosic sandstone, silty shale, and siltstone (Freda Sandstone). Together, the sequence of the Copper Harbor Conglomerate, Nonesuch Formation, and Freda Sandstone form the ~7-kilometer thick Oronto Group (Cannon and Nicholson, 2001).

The Portage Lake Volcanics (PLV) of the main Rift Stage is a sequence dominated by flood basalts, with lesser rhyolitic and intermediate rocks, exposed in the hanging wall west-northwest of the Keweenaw fault system (Figs. 1 - 3). Volumetrically, the PLV is made up of approximately 95% tholeiitic basalt flows, 2% intermediate to felsic volcanics, and 3% conglomerates (Paces, 1988). At least 5 km of volcanic section filled the Lake Superior basin during PLV time within a timespan of less than 5 Ma (White, 1968; Nicholson, 1992). High-resolution age dates from the Copper City Flow (1093.37

± 0.53 Ma) near the base of the section and the Greenstone Flow (1091.59 ± 0.27 Ma) near the top of the PLV stratigraphic section (Fig. 6) constrain the eruptive timing and rate of basalt emplacement (Swanson-Hysell et al., 2019).

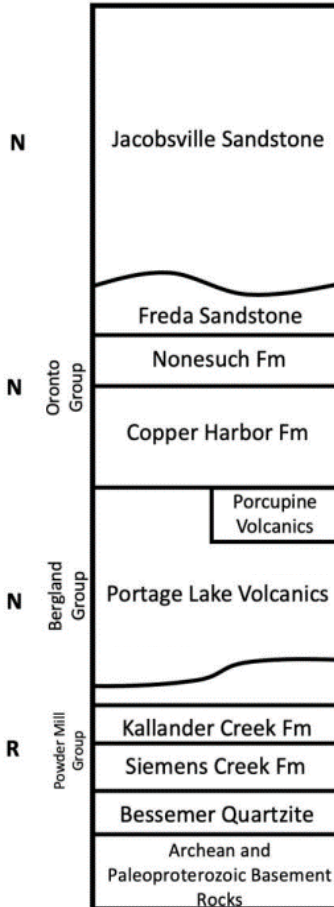


Figure 6: Simplified stratigraphic column of the Western Upper Peninsula of Michigan. Radiometric ages are shown, and ‘R’ and ‘N’ represent time periods of reversed and normal magnetic polarity (Davis and Paces, 1990).

Basaltic lava flows display a variety of textures (Fig. 7) and characteristics that are distributed across a flow’s thickness in predictable but variable ways and are useful for correlation (Fig. 8; Butler and Burbank, 1929; Self et al., 1998). The interiors of PLV lava flows typically exhibit textures described as melaphyric, ophitic, porphyritic, glomeroporphyritic, and pegmatitic, which may be roughly related to flow thickness (Butler and Burbank, 1929). Massive or melaphyric basalts have uniform crystal size

ranging from fine to medium grain and result from relatively fast cooling of thin flows or at the margins of thicker ones. In thicker flows that took longer to cool and solidify, such as the Copper City flow, feldspar and pyroxene crystals may grow larger to form an ophitic texture, featuring pyroxene crystals surrounding feldspar crystals that create a white, circular patchy texture with patches ranging from 0.5 cm to 2 cm across. In very thick flows such as the Greenstone flow, crystal size in the flow interior may exceed 2 cm to form a pegmatitic texture. Porphyritic and glomeroporphyritic textures display bimodal crystal sizes with larger grains distributed evenly or clumped within a finer-grained matrix, respectively.

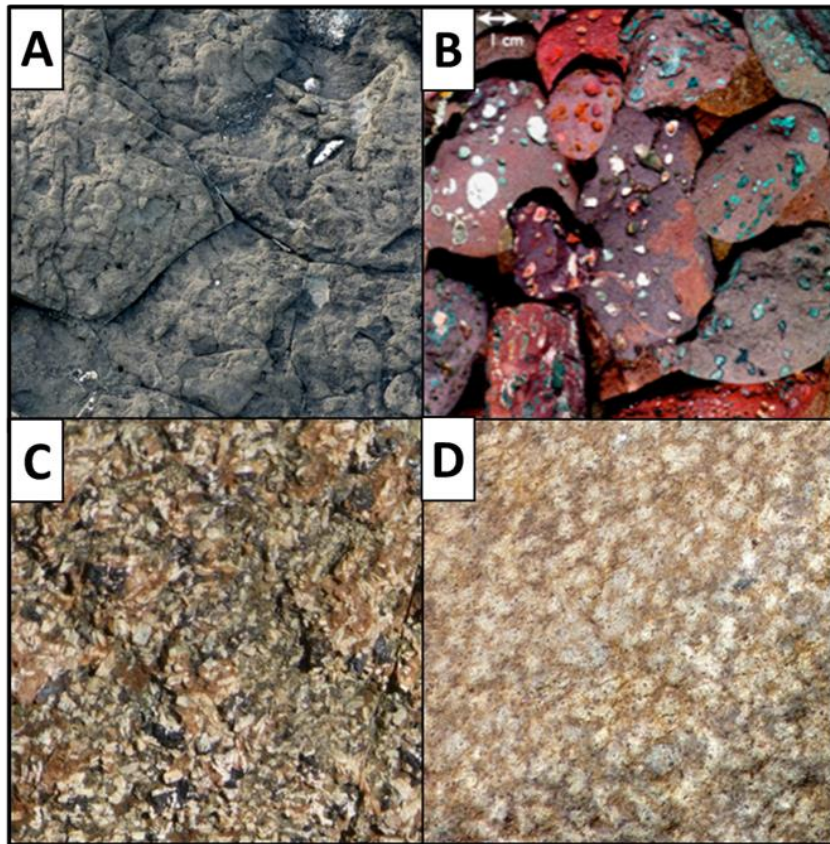


Figure 7: Main PLV basalt textural varieties observed in the map area: A) massive, B) amygdaloidal, C) pegmatite, and D) ophitic. Photos from Keweenaw Geoheritage and Michigan Technological University (Rose, 2020).

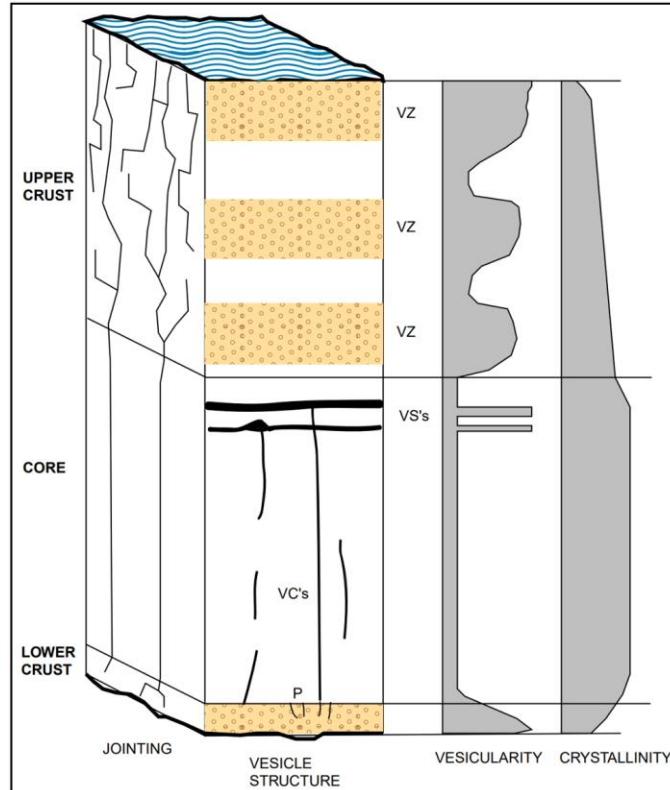


Figure 8: Idealized sketch of a cross section through an inflated pahoehoe lava lobe. Upper crust: 40-60% of the lobe has vesicular texture, often with horizontal vesicular zones (VZs); bubble size increases with depth. Core: Sparse vesicles in vesicle cylinders (VCs) and vesicle sheets (VSs). Lower crust: Vesicular like the upper crust, fewer joints, and 50-90% glass (Self et al., 1998).

The tops and bases of the lava flows are generally vesicular to amygdaloidal, with the upper flow-top zone being better developed and thicker than the lower flow-bottom zone. Amygdaloidal basalt is vesicular basalt with the vesicles filled by secondary mineralization. The amygdules or vesicles range in size from millimeter to centimeter-scale, and they typically have rounded, ellipsoidal, or irregular shapes. Minerals in the amygdules commonly include chlorite, epidote, quartz, copper, calcite, laumontite, prehnite, and pumpellyite. Flow tops are often brecciated, oxidized, and have abundant to moderately abundant amygdules that may be aligned to coalescing. The brecciation that

took place during emplacement (auto-brecciation), promoted subsequent weathering and a crumbled appearance. Flow tops also display a reddish-brown hue due to oxidation and may break down and weather into a lithic sediment during long intervals between eruptions. In contrast, flow bottoms are generally unbrecciated and melaphyric, may have pipe vesicles, and generally have fewer amygdules in a thinner zone than at flow tops.

Rhyolitic bodies have been described as lensoidal flows and dome complexes with associated pyroclastic deposits that are largely associated with the stratigraphic interval of the Bohemia conglomerate (Nicholson, 1992). The rhyolites can be split into two groups primarily based on textural differences and chemical variations. Type I rhyolites make up nearly all of the rhyolitic bodies previously investigated (Nicholson, 1992) and are associated with the bohemia conglomerate well to the northeast of the current project area. They typically have a red to pinkish red color, a very fine-grained ground mass that locally shows flow banding, and sparse small phenocrysts of quartz and plagioclase feldspar. They have a silica content that ranges from 71 to 75 wt% and are slightly enriched in light rare-earth elements (Nicholson and Shirley, 1990). Type II rhyolite is defined by a single body southeast of Copper City and near the level of the St. Louis conglomerate within the current project area (Fig. 14). This Copper City rhyolite body has a grayish green to pinkish gray appearance, fine-grained groundmass, and moderately abundant phenocrysts of quartz and lesser feldspar up to 2.5 mm across. It is characterized by silica content higher than 75 wt%, low rare-earth element abundance, and enrichment in Th, Rb, U, Nb, and Ta (Nicholson and Shirley, 1990; Nicholson, 1992). The Copper City rhyolite accounts for only about 5% of the known PLV rhyolite occurrences and is distinguished from Type I rhyolite in outcrop by having an abundance

of large phenocrysts of subhedral quartz, a larger overall grain size, and a distinctive color (Nicholson, 1992).

Interflow sedimentary units within the Portage Lake Volcanics are easily identifiable and, therefore, are used to correlate within a somewhat monotonous sequence of lava flows.

The finer-grained, sand-prone strata also provide opportunities to obtain accurate bedding measurements. The sedimentary units are mostly conglomerate to conglomeratic sandstone and, less commonly, well-bedded sandstone to siltstone. Conglomerate clasts consist of mafic to felsic volcanic rocks likely derived from rift-related flows and pyroclastic deposits. They are typically sub-rounded to angular in shape and vary in size from 0.5 to 20 cm (Cannon and Nicholson, 1990). The coarse-grained matrix between clasts is usually composed of volcanic rock fragments and minerals like feldspar, quartz, and pyroxene, which locally may display bedding. Interflow sandstone and siltstone layers are typically reddish to purplish to tan in color, have sub-angular to sub-rounded grains similar to the matrix between conglomerate clasts, and are well indurated by calcite or quartz cement, or both.

2.2 Post-rift Compression and Crustal Shortening

During or near the end of post-rift thermal subsidence, one or more compressional events affected the Lake Superior region as part of a new tectonic regime. The resulting crustal shortening led to extensive reverse faulting, such as along the Keweenaw fault, and further deformed the Lake Superior syncline that originated as a sag basin at the end of MRS extension (Cannon et al., 1993, Woodruff et al., 2020). As a result, PLV strata on the hanging wall of the Keweenaw fault dip moderately to steeply northwest, and their dip gradually decreases in a northwest direction towards the synclinal axis beneath Lake Superior (Fig. 9; Cannon et al., 1993, Woodruff et al., 2020). Postulated tectonic causes of the post-rift compression and crustal shortening are the Grenville Orogeny (~1200-980 Ma; Spencer et al., 2015) and the Appalachian Orogeny (~325-260 Ma; Dallmeyer et al., 1986), with the former most often mentioned (Cannon, 1994). Recent updates on the timing of Grenville events suggest that this orogeny involved three stages: Shawinigan (1200-1150 Ma), Ottawan (~1090-1030 Ma), and Rigolet (~1010-980 Ma) (Hynes and Rivers, 2010; Swanson-Hysell et al., 2019).

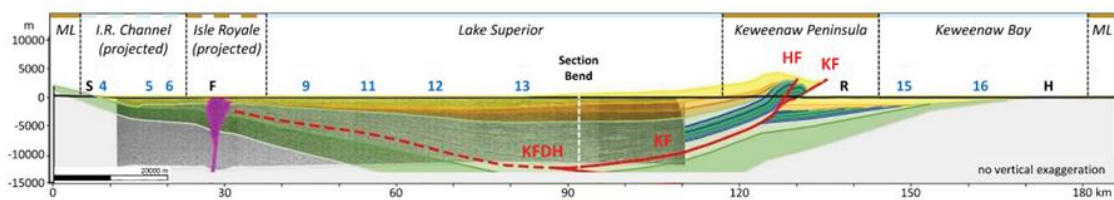


Figure 9: Regional cross section spanning the entire width of the MRS (DeGraff and Carter, 2023).

The Jacobsville Sandstone, deformed in the footwall of the KFS, is the youngest sedimentary unit within the Keweenaw Supergroup. Its age and relationship to post-rift thermal subsidence and later crustal shortening is still debated due to age estimates ranging from 1060 Ma to less than 960 Ma (Cannon et al., 1993; Malone et al., 2020; Hodgin et al., 2022). In a paper about Neoproterozoic sedimentation, Malone et al. (2020) used detrital zircons to infer that part of the JS section is at least 140 million years younger than the end of MRS extension, therefore post-dating thermal subsidence and the Rigolet phase of the Grenville Orogeny. Hodgin et al. (2022), however, used a refined process for detrital zircon analysis to conclude that younger JS strata along the Keweenaw Peninsula were deposited before the end of the Rigolet phase. Based on the latest data and remaining uncertainties, Jacobsville Sandstone in the footwall of the KFS probably was deposited sometime after 1060 Ma and as late as 990 Ma, which places its deposition within the time of the Grenville Orogeny.

Based on limited drilling and geophysical modeling, the Jacobsville Sandstone may attain a thickness of greater than 900 meters and perhaps as much as 3,200 meters in the footwall of the Keweenaw fault (Bacon, 1966; Kalliokoski, 1982; Cannon and Nicholson, 2001). This unit is composed mostly of quartzose to somewhat feldspathic, cross-bedded sandstone and siltstone with lesser conglomerate near the base and shale near the top (Hamblin, 1958; Kalliokoski, 1982). Jacobsville strata often display irregular color bands that alternate between deep to rusty red and opaque to chalky white. Sedimentary features and lithofacies observed in most of the Jacobsville Sandstone are interpreted to represent fluvial and lacustrine depositional systems associated with sediment transport from higher elevations around the sag basin toward its interior. The base of the Jacobsville

southeast of Keweenaw Bay locally consists of basal conglomerate with locally derived clasts that reflect the underlying rock types (Hamblin, 1958). Jacobsville strata low in the exposed section at Natural Wall ravine consists of conglomerate and conglomeratic sandstone with mafic to intermediate volcanic clasts likely derived from PLV strata (Hamblin, 1958). Similar conglomeratic strata found farther northeast in the footwall of the KFS have been interpreted as basal conglomerate of the JS (DeGraff et al., 2020, DeGraff et al., 2022), although they have been interpreted differently by Brojanigo (1984).

2.3 The Keweenaw Fault

The Keweenaw fault was first established as a fault by Irving and Chamberlin (1885), who carefully documented the contact relationships between the PLV and JS along the Keweenaw Peninsula. Based on their convincing observations, the fault trace has since been drawn on maps wherever the Portage Lake Volcanics is in contact with or adjacent to the Jacobsville sandstone. The fault was originally interpreted as a simple reverse or thrust fault, which held through the 1970s (Irving and Chamberlin, 1885; Butler and Burbank, 1929; White, 1972b). In the mid-1980s after acceptance of plate tectonic theory, geologists postulated that the Keweenaw fault began as a rift-related normal fault that later inverted as a reverse fault during post-rift crustal shortening (Cannon et al., 1989; Hinze et al., 1990; Cannon, 1994). More recently, DeGraff and Carter (2023) used modern cross-section construction methods to integrate detailed mining data across the Keweenaw Peninsula and regional geological and geophysical data to infer the downdip geometry of the Keweenaw fault (Fig. 9). The new cross-sectional model interprets the

Keweenaw fault and related faults as parts of a thrust fault system detached at mid-crustal levels, thus contradicting the idea that the Keweenaw fault began as a rift-related normal fault that inverted during post-rift crustal shortening (Figs. 9 and 10).

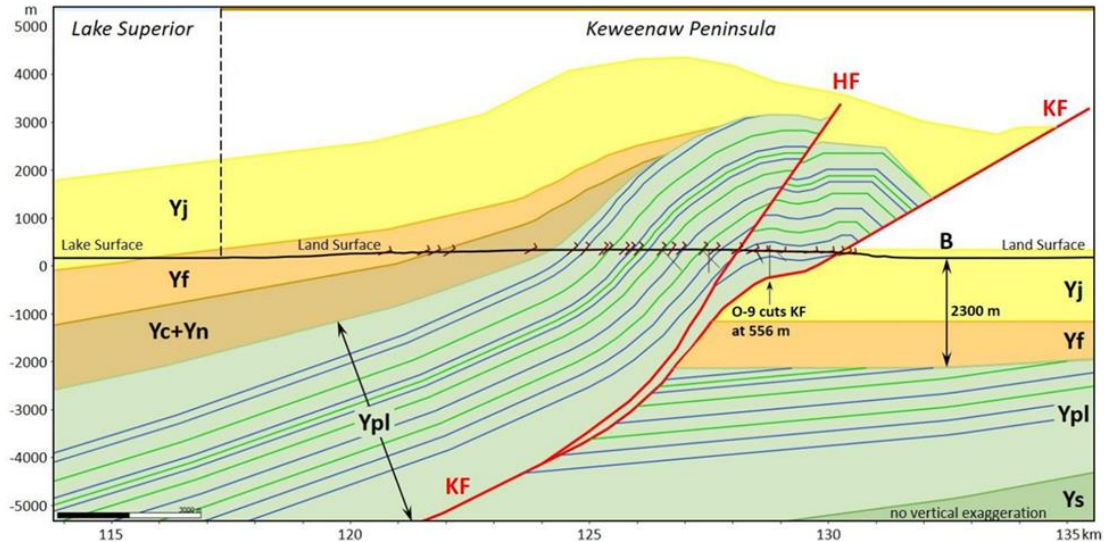


Figure 10: Local cross section across the Keweenaw fault near Dover Creek. HF—Hancock Fault; KF—Keweenaw Fault (DeGraff and Carter, 2023).

The Keweenaw fault generally strikes northeast and dips northwest over most of its length, but it curves to an east-southeast direction near the tip of the Keweenaw Peninsula (DeGraff et al., 2022). Similarly, the northerly dipping PLV strata changes strike by over 90° from N35°E near Hancock to N60°W at Keystone Bay. The curved fault geometry implies that fault-slip characteristics should vary along strike of the fault system. Reverse slip on the Keweenaw fault is estimated to be on the order of 10 km (Cannon and Nicholson, 2001; DeGraff and Carter, 2023), but an important component of right-lateral strike slip has also been documented (DeGraff et al., 2019; Mueller, 2021; Lizzadro-McPherson, 2023).

The timing of fault movement is inferred to have been as early as 1060 Ma, based on reset Rb-Sr dates of biotite in granitic basement (Cannon et al., 1993) and gangue

minerals related to native copper mineralization (Bornhorst et al., 1988; Cannon and Nicholson, 2000). The latest movement on the fault is estimated to be 985 Ma based on U-Pb dates of calcite veins within the fault zone and detrital zircons in deformed JS (Hodgin et al., 2022). This age range for fault movement, which includes both phases of the Grenville Orogeny, may represent more than one period of movement (Irving and Chamberlin, 1885; Butler and Burbank, 1929) or one longer continuous period of movement during Keweenaw time (Cannon and Nicholson, 2001). The nature and timing of fault movement in relation to Jacobsville deposition remains a topic of debate, which may be resolved with more and improved dating results.

The M.S thesis research presented here is based on the 2021-2022 EdMap Project, which was a continuation of the 2017-2018 and 2019-2020 EdMap Projects. The 2021-2022 EdMap project area consisted of two parts (Fig. 13), a southwestern part mapped by Katherine Langfield and a northeastern part that is the subject of this thesis. The specific aims of this M.S project are to:

Characterize and interpret changes in fault geometry and fold patterns along the Keweenaw fault system within the project area.

Interpret updated fold geometry and measured fault-slip indicators in terms of fault kinematics, the related paleostress state, and the tectonic regime responsible for deformation.

Investigate and explain the nature of the Copper City rhyolite relative to other rhyolites in the region.

3 Methods, Equipment, and Materials

Project activities consisted of geologic mapping, rock identification, and structural measurements performed in the field; and construction of geologic maps and cross sections, analyses of fold geometry and fault slip data, sample preparation, geochemistry, and microscopy analyses performed in an office or laboratory. The EdMap project area was divided amongst two Master's students: Katherine Langfield was responsible for investigating the southern section; and I, Nolan Gamet, had the same responsibility for the northern section (Fig. 13). Extensive preparation and planning were needed before the start of each field season to identify areas of interest to target during the field work.

Bedrock geology quadrangle maps for the map area were downloaded as georegistered images, shapefiles, and KMZ files from the USGS website (White et al., 1953; Davidson et al., 1955; Cornwall and Wright, 1956b; Cannon et al., 1999) and imported into ArcGIS Pro and Google Earth Pro as appropriate. Inspection of the legacy maps highlighted locations with interesting or problematic geology near the Keweenaw fault and areas lacking data that could benefit from infill mapping. Property ownership information was obtained from the 2018 plat book for Houghton and Keweenaw counties and from applications such as Onyx Hunt. Lastly, a file and data management system and Excel databases were created prior to beginning field work to store and organize files and a large amount of data were acquired as field work progressed.

The first two weeks of the project consisted of classroom discussions about protocols for geologic mapping, safety, and contacting property owners, along with group visits to field localities near the boundary of the two map areas. These joint activities helped to

ensure that data were collected similarly by both field teams and that precautions were taken to minimize field-related risks and misunderstandings with property owners. Field orientation included training to operate Trimble Geo7x differential geospatial positioning system (dGPS) units to obtain site positions and record basic site data, take and organize field book notes, make structural measurements, collect and mark samples, as well as opportunities to discuss uncertainties that arose.

3.1 Field Operations

Traditional geologic mapping techniques used during the project were enhanced with modern advancements in technology. Traditional field gear included a rock hammer, Brunton compass, measuring tape, hand lens, safety glasses, field book, and high-visibility safety vest. These items were supplemented with satellite-assisted systems such as Trimble Geo7x units with submeter positional accuracy and personal-device applications for navigation, figuring out property ownership, and making structural measurements. Whereas previous mappers relied on aerial photography, pace-and-compass methods, and physical maps to navigate and locate outcrops, we used Avenza Maps iOS and Google Earth Pro with georeferenced USGS quadrangle maps for the same tasks.

Prior to field work, a data dictionary was created and installed on the Trimble Geo7x to aid with data collection and to ensure data consistency between both MS projects. A data dictionary is a user-designed data-entry protocol that presents a screen with data fields and pick lists that allow a user to specify rock units, major lithologies, exposure types,

structures, and brief notes for each field site. At the end of each day, data files from the Trimble Geo7x unit were transferred to a computer running GPS Pathfinder Office and converted to SSF and CSV files to be imported to ArcGIS Pro and an Excel database. Additional site information recorded in a field book was transferred to the same Excel database and subsequently formatted for various analytical operations explained below (Table 1). The newly obtained site data were then used to modify previous geologic maps and to construct cross-sections in selected areas.

Table 1: Data acquired at field sites; modified from Mueller (2021).

Data Type	Description	
Site Number	Sequential number that indicates each site throughout data processing	
Setting	Location relative to nearby sites, topographic position, topographic features and expressions, drainage beds, ridge trends	
Exposure Type	Description of exposure (outcrop, subcrop, float), relative extent and size of exposure, visible structures and contacts, where GPS point was taken	
Lithology	Hand sample description of dominant rock types and observed mineralogy; notes tracking when samples are collected (including number of samples taken)	Igneous rocks: color, texture, grain size, mineralogy (groundmass, amygdules, phenocrysts), secondary mineralization and alteration
		Sedimentary rocks: color, grain size, shape, sorting, induration, binding agent, clasts and their constituents, identifiable minerals, sedimentary features and small-scale structures
Structural Features	Structures observed at the site such as deformed strata (tilting, folding, faults, veins, joints); describes and interprets structures and the relationship between them	
Structural Measurements	When applicable, strike-dip of surfaces, rake or plunge-azimuth of lineations on fault surfaces, identifies feature type, confidence level, measurement method, and the measurer	

A typical field day began with a discussion about possible safety hazards and objectives for the day. The date, location, personnel, and basic objectives for the day were recorded on a new page within the field book. Most days were spent in the same general area navigating to outcrops noted on published bedrock geology maps or searching for new outcrops along dry ravines, creek beds, roadside ditches, or elsewhere where topography seemed favorable. On some days, multiple areas were visited because of outcrop scarcity or complications due to weather, availability of field assistants, or access to properties. Conversations with property owners occurred frequently and flyers explaining the purpose of the project were created and delivered to rural mailboxes to facilitate requests to access private property.

Around 2% of the 1,045 sites in the project area had limited satellite reception. The Trimble Geo7x uses the Global Navigation Satellite System (GNSS) of satellite constellations to obtain geospatial coordinates, and it requires a special reference signal to achieve the desired submeter horizontal accuracy. This project relied on geostationary satellite signals that commercial airliners use to obtain submeter positional accuracy, namely the Satellite-based Augmentation System (SBAS). In northern Michigan, SBAS satellites are found low on the southwestern horizon such that their signals are blocked by terrain when field sites are within deep ravines or adjacent to steep northeast-facing slopes. For these and other situations without an SBAS signal, a distance offset method ([Trimble Geo 7x handheld user guide, 2013](#)) was implemented whereby a laser rangefinder was used to measure distance and direction from a site with submeter positional accuracy to a targeted feature, and then the target's coordinates were computed trigonometrically with provided software.

Upwards of 1,800 surface orientations and lineations were measured over the course of two field seasons for this MS project. This robust dataset allowed various structural analyses to be performed on different data subsets to investigate changes in fold geometry and fault-slip characteristics within the project area. Wherever possible, bedding orientation at a site was measured on five or more separate surfaces to obtain a site average with subsequent data processing. Fracture orientations in different sets were measured at sites in a similar way and with the same intent to compute site averages. Slip lineations, such as slickenlines, were also measured nominally five times per fault surface to obtain an average slip direction for each fault. Surface orientations generally were measured as strike and dip with FieldMOVE Clino on iOS devices, whereas lineations were measured with a Brunton compass as apparent rake or plunge azimuth.

FieldMOVE Clino (FMC) was found to be operationally very efficient and helpful when measuring orientations in difficult spots such as confined spaces, underhangs, areas with strong magnetic anomalies, and on steep slopes where footing was difficult. The iOS version of the application was used instead of the Android version due to better sensor accuracy of iOS devices ([Allmendinger et al., 2017](#)). At each field site, the geographical position and declination used by FieldMOVE Clino were refreshed and comparative measurements were taken on the same planar, non-magnetic surface using a Brunton compass and FMC to ensure data consistency.

3.2 Data Management and Analysis

Field data were formatted and processed using different workflows for geospatial and geologic data (Fig. 11). Geospatial data files were saved on multiple storage devices and shared to a Google drive daily to ensure that no data was lost in case of storage or file-related issues. These data files were then exported as CSV files and saved to a master Excel workbook containing three main worksheets or tabs for different data types, namely site geologic data, feature orientation data, and sample data. Most of the data processing involved feature orientation data that needed to be structurally corrected and averaged to obtain characteristic site values. To facilitate the processing, a new Excel tab was created after each major processing step to improve efficiency and to minimize confusion when implementing equations and Excel macros. Processed data were then formatted to be compatible with other software tools discussed below.

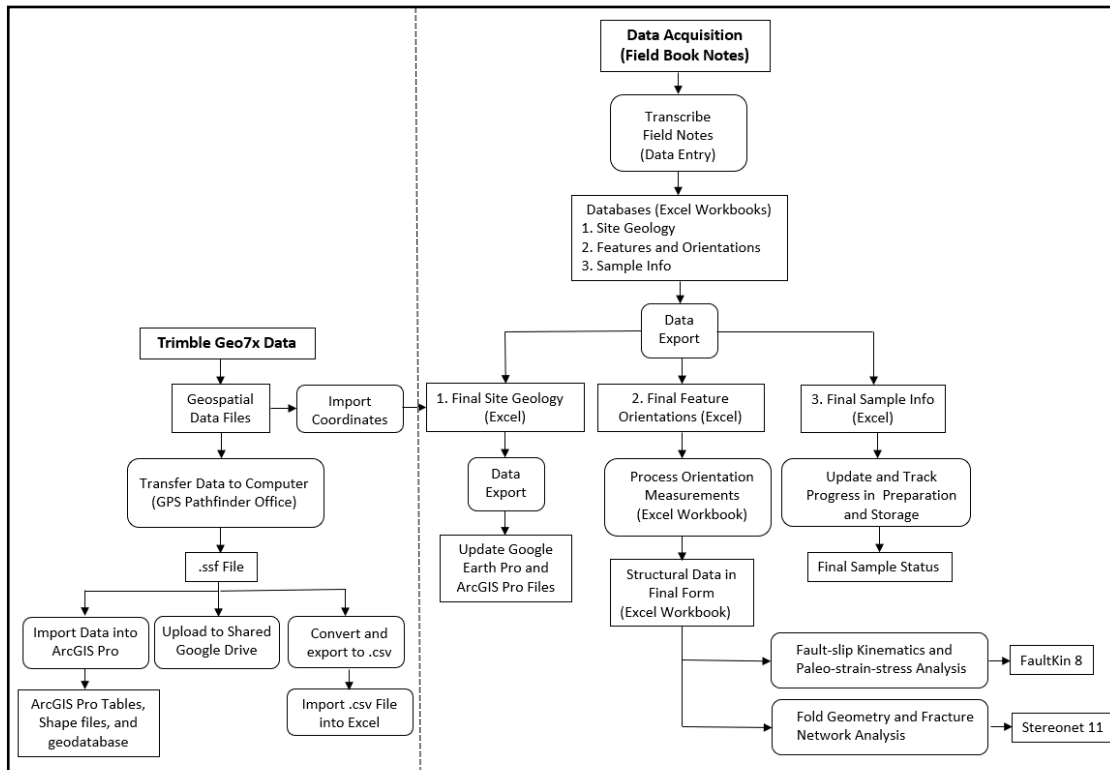


Figure 11: Workflow for geospatial data transfer from Trimble Geo7x units and export to other systems (left); and for geological data transfer from field books, subsequent processing, and structural analysis (right).

Orientation measurements taken at each site first were grouped by feature type, such as bedding or lineations on a single fault surface, and then were averaged to obtain characteristic values for the feature class of interest. In some cases, multiple measurements of the same feature were taken and then averaged, such as when measuring large undulous surfaces whose orientation varied with position or when using different measuring methods, devices, or personnel to check for consistency. Repeated measurements of a feature class like bedding at one site or of an individual feature improved confidence in the average characteristic values by compensating for variability within a site or on a surface. These site-averaged orientations were then imported into Stereonet and FaultKin (Allmendinger, 2020) for fold and fault-slip analyses.

Following data processing and analysis, ArcGIS Pro was used to update legacy bedrock geology maps using the new outcrop data and structural measurements. A database containing geologic map layers and supporting data was downloaded from the USGS to use as a starting point for the map construction (Cannon et al., 1999). Field sites with accompanying feature orientation data were then imported into ArcGIS Pro and used to modify existing geologic unit polygons and fault line features. The geologic unit polygons were adjusted based on newly documented outcrops, ridge trends, and other useful data from the mapping work. Other legacy map objects that were modified based on the new field work included diamond drillholes, water wells, and mineshafts.

The updated bedrock geology map and processed orientation data were used to construct four cross sections that transect the KFS normal to its local strike. The cross sections were created using geoprocessing tools and layout views in ArcGIS Pro. Topographic profiles were created using a DEM mosaic that has 2-foot horizontal resolution between imaged LiDAR points on a single raster cell and sub-foot vertical precision with a cell value of 19.6 centimeters. Cross-sectional geometries have been constrained with characteristic values of bedding and fault orientation converted from true dip to apparent dip along the cross-section lines, and by the results of fold and fault-slip analyses.

3.3 Sample Preparation and Analysis

Over 400 grab samples were collected over the course of both field seasons, most of which were cut in the laboratory to observe a fresh face and improve rock identification. Samples were organized based on site number and stored in a rock storage room. Samples from sites of particular interest or having unusual lithology or mineral assemblages were selected for thin section work, geochemistry, and age dating. Over 20 specimens for external lab work were prepared in Michigan Tech's rock lab according to the type of anticipated analyses, and then sent to various laboratories for thin section preparation, whole-rock geochemistry, and mineral separation for age dating.

Cut billets were sent to Wagner Petrographic for the preparation of 12 polished thin sections. Finished thin sections were examined using a transmitted light microscope (Leica DM750P polarizing microscope) in cross-polarized and plane-polarized light to identify major mineral components, textures, and microstructures. Six rhyolite samples, two basalt samples, and two conglomerate samples were sent to ALS Global for whole-rock geochemical analyses including trace elements. Lastly, two rhyolite samples were cleaned, broken into hand sample-sized pieces, and sent to Zirchron LLC for zircon extraction required for obtaining age dates. Zircons were successfully separated from one of the two samples, but they are yet to be submitted for TIMS work and results probably will not be available until 2024.

4 Results and Findings

The recent 2021-2022 EdMap project area is approximately midway between the base and tip of the Keweenaw Peninsula, and it lies at the southwest end of a broad arc formed by the KFS as it curves rightward going toward the peninsula's tip (Fig. 1). Results of the EdMap project have been submitted to the USGS as an updated map (Fig. 13) and as a technical report with detailed maps focused on complex areas of particular structural interest (DeGraff et al., 2022). Those products contain the results of the work for this M.S. thesis, and so they are summarized in the next section to provide context for subsequent sections. A comparison of these new results with those from areas farther along the curve of the fault system is made later in the Discussion section.

4.1 Overview of EdMap Project Results

The integration of field data and exploratory drillhole data indicates that the Keweenaw fault (KF) is not one continuous slip surface offset by smaller cross faults, but instead is a complex system of fault segments that we call the Keweenaw fault system (KFS). In the recent EdMap project area, the KFS can be divided along its length into three main sections that differ in geometry and stratigraphic position, but whose principal slip surfaces are connected along strike (Fig. 13, KFS-1, KFS-2, KFS-3). The two sections of the fault system farthest to the southwest (KFS-1, KFS-2) define the average N35-40°E trend of the fault system here and account for most of its length. The third section to the northeast (KFS-3) has an average trend of N55°E, which represents an abrupt change in

direction from the other two sections where the Allouez Gap fault intersects the KFS. At this abrupt bend in the KFS, the main slip surface shifts down stratigraphically from near the base of St. Louis conglomerate southwest of the bend to ~650 meters deeper northwest of the bend (DeGraff et al., 2022). Geometric and stratigraphic differences between the two fault segments farthest to the southwest will be discussed in more detail by the companion M.S. thesis in preparation by Langfield.

At a finer level of detail, individual faults of the KFS can be categorized by direction into three sets: 1) major NNE-trending segments that define the fault system's overall trend and probably have mostly reverse slip; 2) NE-trending segments that branch off the major fault segments and define wedge-shaped fault blocks; and 3) NNW-trending segments that connect faults of the first two types. More specifically, Set 1 faults make up most of sections KFS-1 and KFS-2, strike N15-40°E, and dip 15-50°NW. Set 2 faults, striking N35-70°E and dipping 35-50°NW, include most of section KFS-3, the Hancock fault, and footwall splays branching off the main Set 1 faults. Set 3 faults, striking N5-20°W with poorly constrained, include connectors between the other two fault sets and the Allouez Gap fault (DeGraff et al., 2022).

These three directional fault sets define multiple fault blocks of PLV strata that vary greatly in size and whose long dimension typically trends in a northeasterly direction. The largest of these fault blocks is in the hanging wall of the fault system between the Hancock fault and two of the main Keweenaw fault sections (KFS-1, KFS-2). A second large fault block, referred to as the Mayflower fault block (MFB), is in the footwall of the fault system at the abrupt bend between sections KFS-2 and KFS-3. Southwest of the

Mayflower fault block, two much smaller, contiguous, fault blocks are defined by Set 2 splay faults in the footwall of main Set 1 fault segments. The three contiguous footwall fault blocks are wedge-shaped, widen toward the northeast, and increase in size in the same direction.

Other significant changes shown on the new bedrock geology map are the reinterpretation of two cross faults at offsets of the Keweenaw fault on published maps and extension of the Copper City rhyolite along strike. The fault reinterpretation has the Allouez gap fault terminating against one of the main KF segments near the northeast end of the Mayflower fault block, rather than cutting across the KF and presumably offsetting it. In the same general area, a complex intersection of four faults is proposed to accommodate the abrupt change in direction and stratigraphic level of the KFS. Regarding the Copper City rhyolite, additional outcrops were discovered ~1 kilometer southwest of the previous southwestern extent of the main rhyolite body along the old Calumet and Hecla railway, ~0.2 kilometers northeast of the previous northeast extent in a newly opened quarry, and ~3.6 kilometers northeast of the quarry near the northeast boundary of the project area. Together, these new exposures extend the Copper City rhyolite over ~6 kilometers along strike.

In the broader context of the 2021-22 EdMap project, this M.S thesis project has focused on the northeastern part that extends along the KFS from Lake Linden to Mohawk, Michigan. Many of the observations were made at well-known localities such as Houghton-Douglass Falls near Lake Linden, St. Louis and Natural Wall ravines east of Calumet, and the Copper City rhyolite near that town. These localities have been of

interest to geologists for over 150 years and they provide examples of how fault geometry can change over a relatively short distance. The following sections present detailed mapping results for three focus areas along the KFS where four cross-sections were constructed across the Keweenaw fault (Fig. 13, Locations A, B, C).

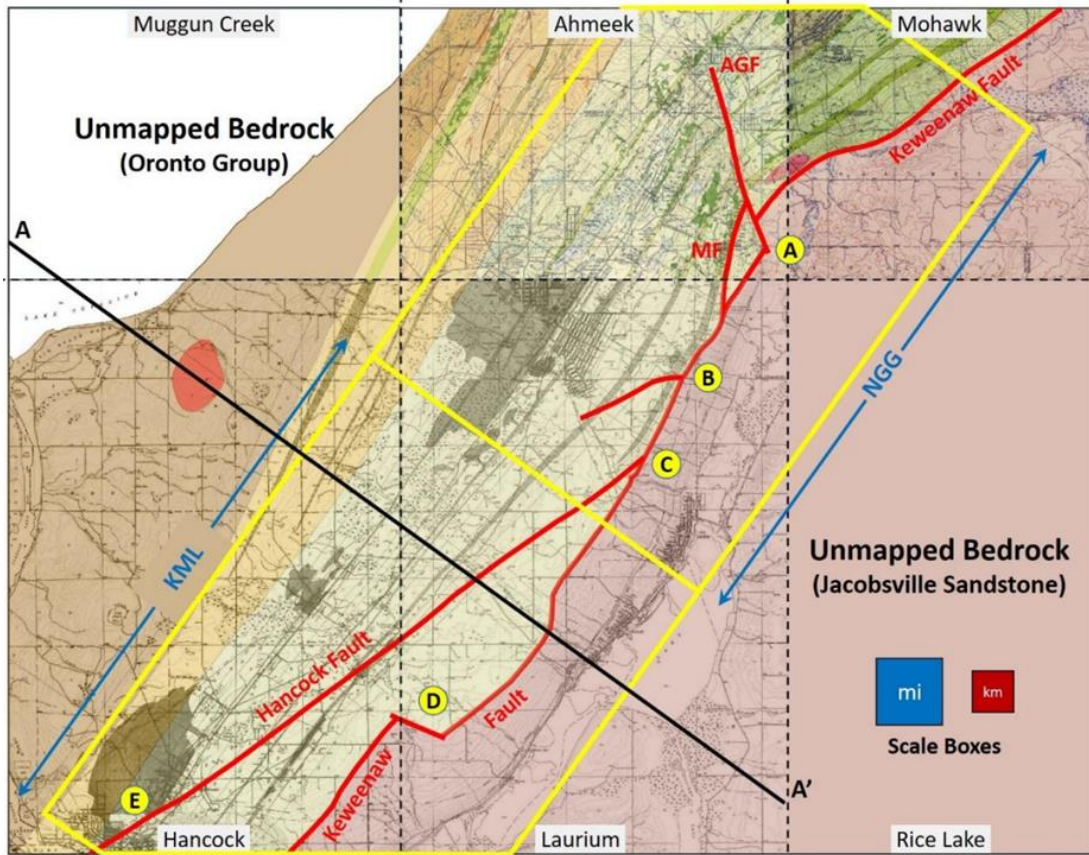


Figure 12: Legacy bedrock geology map of the Keweenaw Peninsula north of Portage Lake. The 2021-2022 EdMap project is outlined in yellow. Yellow circles with letters denote key localities: A – Mayflower Fault block, B – St. Louis ravine and large splay fault, C – junction between Keweenaw and Hancock faults near Houghton-Douglass Falls. D – unusual offset in Keweenaw fault, and E – Hancock fault inside the Quincy Mine adit. Map adapted from Cannon and Nicholson (2001).

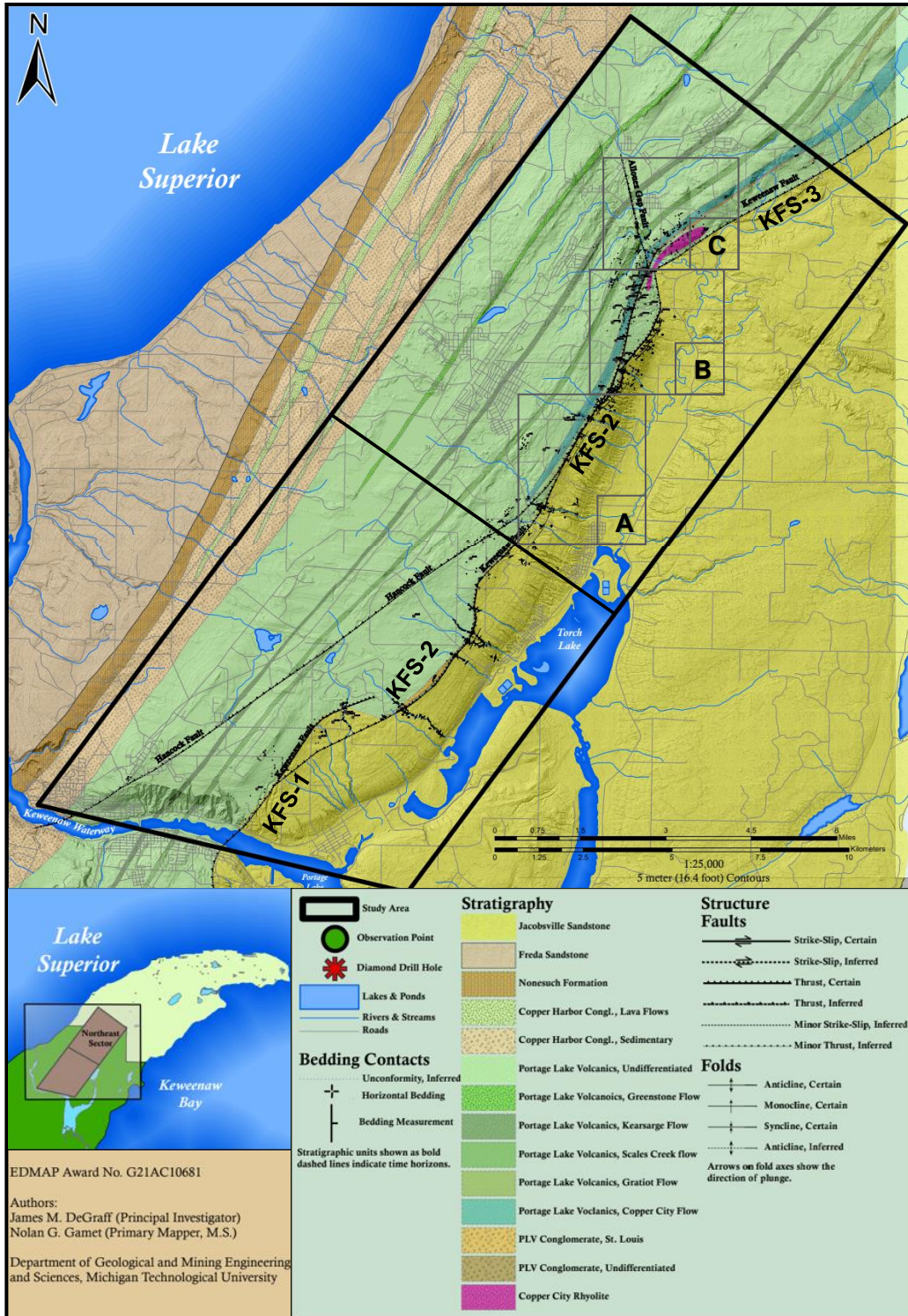


Figure 13: Updated bedrock geology for the 2021-2022 EdMap project area. Inset shows the area relative to the Keweenaw Peninsula and subareas for two M.S. projects. Focus areas are outlined with black boxes: A) Houghton-Douglass Falls and St. Louis Ravine; B) Natural Wall ravine and Mayflower Fault Block; and C) Copper City rhyolite. Main sections of the Keweenaw fault system: KFS-1, KFS-2, and KFS-3.

4.2 Houghton-Douglass Falls and St. Louis Ravine

The Keweenaw fault within this focus area, defined to be the main slip surface of the KFS, is intersected on its hanging wall by the Hancock fault and a small fault farther north, and on its footwall by an unnamed splay at the north edge of the focus area. The Keweenaw fault is interpreted to lie at or just below the level of the St. Louis conglomerate, which itself lies at or just below the base of the thick Copper City flow (Fig. 14), based on new mapping along many ravines crossing the fault, examination of exploratory drill core logs (White, 1985), and reinterpretation of published maps and reports (White et al., 1953; Davidson, 1955; Cornwall and Wright, 1956b). The connection between the St. Louis conglomerate and the KF is an important update to previous interpretations regarding the geology adjacent to the fault. Hubbard (1898) came closest to making this connection when he documented the so-called “contact” conglomerate northeast and southwest of Hungarian Falls along Dover Creek, speculating that it and a sedimentary layer near the base of Houghton-Douglass Falls could be the St. Louis conglomerate. White et al. (1953) later connected the Mayflower fault (Fig. 12) to the St. Louis conglomerate within the Ahmeek bedrock geology map and on accompanying cross-sections. The “contact” conglomerate of Hubbard (1898) in the hanging wall of the KF at Hungarian Falls was later interpreted to be the St. Louis conglomerate (DeGraff and Carter, 2023), based on its field characteristics, down-dip correlation to drill hole penetrations, and relative stratigraphic position on both sides of the Hancock fault.

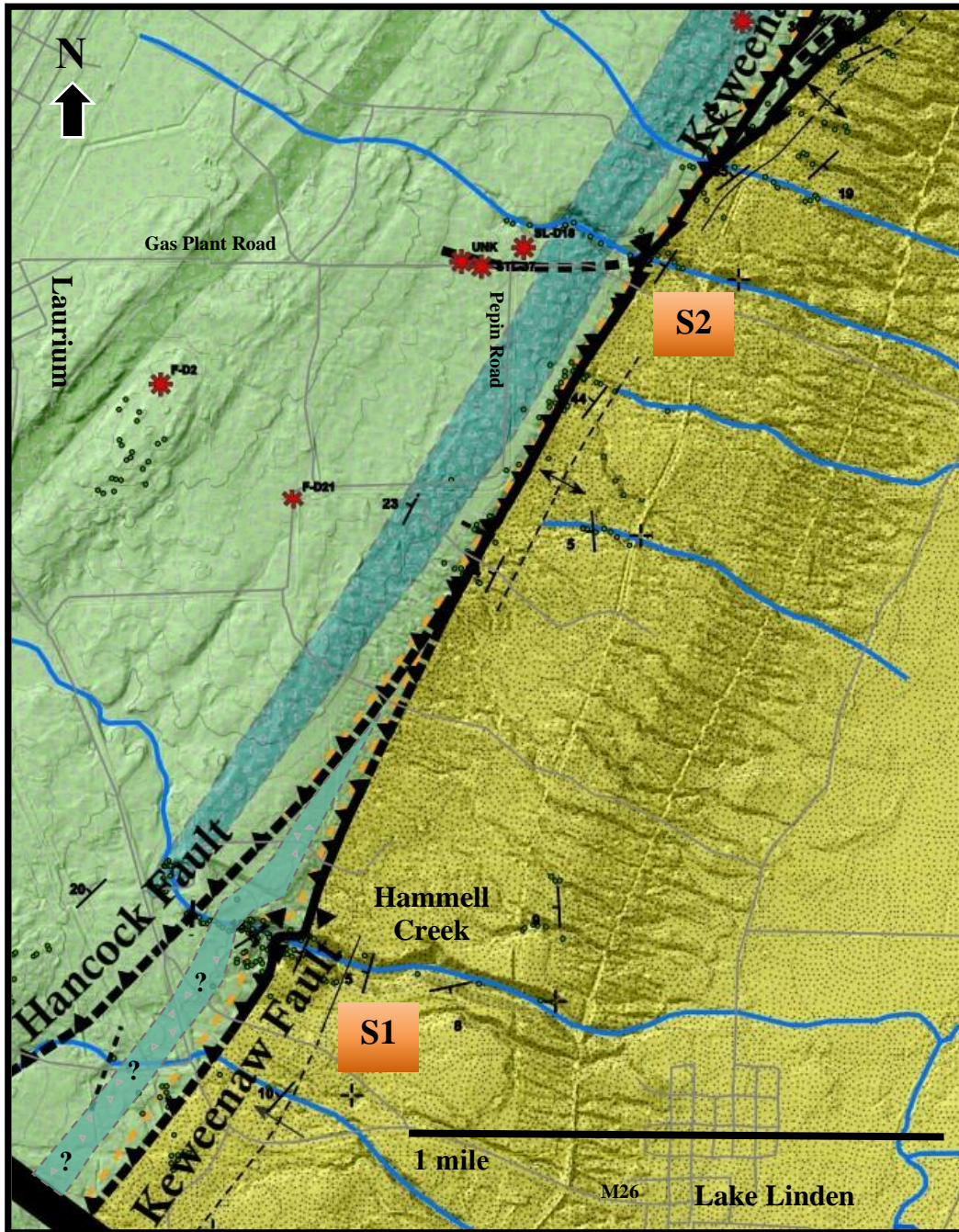


Figure 14: Zoomed in view of new bedrock geology map for the area containing Houghton-Douglas Falls and St. Louis ravine. Colors and symbols explained in the map legend of Figure 13. Localities mentioned in text: S1 – Houghton-Douglas Falls; and S2 – St. Louis ravine.

Houghton-Douglass Falls is located 2.9 km northwest of Lake Linden and exposes a kilometer-long stretch of bedrock along Hammell Creek in both the hanging wall and footwall of the Keweenaw fault. The faulted PLV-JS contact is well constrained here by outcrops and excavations made by Irving and Chamberlin (1885), some of which were located during the recent mapping (Fig. 14, S1). Irving and Chamberlin (1885, their Fig. 6 and Plate VII) indicated by their drawings that the Keweenaw fault dips 25-30° NW, slightly steeper than PLV strata in the hanging wall, which dips ~15°NW based on measurements made for this project. The fault's strike and dip were calculated for this study to be 240°/19° NW by applying a three-point method to locations along the V-shaped PLV-JS contact across Hammell Creek. Less accurate site-line dip measurements made in the field averaged to be 16° NW, in good agreement with the three-point calculation.

Hanging-wall PLV strata are highly brecciated, sheared, and altered from the PLV-JS fault contact on Hammell Creek to ~60 meters upstream at the base of Houghton-Douglass Falls. The geometry of basaltic flows over this distance is not apparent because of this deformation, but the approximate stratigraphic thickness that is represented is calculated to be about 20 meters. About 10 meters up the face of the waterfall, a 2-m-thick conglomerate layer below a ~10-cm-thick sandstone layer is the only PLV sedimentary unit observed anywhere along this section of Hammell Creek. It provides a reliable orientation for PLV hanging-wall strata of 236°/16° NW. The main vertical face of the waterfall was not examined directly, but from a side view it appears to be a single thick flow that exhibits a coarse fabric dipping shallowly to the northwest. At the top of the falls, an average orientation for this flow was determined to be 242°/15° NW by

measuring several surfaces parallel to amygdaloidal layers, which measurement agrees with the more reliable measurement made on the interflow sedimentary layer below. Given the above relationships, we interpret that both the St. Louis conglomerate and Copper City flow are present in the KF hanging wall at Houghton-Douglass Falls and that they extend northeastward to a truncation on the footwall of the Hancock Fault (Fig. 14). This interpretation results in an apparent left-lateral offset of these two units across the Hancock fault, which matches the apparent sense of offset shown on legacy maps for PLV layers higher in the section (Fig. 12).

The Hancock fault had been mapped as intersecting the Keweenaw fault just north of Houghton-Douglass falls, but PLV units northeast of the Hancock fault were not carried across to its southwest side (Cornwall and Wright, 1956b). The Hancock fault here is not exposed in outcrop. Instead, its surface trace was inferred from drill hole penetrations less than 0.8 kilometers southwest of Hammell Creek, other drill hole penetrations farther southwest, and finally exposures underground at the Quincy Mine (Cornwall and Wright, 1956a; Cornwall and Wright, 1956b). The updated trace of the Hancock fault (Fig. 14) is adopted from the Laurium bedrock geology map at points away from the Keweenaw fault intersection but modified near the Keweenaw fault based on the new field data. Relative to earlier maps, the intersection of the Hancock fault with the Keweenaw fault has been moved ~800 meters northeast on the updated map, and the St. Louis conglomerate and Copper City flow have been correlated across the Hancock fault with slight modifications to their positions north of that fault.

The St. Louis ravine is located ~1.5 kilometers north of the re-interpreted intersection between the Hancock and Keweenaw faults and about 2 km southeast of Laurium (Fig. 14, S2). Field and subsurface relationships between the KF, the St. Louis conglomerate, and Copper City flow here are relatively well established from the new mapping and previous work by USGS geologists. Erosion by the SE-flowing creek in this ravine has exposed the fault contact and much of the adjacent hanging-wall and footwall stratigraphy. These outcrop exposures were first examined by Irving and Chamberlin (1885) who noted a steeply dipping (S/D = $242^{\circ}/70^{\circ}$ NW) JS conglomerate against overlying PLV strata. These exposures were located during this project and described in more detail as follows.

The Keweenaw fault is crossed by this ravine ~5 meters ESE of a 2-meter-tall waterfall over basalt that lies above a PLV felsic conglomerate with a thin layer that are interpreted to be the St. Louis conglomerate. The immediate hanging wall of the fault has ~7 meters of a horizontally continuous exposure of brecciated St. Louis conglomerate overlain by amygdaloidal basalt with mineralized zones and fractures filled mostly with calcite and quartz. The PLV interflow sandstone layer strikes N32°E and dips ~34° NW and is subparallel to the overlying conglomerate and the Copper City flow measured ~400 meters to the northwest (S/D = $214^{\circ}/32^{\circ}$ NW). The fault's orientation here is taken to be nearly parallel to the orientation of hanging-wall PLV strata. At the base of the St. Louis conglomerate, the creek turns sharply toward the northeast to flow along the fault contact for about 10 meters, before turning again to resume its southeasterly course. Upstream from the St. Louis conglomerate, the upper part of the thick Copper City flow is marked by another jog in the creek around a large resistant NW-facing slope (Fig. 14). Here, the

Copper City flow and St. Louis conglomerate are not in direct contact as they are farther northeast ([White et al., 1953](#)), but instead have one or more basaltic flows between them.

Footwall JS strata are exposed along the NE-trending jog in the creek and at a 4-meter-tall waterfall located ~15 m southeast of the fault. Along this part of the creek, JS strata consist of sandstone, conglomerate, and silty mudstone layers that strike parallel to the fault trace and are subvertical to overturned ($S/D = 214^{\circ}/62^{\circ}$ NW). Downstream below the main waterfall, JS strata become nearly horizontal at ~170 m southeast of the fault, where they strike $N76^{\circ}E$ and dip $7^{\circ}SE$. A lack of outcrop between this point and the main waterfall to the northwest obscures the manner in which this large dip change occurs, and so the footwall fold geometry here has been modeled in a cross-section presented later by combining data from St. Louis ravine with data from the Houghton-Douglass Falls area.

The legacy bedrock geology map shows a small splay fault as a dashed trace that diverges in a southwesterly direction from the hanging wall of the main KF and offsets the St. Louis, Copper City, Bohemia, and Scales Creek units with an apparent left-lateral slip sense ([Cornwall and Wright, 1956b](#)). Although this SW-trending splay is not observed in outcrop, examination of core logs for two exploratory drill holes closest to the fault (St. Louis-18 and 37; [Appendix A3](#)) help support its existence and general position. We interpret that the fault generally strikes east-west and passes between the two boreholes rather than south of both boreholes in a southwesterly direction, as shown on the published bedrock geology map. The drill holes support the apparent left-lateral offset at the top of the Copper City flow as shown on published maps, but neither cored drill hole intersects a significant fault. Field mapping in this area also did not find surface

evidence for this fault or the offset of the PLV units shown on the Laurium bedrock geology quadrangle. This splay was omitted in a later map compilation of the Keweenaw Peninsula for reasons unknown ([Cannon and Nicholson, 2001](#)). All of the above suggests that this fault is a minor feature along the Keweenaw fault system and probably allows local adjustment of strata displaced along the larger faults.

4.3 Natural Wall Ravine and Mayflower Fault Block

The Natural Wall, in a ravine of the same name, is the next prominent locality along the KFS with abundant outcrop exposures of deformed JS strata adjacent to the Keweenaw fault. It was first described by Irving and Chamberlin (1885) as a vertical wall of indurated quartzose sandstone projecting from softer conglomerate to conglomeratic sandstone and muddy siltstone that has been removed by erosion along the creek. This prominent locality lies at the southern end of the Mayflower fault block where the legacy bedrock geology map shows the Mayflower fault diverging northward from the Keweenaw fault up to the Allouez Gap fault (Fig. 13; Cornwall and Wright, 1956b; White et al., 1953). Similar to the previous focus area, the Keweenaw fault in this area is interpreted to lie at or just below the level of the St. Louis conglomerate, which itself lies at or just below the base of the thick Copper City flow (Fig. 15; White et al., 1953). Unlike the previous area, splay faults intersecting the main fault occur only in its footwall and become increasingly prominent toward the north. These NE-trending splays and their connections define a series of three fault blocks that are elongated in a northeast direction and become wider and larger in that direction, culminating with the Mayflower fault block. Their geometry and arrangement imply that the bounding splay faults have a component of right-lateral strike slip as well as west-side-up reverse slip (Fig. 15, S1).

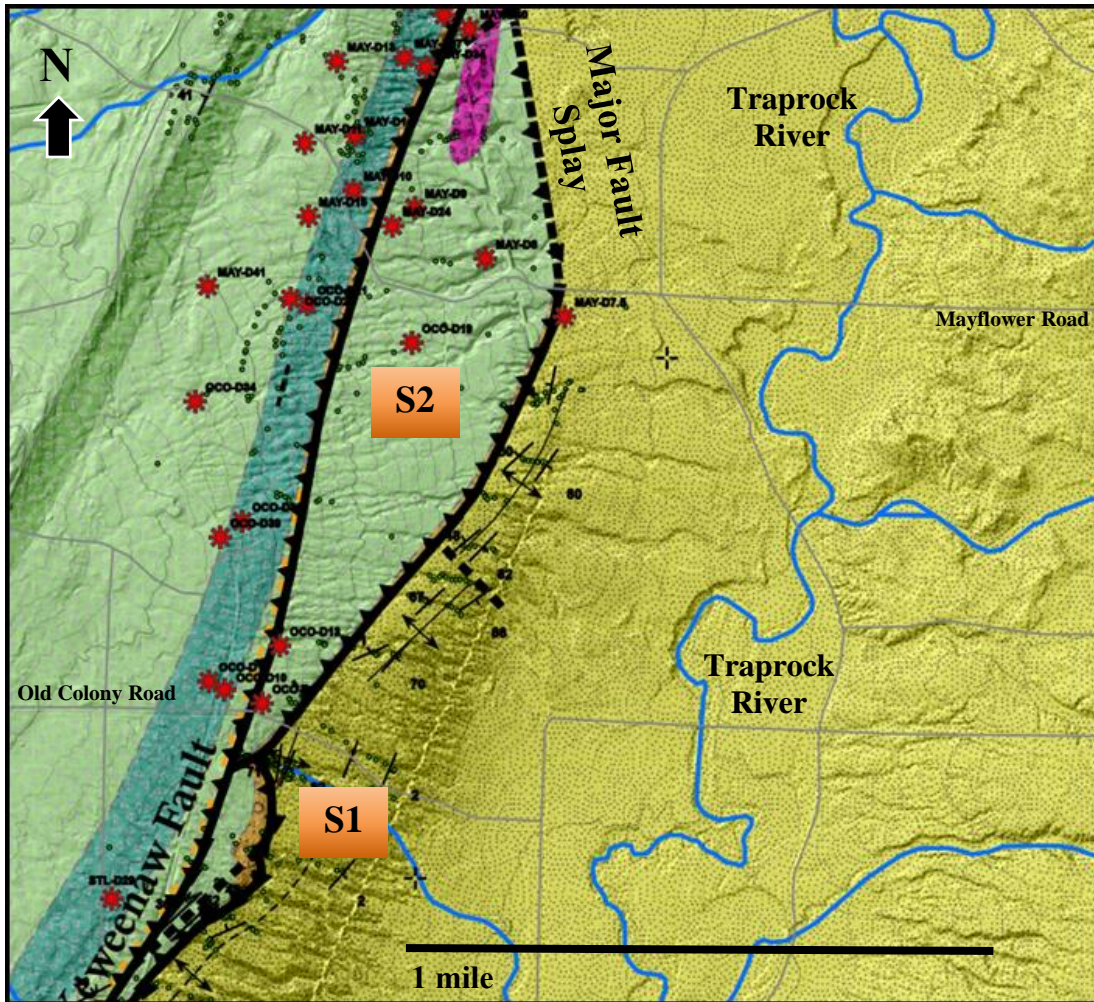


Figure 15: Zoomed in view of new bedrock geology map showing multiple fault segments within focus area B. Colors and symbols explained in the map legend of Figure 12. Localities with primary interests: S1 – Natural Wall; and S2 – Mayflower Fault Block.

Natural Wall ravine is ~2 km east of Calumet, MI and close to the junction of the Keweenaw fault with a large footwall splay at the southern end of the Mayflower fault block (Fig. 15, S1). The fault system here is interpreted to be more complex than shown on the published bedrock geology map (Fig. 12). Based on the new mapping and distribution of conglomerate units, Natural Wall ravine is interpreted to lie at the intersection of the largest of the footwall splay faults with a connector fault from the next

splay to the south (Fig. 15). The large splay fault continues northeast from the Natural Wall to define the southeastern boundary of the Mayflower fault block and extends in the opposite direction to connect with the main Keweenaw fault less than 90 meters away. The connector fault terminates against the large splay fault and extends south-southeast for ~340 meters before curving southwest to a connection with a smaller, NE-trending, splay fault. The footwall fault blocks defined south of Natural Wall ravine have the main KF along their western boundaries and, according to the new interpretation, have the St. Louis conglomerate duplicated along their southeastern and northeastern margins in a set of arcuate outcrop belts. This updated map pattern defines a set of small fault blocks or slices in the footwall of the main fault that partly duplicate the PLV section containing the St. Louis conglomerate.

Outcrops in the immediate vicinity of the Natural Wall are nearly continuous upstream to just beyond the major NE-trending splay fault and downstream for several hundred meters. Upstream from the Natural Wall, a fault contact was excavated by Irving and Chamberlin (1885), who described it as juxtaposing a PLV conglomerate layer in the hanging wall with vertical JS layers in the footwall along a NW-trending fault. Based on their description, we interpret the fault they excavated as being the connector fault shown on the new map rather than the large NE-trending splay fault or the main Keweenaw fault. The hanging-wall conglomerate is again interpreted to be the St. Louis conglomerate, but here the PLV section above is not well exposed to confirm this inference.

Footwall Jacobsville strata along Natural Wall ravine are mostly poorly indurated, mud-prone conglomerate to siltstone with an occasional well-indurated sandstone layer that may reach 2 meters in thickness, such as at the Natural Wall itself. The strata are more complexly folded than has been reported previously in publications. The Natural Wall lies on the shared limb of an asymmetric syncline downstream to the southeast (Irving and Chamberlin, 1885) and a tighter anticline upstream to the northwest (Fig. 15). This fold configuration occurs at the inside corner defined by the intersection of the two fault segments in this area and is discussed further in a later section on fold analysis. It seems likely that the tightness of folding here is partly due to the abundance of poorly indurated, pliable strata that can readily accommodate such deformation.

North from the Natural Wall ravine, the Mayflower fault block (MFB) is defined by a Set 1 fault on its northwestern side, a Set 2 fault along its southeastern side, and a Set 3 fault to the northeast. Starting with the southeast side of the MFB, the bounding fault is penetrated by two exploratory drill holes that from southwest to northeast are OC-8 and MAY-41. The fault is not observed at surface but is relatively well constrained by JS outcrops in the footwall and by limited PLV outcrops in the hanging wall (Fig. 15, S2). Footwall JS strata along the southeast margin of the MFB commonly are overturned and dipping steeply northwest near the bounding fault and become nearly horizontal away from the fault towards the southeast. These stratal orientations define broad folds that can be traced across multiple EW-trending drainages to the north of Wall Ravine (Fig. 15, S2). Abundant orientation measurements collected from footwall JS strata along the southeast side of the MFB are analyzed later in terms of their fold characteristics. The Set 2 fault here has been reinterpreted as a major footwall splay fault of the KFS rather than

the Keweenaw fault itself. It is now considered to be the major splay that crosses upstream of the Natural Wall and is similar to the smaller splays south of Natural Wall ravine.

The northwest side of the MFB is bounded by a NNE-trending fault segment shown on published maps as the Mayflower fault (Fig. 15, S2; White et al., 1953; Cornwall and Wright, 1956b; Cannon and Nicholson, 2001). The Mayflower fault has been mapped as a splay fault that diverges north-northeast from the main NE-trending Keweenaw fault and terminates against the Allouez Gap fault. The fault is well defined by many exploratory drill holes (OC-14, OC-15, OC-21, OC-28, May-39, and MAY-41; White, 1985) and underground workings of the Mayflower and Old Colony mining companies, as well as by PLV outcrops in its hanging wall, including those of the Copper City flow and St. Louis conglomerate.

The well-defined fault on the northwest side of the triangular MFB is parallel to PLV layers in the hanging wall and near the base of the St. Louis conglomerate (White et al., 1953). Previous interpretations show this fault striking N15°E and dipping 60°NW and with the same hanging-wall stratigraphy and general geometry as the Keweenaw fault southwest of the MFB. As should become clear in presenting the cross-section results, the previously named Mayflower fault has all the characteristics of the Keweenaw fault southwest of the MFB. It is therefore reinterpreted to be the northeastern continuation of the Keweenaw fault that follows the mostly overlying St. Louis conglomerate into this area from the southwest.

The northeast edge of the MFB was delimited on published maps by the Allouez gap fault (AGF), which appeared to displace the Keweenaw fault with apparent left lateral offset or was simply positioned at such a jog (White et al., 1953; Cannon and Nicholson, 2001). As explained in more detail in the next section, the Allouez gap fault is now reinterpreted as not crossing the main segments of the KFS and instead is limited to the hanging wall of the fault system. The AGF in the new interpretation does not bound the northeast edge of the MFB. Instead, the northeast edge of the MFB is defined by a separate Set 3 fault somewhat parallel to the AGF but terminating against an ENE-trending KF segment (Set 2) that cuts beneath the Copper City rhyolite body. The interpretation of KFS segments in this area shows the NNW-trending Set 3 fault terminating against the ENE-trending Set 2 KF segment that passes below the base of the main Copper City rhyolite body. A rhyolite outcrop found along an EW-trending valley at the base of the old Calumet and Hecla railroad culvert (Fig. 15, S1, green sites) and rhyolite cut by drill holes within the MFB are probably correlated with the Copper City rhyolite across the complex intersection of faults in the northeast part of the MFB. The 4-m by 3-m exposure and drill hole penetration are positioned at a similar stratigraphic position as the main Copper city rhyolite body, as discussed further in the next section.

4.4 Copper City Rhyolite and Allouez Gap Fault

The Keweenaw fault system undergoes a major change in trend and stratigraphic level within this focus area, which is structurally complex at the junction of these two fault sections (KFS-2, KFS-3), the Allouez Gap fault in the hanging wall, and the Mayflower fault block in the footwall (Fig. 16). Moreover, the Copper City rhyolite northeast of the Mayflower fault block is interpreted to extend southwest into this already complex area.

The broad structural geometry in the hanging wall of the KFS is relatively simple, however, and characterized by a general conformance of PLV layers with the strike of the main underlying fault segments. Southwest of the Allouez Gap fault (AGF), the main KF segment is at or near the base of the St. Louis conglomerate and strikes N20°E, as do the overlying PLV layers. Northeast of the AGF, the main KF segment is about 650 m deeper, below the Copper City rhyolite, and strikes N55°E like the overlying PLV layers. Clearly, the AGF is located in the hanging wall of the KFS where this abrupt directional change occurs and, therefore, is probably related to an anomalous stress state in this region during faulting.

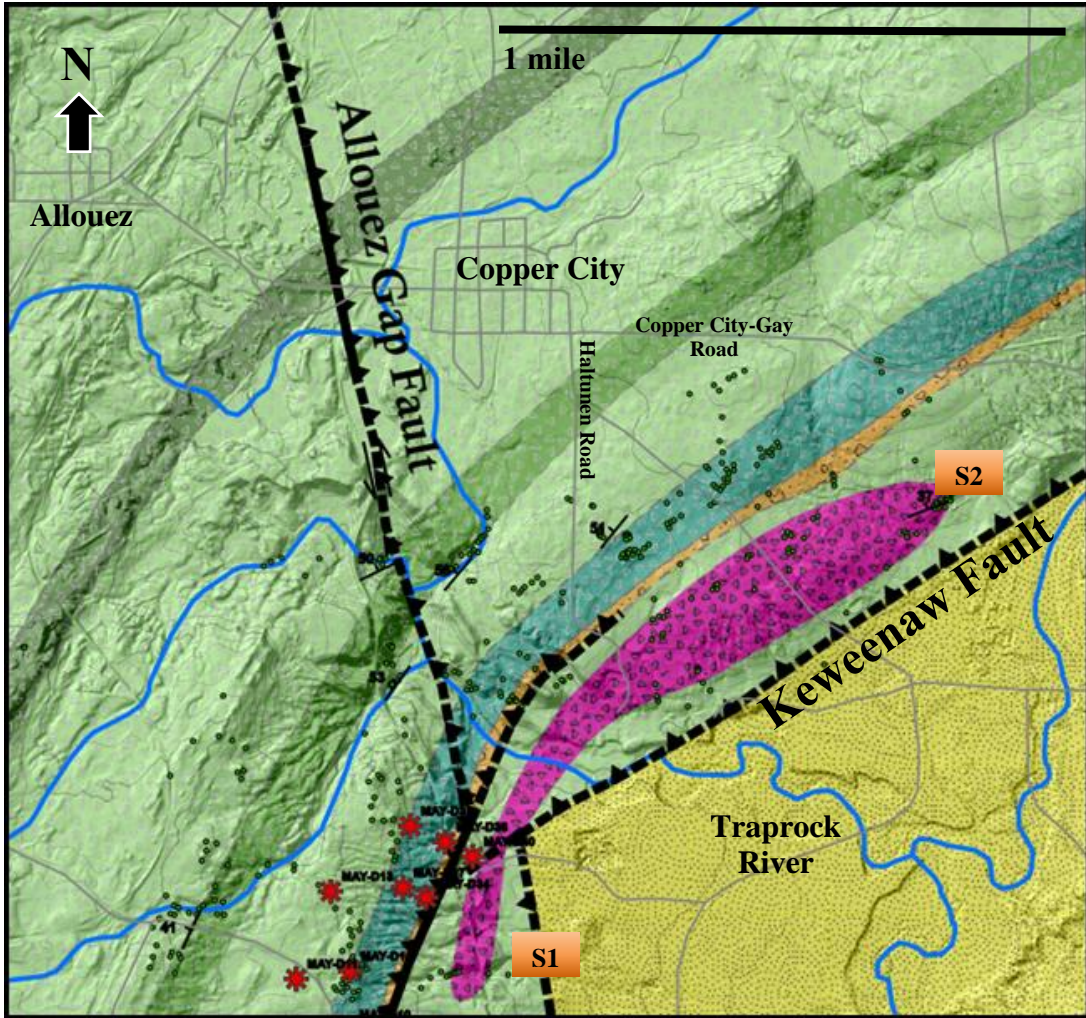


Figure 16: Zoomed in image of new bedrock geology map showing multiple fault segments within focus area C. The Copper City Rhyolite is the primary focus and is displayed as the pink oblong-shaped unit. S1 – rhyolite quarry; Colors and symbols explained in the map legend of Figure 12.

The Allouez Gap fault, shown on the legacy Ahmeek bedrock geology map as cutting across the Keweenaw fault in this area (White et al., 1953), has been reinterpreted as being confined to the hanging wall of the KFS and terminating on one of the main KF segments (Fig. 12). The Allouez Gap fault was first described formally by White et al. (1953) as dipping 65-85° NW where it cuts the Kearsarge flow in underground mine workings. While this dip magnitude may be correct, the northwesterly dip direction is

unlikely given the N12°W strike of the AGF on their map. Furthermore, White et al. (1953) state that most faults with this strike direction dip steeply northeast. Based on apparent map offset of PLV units crossing the AGF, it may have left-lateral strike slip or east-side-up dip slip or a combination of these components. If the AGF dips steeply northeast as concluded here from the Ahmeek quadrangle information, then inferred east-side-up movement would be reverse slip. This sense of slip contrasts with the opposite sense of movement inferred to have occurred along the northeast bounding fault of the Mayflower fault block that roughly aligns with the AGF but must have been west side up to explain the older PLV rocks exposed on higher elevations to the west. Mostly for this reason, the AGF is not extended southeast of the main KF segment on the new map. Additionally, offset on the AGF as shown on the published Ahmeek geologic map sheet is far less than shown for the main KF (former Mayflower fault) or estimated by other cross-section work (Cannon and Nicholson, 2001; DeGraff and Carter, 2023), making it likely that the AGF is a splay fault formed in response to larger fault movements.

An important unit in this focus area is the Copper City rhyolite, located east-southeast of Copper City, which was last investigated along with other rhyolites of the Keweenaw Peninsula by Nicholson (1992). Based on its distinctive characteristics, Nicholson (1992) placed this rhyolite in a class of its own, unique from all other rhyolites sampled to the northeast along the peninsula and left open its mode of emplacement due to ambiguous field relationships. Other small occurrences of rhyolitic rocks southwest of Copper City have been reported as far as between Lake Linden and Calumet (Hubbard 1898; Butler and Burbank, 1929), but are not well documented and are not shown on the latest published maps.

The new mapping of rhyolite exposures in the project area has focused on the relatively well exposed Copper City rhyolite located ~1.2 kilometers SE of Copper City, MI (Nicholson, 1992). Based on newly documented exposures and exploratory drill hole data, the main Copper City rhyolite body has been extended along strike to the SW by at least 1,000 meters and perhaps as much as 3,600 meters to the NE (Fig. 13; Fig. 16). It lies stratigraphically beneath the Copper City Flow and either at or slightly below the St. Louis conglomerate. New observations at a recently opened quarry (Fig. 16, S2) northeast of the Copper City rhyolite as shown on published maps provide evidence that the rhyolite body is extrusive. The quarry exposes ~25 meters of PLV section that has two main rhyolitic intervals separated by a ~50-cm-thick interval of conglomerate or breccia consisting of subangular to angular rhyolite clasts and fragments up to 6 centimeters across. Multiple contact and remotely sighted bedding measurements were taken on the conglomerate layers and on an interbedded quasi-planar seam (Fig. 16), yielding an average strike and dip of 249°/37° NW. Around 160 meters southwest of the quarry, small exposures of a similar conglomerate or breccia occur roughly midway through the stratigraphic extent of mapped rhyolite outcrops. Although correlation of these conglomerate exposures cannot be made with confidence, they indicate that the Copper City rhyolite is an extrusive complex consisting of rhyolitic flows, thin intervals of felsic conglomerates, and probably pyroclastic layers. These new observations indicate that the Copper City rhyolite complex is a stratigraphic unit that lies below the level of the Type I rhyolite occurrences mapped along the Keweenaw Peninsula to the northeast, which may explain its unique character. The Copper City rhyolite seems to be closely

associated with the St. Louis conglomerate, whereas the Type I rhyolites to the northeast are closely associated with the Bohemia conglomerate.

Other rhyolite occurrences within the project area also occur at or near the St. Louis conglomerate and mostly southwest of the Copper City rhyolite complex. Within the Mayflower block, for example, an outcrop ~4 meters in diameter is located less than 2,000 meters SSW of the southwest extent of the original outline of the Copper City rhyolite along a drainage culvert of an old Calumet & Hecla railway (Fig. 17, S2). About 2.4 kilometers farther south-southwest at Natural Wall ravine, a 3-meter exposure of a felsic rock displaying spherulites and flow banding was noted by Hubbard (1898) and found during this project. This felsic rock is interpreted as rhyolite and lies stratigraphically below PLV basalt and the inferred St. Louis conglomerate. Another rhyolite occurrence was located and sampled north of Lake Linden and about 100 meters east of the old Calumet and Hecla railroad along an old drainage ditch (see also Irving and Chamberlin, 1885; Hubbard, 1898), again about at the level of the St. Louis conglomerate. Yet another rhyolite outcrop was reported by Hubbard (1898) from a waterfall at the Keweenaw fault, located ~2 kilometers SE of Laurium, MI off Pepin Road. This occurrence is on private land for which access was not granted. Rhyolite reported at Houghton-Douglas falls was not found in outcrop (Butler and Burbank, 1929), but abundant rhyolitic floats were found southwest of the falls, suggesting the presence of outcrops that may now be covered by overburden.

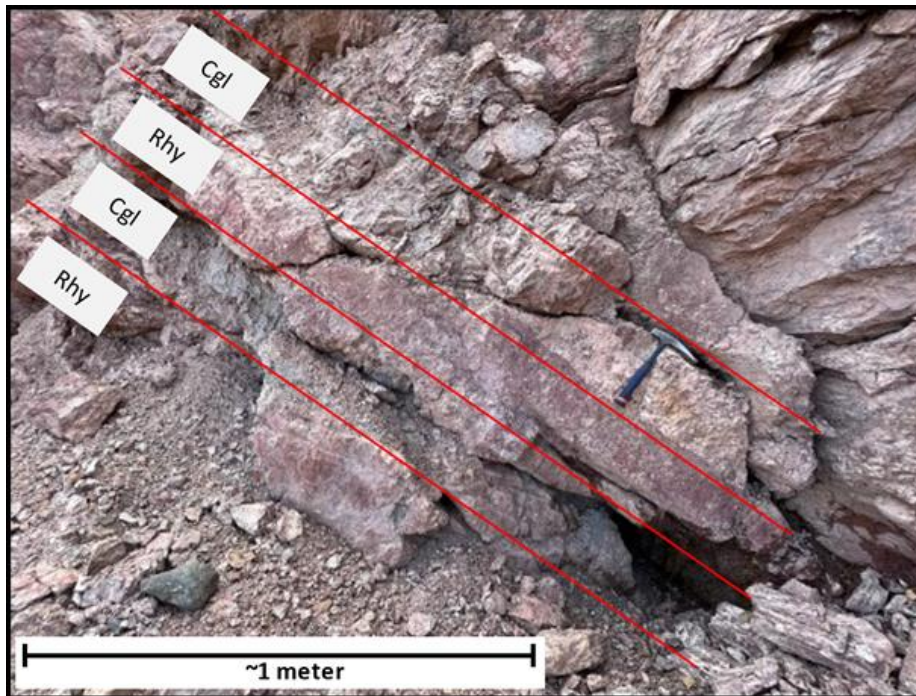


Figure 17: Copper City rhyolite complex: Interbedded rhyolite (Rhy) and conglomerate layers (Cgl) dipping 37° NW. Image taken facing SW in a private quarry ESE of Copper City, MI (Fig. 16, S2). Unit boundaries denoted with red lines. Rock hammer for scale.

Near the northeastern edge of the project area, a set of rhyolitic outcrops are exposed along a small creek bed northeast of the Mohawk-Gay Road near the intersection with Jack Kivela Road (Fig. 18; Mueller, 2021). These weathered and fractured exposures have felsic volcanics as well as conglomerate with subangular to angular felsic clasts or perhaps pyroclastic breccia. While it is difficult to determine the relationships here, felsic volcanic rocks appear to be stratigraphically below an 80-m by 45-m semi-continuous conglomerate exposure, which is interpreted as the St. Louis conglomerate and shown on the new map (Fig 13).



Figure 18: Copper City rhyolite near boundary of the 2020 and 2022 EdMap projects. Image taken facing towards the SW. Rock hammer for scale.

To better characterize rocks of the Copper City rhyolite complex and its possible extension along strike, a series of analyses were undertaken that include petrographic descriptions, whole rock geochemical analysis, and mineral separation for age dating. The petrography and geochemistry results were compared with what was available from earlier descriptions and analyses. Compilation of the data was then used to further examine a possible correlation of the Copper City rhyolite along strike.

The thin section analysis reveals similar primary and alteration minerals in three rhyolite samples (EM3A-327, EM3A-639a, and EM3A-780) that were selected for a comparative analysis of rhyolite mineralogy away from the Copper City complex (Fig. 19). These samples were collected across the mapped area from locations positioned

stratigraphically below the St. Louis conglomerate. Sample EM3A-327 is a float sample taken from ~250 meters SSW of Houghton-Douglass Falls and has been interpreted as a rhyolite porphyry ([Hubbard, 1898](#)); sample EM3A-639a is from the southeast edge of the main Copper City rhyolite body near its contact with undifferentiated PLV basaltic rock; sample EM3A-780 is from the northeast end of the rhyolite quarry ([Fig. 16, S2](#)).

Petrographic work revealed that the main phenocrysts are subhedral to euhedral quartz up to 4 mm across, along with plagioclase and alkali feldspar laths less than 2 mm across that are commonly altered or replaced by clay minerals, oxides, and carbonate minerals. The phenocryst volume of the bulk rock is ~5-10 % and quartz makes up approximately 60% of phenocrysts. The quartz phenocrysts display resorbed margins, or sieve textures, which suggests dissolution of quartz back into the magma from which the crystals formed ([Strekeisen, 2020](#)). Quartz grains with these textures were observed in all of the examined thin sections. Textures such as embayed quartz, secondary alteration, and opaque mineral inclusions were similar to what was described by Nicholson ([1992](#)) for a Type II rhyolite, therefore distinguishing these new samples from Type I rhyolites found to the northeast in association with the Bohemia conglomerate.

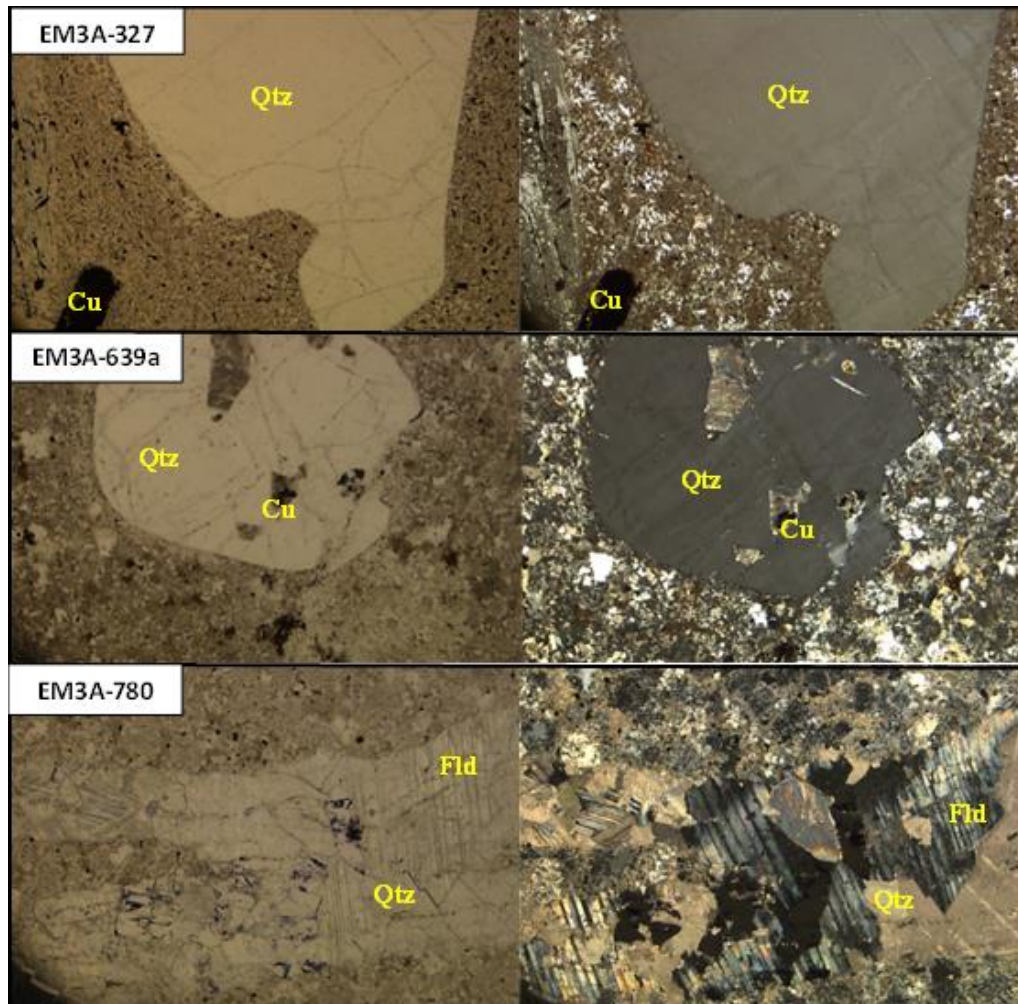


Figure 19: Transmitted light microscope images taken at 4x magnification showing phenocrysts of embayed quartz (Qtz), plagioclase feldspar (Fld), and likely native copper (Cu) inclusions in a porphyritic rhyolite. Photos taken in plane polarized light (left) and crossed polarized light (right) by the author.

New geochemical data ([Table 2](#)) confirms that the main Copper City rhyolite occurrence northeast of the AGF has geochemical affinities with the smaller exposures located southwest along strike. Rhyolite samples analyzed for this project yielded an average weight percent of 73.5 wt% SiO₂, which may be lower than their original content because of an average loss on ignition of 2.06 wt%. As stated earlier, Type II rhyolites are characterized by silica content of 75 wt% or more, low rare-earth element abundance, and enrichment in Th, Rb, U, Nb, and Ta ([Nicholson and Shirley, 1990](#); [Nicholson,](#)

1992). Given these criteria, the six rhyolite samples analyzed for geochemistry are categorized as Type II rhyolites.

Trace element abundance in parts per million and oxide weight percentages were averaged ($N = 6$) to compare with averaged Type II rhyolite samples analyzed by Nicholson (1992). The relative enrichment or depletion of Rb, Ba, Sr, Th, U, Nb, and Zr in each of the selected samples supports the idea that they are all Type II rhyolites and share an affinity with the main Copper City rhyolite body. Depletion in parts per million (ppm) is shown by the average Rb of 371.5 ppm and the lower Zr average of 134.3 ppm amongst the selected samples. Enrichments in transition metals such as Cu, Cr, Nb, and Zr are observed in samples EM3A-923 and EM3A-683. Sample EM3A-923 was collected from the small outcrop located off the old Calumet and Hecla railway culvert near the northeast part of the MFB. Sample EM3A-683 was collected from the northern most part of the main rhyolite body approximately 500 meters west from the rhyolite quarry. Sample EM3A-923 has the highest copper value at 3,340 ppm, which may be due to its proximity to the Keweenaw fault if the fault was a fluid flow pathway during copper mineralization.

Enrichment in Cu and Cr coupled with alteration seen in thin sections suggests that the Copper City rhyolite was affected by metasomatism perhaps associated with movement of fluids along faults. Increased K_2O content and decreased Na_2O content suggests local metasomatism that likely occurred after rifting waned and magmatism slowed (Nicholson and Shirley, 1990). The petrographic and geochemical similarities among the analyzed samples and with the main Copper City rhyolite, and their shared stratigraphic position

over a long strike distance, supports the idea of a significant rhyolitic stratigraphic interval beneath the Copper City flow and associated with the St. Louis conglomerate.

This idea is supported by the similarities in petrographic and geochemical results reported here with those of Nicholson (1992) for rocks she identified as Type II rhyolites.

Table 2: Geochemical data for bulk rock samples showing trace element abundance in ppm and as ratios (top) and major oxide weight percents (bottom).

Sample #	EM3A-595	EM3A-639A	EM3A-683	EM3A-780	EM3A-783	EM3A-923	Average	Type II Rhy
Trace Elements:	(N = 1)	(N = 1)	(N = 1)	(N = 1)	(N = 1)	(N = 1)	(N = 6)	(N = 4)
Cr	5.0	12.0	12.0	37.0	5.0	32.0	17.17	3.2
Ni	1.0	<1	2.0	3.0	3.0	6.0	3.0	<40
Hf	7.0	6.9	8.1	7.5	7.7	6.0	7.20	6.3
La	15.5	21.2	6.9	19.2	26.2	18.0	17.83	12
Nb	42.5	47.2	57.2	54.5	55.2	40.7	49.55	51
Rb	449.0	435.0	491.0	482.0	345.0	27.1	371.52	465
Sm	6.6	10.7	4.9	6.8	5.8	7.5	7.05	6.9
Sr	29.4	23.3	24.9	18.8	21.1	65.4	30.48	28
Ta	3.7	4.4	5.7	5.1	5.1	3.3	4.55	4.9
Tb	1.2	2.0	1.2	1.4	1.2	1.4	1.40	1.85
Th	66.1	46.7	53.8	51.6	59.8	50.7	54.78	63
Y	47.7	96.9	52.0	66.7	57.2	61.4	63.65	74
Yb	5.8	12.8	7.1	8.2	7.1	6.6	7.93	7.68
Zr	140.0	127.0	144.0	143.0	130.0	122.0	134.33	144
Trace Element Ratios:								
Rb/Sr	15.3	18.7	19.7	25.6	16.4	0.4	12.19	16.66
Zr/Nb	3.3	2.7	2.5	2.6	2.4	3.0	2.71	2.88
Nb/Rb	0.1	0.1	0.1	0.1	0.2	1.5	0.13	0.11
Ba/Rb	1.1	0.5	0.5	0.5	0.5	4.2	0.66	0.87
Ba/Th	7.4	4.3	4.7	4.7	2.9	2.2	4.5	6.23
Zr/Hf	19.9	18.5	17.8	19.0	16.8	20.4	18.7	23.01
Ce/Yb	6.6	3.2	2.7	5.0	3.5	9.3	4.7	5.89
Other Anomalies:								
Cu	18.0	32.0	76.0	13.0	18.0	3340.0	582.83	
Ba	486.0	200.0	253.0	240.0	172.0	112.5	243.92	
Ce	38.2	41.3	18.9	40.8	25.1	61.3	37.60	
Li	<10	10.00	10.00	10.00	<10	10.00	10.00	
Ga	27.40	27.70	30.70	28.30	24.10	21.20	26.57	

Sample	EM3A-595	EM3A-639A	EM3A-683	EM3A-780	EM3A-783	EM3A-923	Average	Type II Rhy
Major Oxides:	(N = 1)	(N = 1)	(N = 1)	(N = 1)	(N = 1)	(N = 1)	(N = 6)	(N = 4)
SiO ₂	74.2	69.7	74.9	72.2	75.5	74.2	73.45	75.74
Al ₂ O ₃	13.3	11.8	14.1	12.9	13.3	13.0	13.03	13.28
Fe ₂ O ₃	1.6	1.4	1.4	2.1	2.0	1.8	1.71	0.44
CaO	0.2	5.0	0.6	2.1	0.4	0.4	1.46	1.38
MgO	0.1	0.2	0.1	0.2	0.1	0.9	0.27	0.14
Na ₂ O	2.7	1.1	2.9	1.0	4.0	6.4	3.02	2.48
K ₂ O	5.8	4.7	5.6	5.4	3.9	0.8	4.35	5.60
TiO ₂	0.1	0.0	0.0	0.0	0.0	0.1	0.05	0.05
MnO	0.0	0.0	0.0	0.0	0.0	0.0	0.03	0.04
P ₂ O ₅	<0.01	<0.01	<0.01	<0.01	0.0	0.0	0.01	0.02
LOI	0.77	5.27	1.26	3.25	0.94	0.86	2.06	-
Oxide Ratios:								
Na ₂ O/K ₂ O	0.47	0.23	0.52	0.19	1.03	8.38	0.69	0.44

5 Structural Analysis and Interpretation

Various structural analyses were performed to quantify the deformation observed along the Keweenaw fault system in the project area and then to relate this deformation to tectonic events. Bedding orientations used for fold characterization with a stereonet were more abundant and reliable for well stratified JS in the KFS footwall than in thick, irregular PLV strata in the hanging wall. Stratal orientation in the PLV, for example, could only be measured accurately when flow contacts or interflow sedimentary units were exposed. Site averaged bedding measurements were imported into Stereonet v.11 to quantify fold geometry wherever possible but mostly for JS in the KFS footwall. Fault-slip measurements were characterized using rake histograms to determine the relative contributions of dip slip and strike slip to overall motion along the KFS. The same data along with slip sense determinations were analyzed using FaultKin to compute principal strain directions and thus to infer regional stresses and tectonics that drove faulting in the area. Lastly, four cross-sections, constrained by the results of these analyses, were constructed to be perpendicular to the local trend of the fault system in order to infer its subsurface geometry and that of the associated deformation its hanging wall and footwall.

5.1 Stratal Deformation and Fold Analysis

The following characterization of stratal deformation and folding has grouped bedding orientation data into subareas with internally similar structural characteristics to avoid blending and blurring important changes along the fault system. The data analysis begins at Houghton-Douglass Falls and proceeds northeastward to the area of the Copper City rhyolite complex.

At Houghton-Douglass Falls, large-scale footwall deformation of JS strata is best categorized as a broad open anticline based on field observations and examination of footwall bedding orientations (Fig. 20, left), though the breadth of the structure gives the impression of a monocline facing toward the KF. Footwall measurements of JS stratal orientation, minus local fold measurements analyzed separately below, define a fold axis (T/P = $198^{\circ}/01^{\circ}$) plunging shallowly towards the SW, an interlimb angle of 156° , and an axial plane (S/D = $18^{\circ}/78^{\circ}$ E) dipping steeply away from the KF. A tightly folded package of JS strata ~200 meters ESE of the KF contains an anticline-syncline pair that is 9 meters wide by 4 meters tall and has axial surfaces tilted northwest toward the KF. Calculations on a series of closely spaced bedding orientations across the two folds define a composite fold axis (T/P = $216^{\circ}/02^{\circ}$) plunging shallowly to the SW, an interlimb angle of 94° , and an axial plane (S/D = $216^{\circ}/55^{\circ}$ W) dipping moderately northwest towards the Keweenaw fault (Fig. 20, right). The geometry of this small-scale folding implies a top-to-southeast shearing of strata within JS footwall strata, which is consistent with a component of southeastward thrusting on the KF.

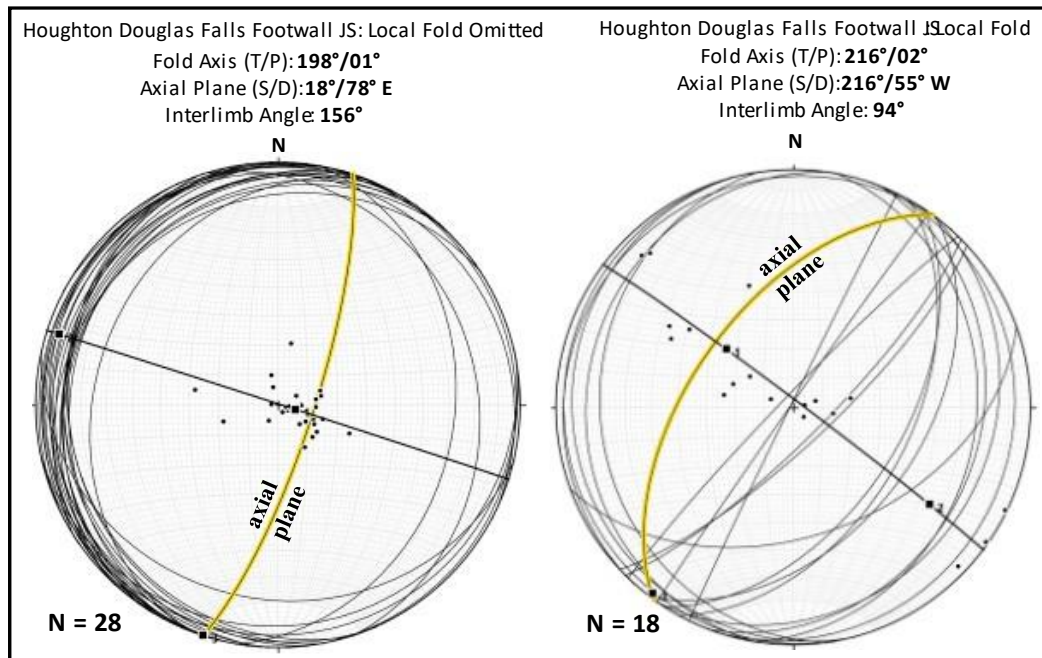


Figure 20: Equal area stereonet plots and analyses of footwall JS stratal orientation from Houghton-Douglas Falls. Plotted values are site-averaged data. Thin black arcs are bedding planes; black dots are poles to planes. Thick black arcs are best-fit surfaces to bedding poles. Left plot shows all data minus data from the small fold. Right plot shows data from the small fold within the large anticlinal structure.

As discussed previously, hanging-wall PLV strata at Houghton-Douglas Falls dip shallowly northwestward based on measurements within the St. Louis conglomerate near the base of the cliff and on flow structure in the Copper City flow at the top. The average orientation of PLV strata (Fig. 21, black arcs) in the hanging wall (S/D = 242°/15° NW) is very similar to that of the KF (S/D = 240°/19° NW) at this location (Fig. 21, yellow arc), which implies that the hanging wall became detached along a horizon just below the St. Louis conglomerate. The ENE trending strike of the KF and hanging-wall PLV strata is oriented clockwise relative to NNE-trending fold axes in footwall JS strata. If the local shortening direction is normal to the JS fold axes, this would imply a component of right-lateral slip on the KF in addition to its reverse slip component.

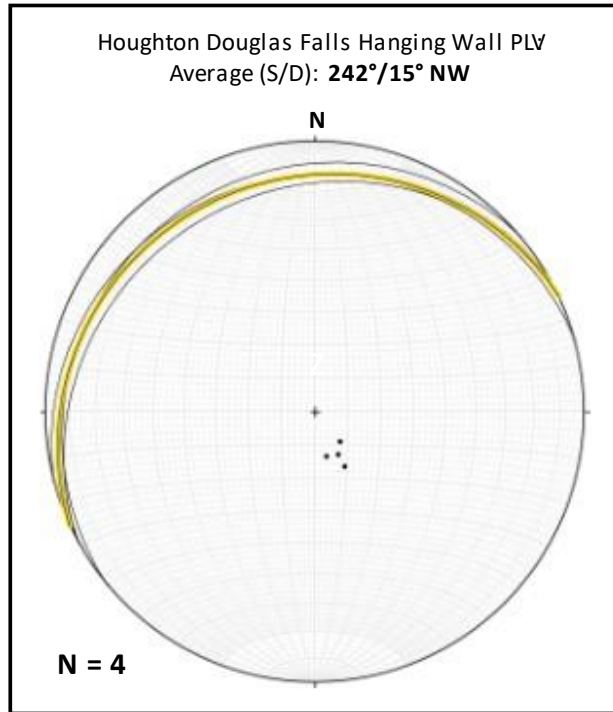


Figure 21: Equal area stereonet plot of hanging-wall PLV stratal orientations at Houghton-Douglas Falls. Symbology the same as in Figure 18. Thin black arcs are averaged bedding orientation measurements taken on St. Louis conglomerate near base of falls and on Copper City flow amygdaloids at top of falls; black dots are poles to the planes. Yellow arc shows Keweenaw fault orientation.

At the Natural Wall ravine, an anticline-syncline pair is exposed along a deeply incised valley that exposes the well-known Natural Wall of Jacobsville Sandstone (Fig. 14).

Folding of footwall JS strata was first analyzed using all data (Fig. 22), which identified two groups of measurements that were subsequently analyzed separately (Fig. 23). The first group is from site locations at and near the Natural wall and captures the synclinal fold downstream to the southeast. The second group is from sites upstream to the northwest from the Natural Wall and captures folded strata closest to the fault intersection in this area. The complete data set defines a composite fold axis (T/P = $202^{\circ}/38^{\circ}$) for the anticline-syncline pair as plunging moderately south-southwest, an interlimb angle of 95° , and a composite axial plane (S/D = $174^{\circ}/58^{\circ}$ W) that trends

roughly oblique to the nearby faults composing the KFS but more parallel to the NNE-trending connector fault near the fault intersection.

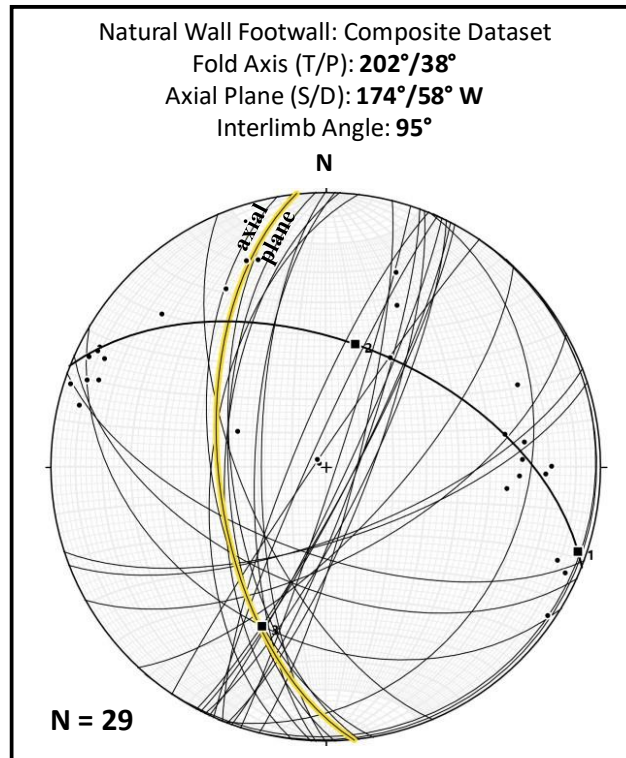


Figure 22: Equal area stereonet plot and analysis of all JS stratal orientations from the Natural Wall. Thin black arcs are bedding planes; black dots are poles to planes. Yellow arc indicates axial plane. Thick black arc is best-fit surface to bedding poles.

To further understand the geometry of this footwall deformation, a fold analysis was done separately for the two groups defined above. Regarding the main syncline downstream from the Natural Wall, the steep west limb at the wall and shallow east limb to the southeast define a shallow plunging fold axis (T/P = $197^{\circ}/19^{\circ}$) and an axial plane (S/D = $181^{\circ}/51^{\circ}$ W) dipping moderately towards the KFS (Fig. 23, left). Upstream from the Natural Wall, anticlinal folding defined by Group 2 has a fold axis (T/P = $218^{\circ}/50^{\circ}$) plunging moderately southwest and an axial plane (S/D = $192^{\circ}/70^{\circ}$ W) dipping steeply towards the KFS (Fig. 23, right). The axial planes for both groups are subparallel to the main Keweenaw fault. The steeply plunging fold axis of Group 2, however, is nearer to

the major NE-trending fault splay and to its intersection with the NNW-trending connector fault, which implies more deformation and complexity.

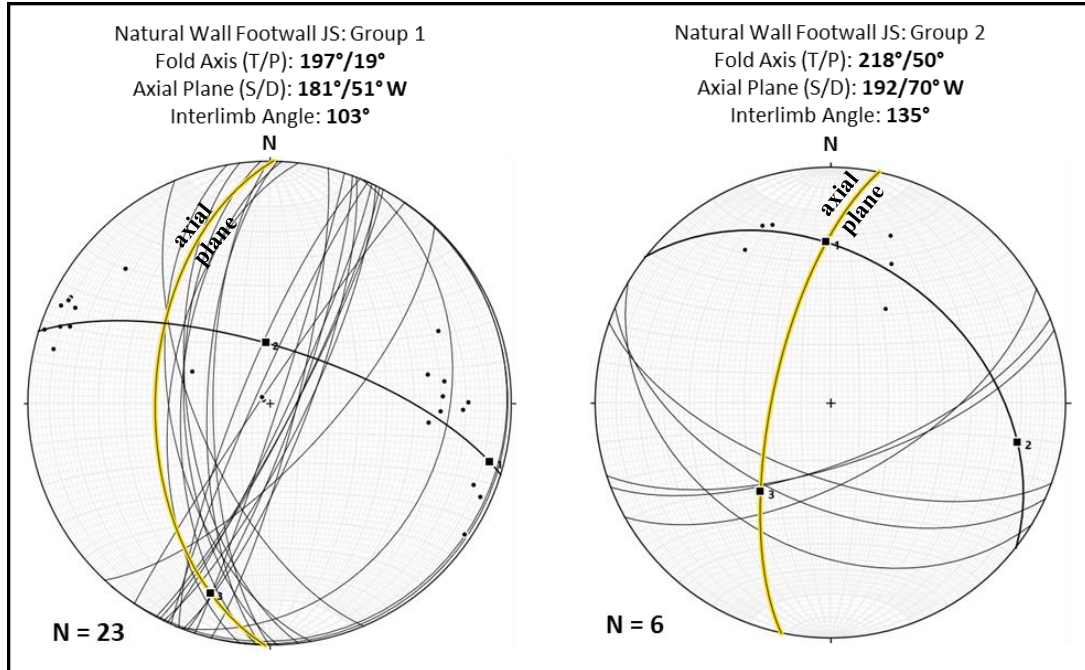


Figure 23: Equal area stereonet plot and analysis of two groups of JS stratal orientations at Natural Wall. Thin black arcs are bedding planes; black dots are poles to the planes. Thick black arcs are best-fit lines to bedding poles. Yellow arcs indicate axial planes.

The style of folding at Natural Wall ravine continues northeast to the southern part of the Mayflower Fault block, where abundant outcrops allowed stratal orientation to be measured on subvertical and overturned beds near the major footwall splay along the southeast edge of the MFB and on sub-horizontal beds to the southeast. Footwall exposures of JS near Old Colony Road and Mayflower Road show a complex series of vertical and overturned strata (Fig. 24). Most measurements were taken on quartzose sandstone beds with occasional siltstone and conglomeratic sandstone layers located within ~100 meters of the fault bounding the southeast edge of the MFB. Fold analysis of the composite dataset yields a composite fold axis (T/P = 42°/4° E) plunging slightly

northeast and a composite axial plane dipping moderately northwest towards the major footwall splay (S/D = 225°/52° N). This composite dataset was then geographically split into two areas near Old Colony Road and Mayflower Road (see Fig. 15).

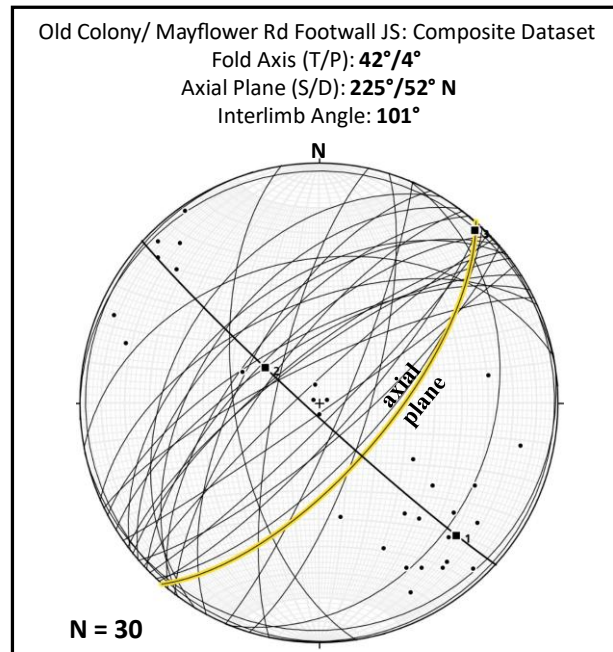


Figure 24: Equal area stereonet plot and analysis of JS stratal orientations. Composite data set of measurements from Old Colony Rd to Mayflower Rd. Thin black arcs are bedding planes; black dots are poles to planes. Yellow arc indicates fold axis.

Near Old Colony Road (Fig. 25, left), field observations reveal a tight syncline with a steeply dipping NW limb, and analysis of stratal orientations computes a fold axis (T/P = 48°/01°) plunging very slightly northeast and an axial plane (S/D = 229°/50° N) dipping moderately northwest toward the major footwall splay. These results are very similar to those of the full dataset in this area, but should be a better estimate of fold characteristics because they are geographically more restricted. Near Mayflower Road (Fig. 25, right), JS stratal orientations suggest a similar trending fold or folds as shown near Old Colony Road and may define a tight fold. However, the sparse data and variability of bedding

orientations makes this difficult to determine. Fold axes calculated from the composite and Old Colony Road datasets have similar trends to that of the nearby major footwall splay fault (N34°E) that bounds the southeast side of the MFB. This general result shows that footwall fold trends here are parallel to the nearby fault as expected and without any apparent complications.

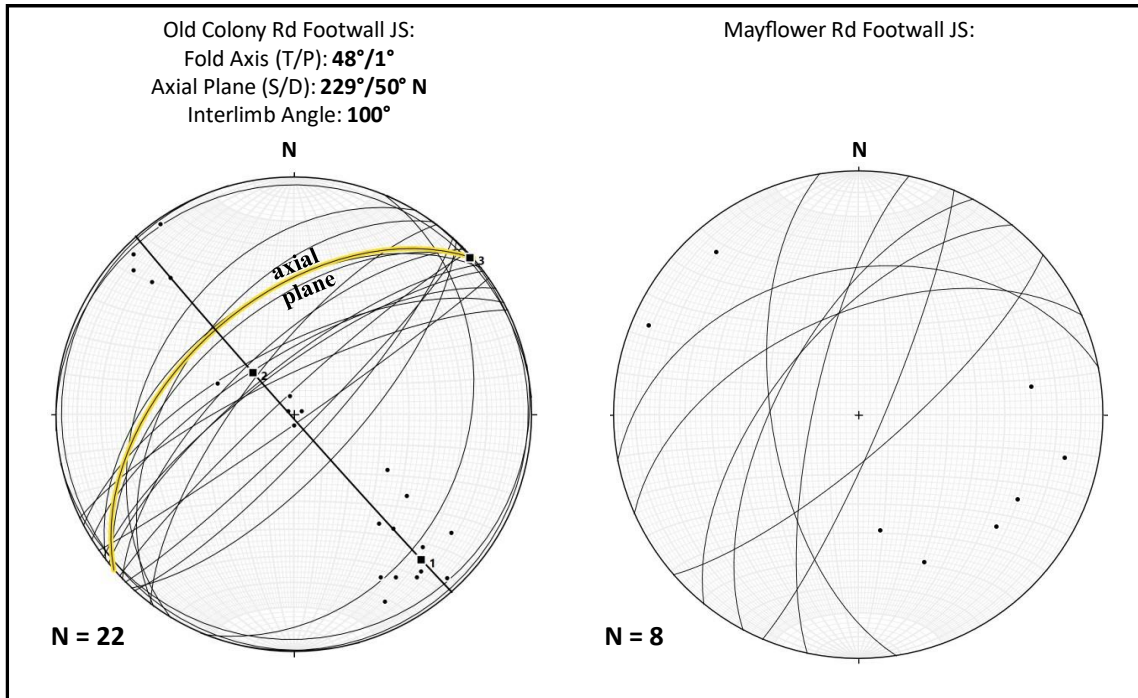


Figure 25: Equal area stereonet plot and analysis of JS footwall stratal orientations between Old Colony Road and Mayflower Road, separated by location. Thin black arcs are bedding planes; black dots are poles to planes. Yellow arc represents axial plane. Thick black arcs are best-fit lines to bedding poles.

Orientations of PLV strata in the hanging wall of the main footwall splay and near the center of the Mayflower fault block are defined by two groups of sites based on their position north and south of Mayflower Road, which crosses the center of the Mayflower fault block. South of Mayflower Road, PLV strata strike parallel to the major footwall splay and dip moderately northwest (Fig. 26, left; S/D = $237^{\circ}/30^{\circ}$ NW), whereas PLV strata north of Mayflower Road dip more steeply northwest (Fig. 26, right; S/D =

225°/48° NW). These average trends reflect the major fault splay on the southeast part of the MFB more than the main KF on the northwest part of the MFB.

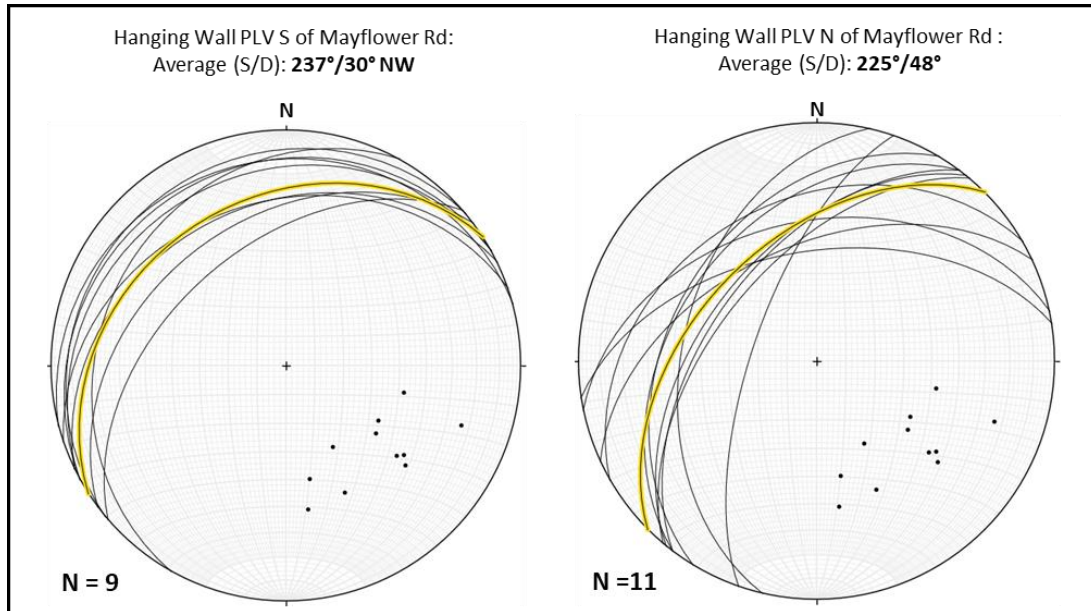


Figure 26: Equal area Stereonet plot of PLV hanging wall stratal orientations. Data grouped relative to Mayflower Road. Thin black arcs are bedding planes; black dots are poles to planes. Yellow arcs indicate average bedding orientations.

The private rhyolite quarry, located ~1 kilometer ESE of Copper City, exposes felsic conglomerate layers within the Copper City rhyolite complex that dip to the northwest (Fig. 27; S/D = 249°/37°). The rhyolite unit has an average dip that is 14° less than the dip of the overlying Copper City basalt flow (Fig. 27, black arc), which suggests a broad roll in the dip of hanging-wall PLV strata shown on a subsequent cross-section.

Otherwise, the average stratal orientation of the Copper City rhyolite is similar to the orientations of nearby PLV strata within the Mayflower fault block (Fig. 27, blue arcs).

5.2 Fault-Slip Characterization and Kinematic Analysis

Many faulted surfaces display aligned narrow striations and wider ridges and grooves that form parallel to the slip direction by scraping, gouging, scratching, and mineralization during slip (Fig. 28; Billings et al., 1972; Burg, 2020). A fault's slip sense often can be determined by inspection of asymmetric steps that form roughly perpendicular to the slip lineations (Fig. 29; Allison, 2020). Fault slip direction can be specified by the rake of a surface lineation, defined as the angle measured on the fault surface between a strike line and the lineation, or by its plunge azimuth combined with strike and dip of the host surface (Fig. 30; Burg, 2020). Slip lineations measured for this project were mostly on fault surfaces with secondary mineralization in the Portage Lake Volcanics. The slip lineations were not always paired with asymmetric surface steps, so the slip sense was determined less frequently than the slip direction. Weathered surfaces, poor lighting, and accessibility to the surface also made determining a fault's slip sense difficult or not possible.

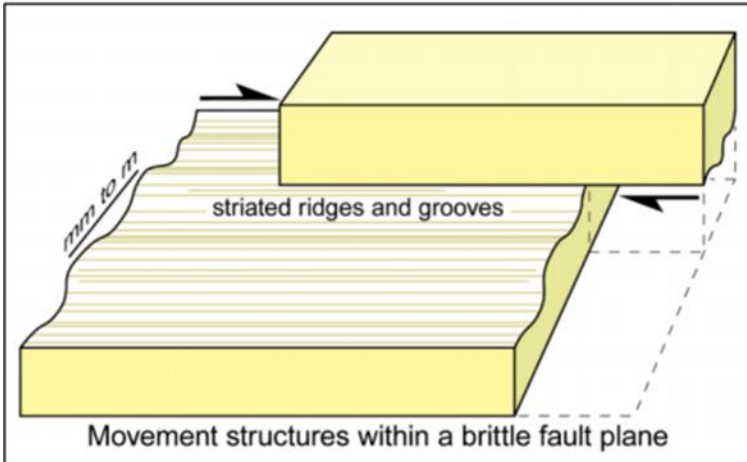


Figure 28: Fault surface lineations parallel to the slip vector (Burg, 2020).

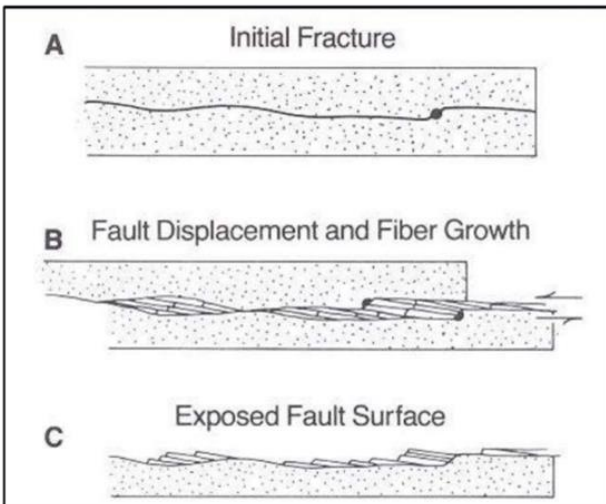


Figure 29: Relationship between slip sense and asymmetry of steps formed by synkinematic mineralization (Allison, 2020).

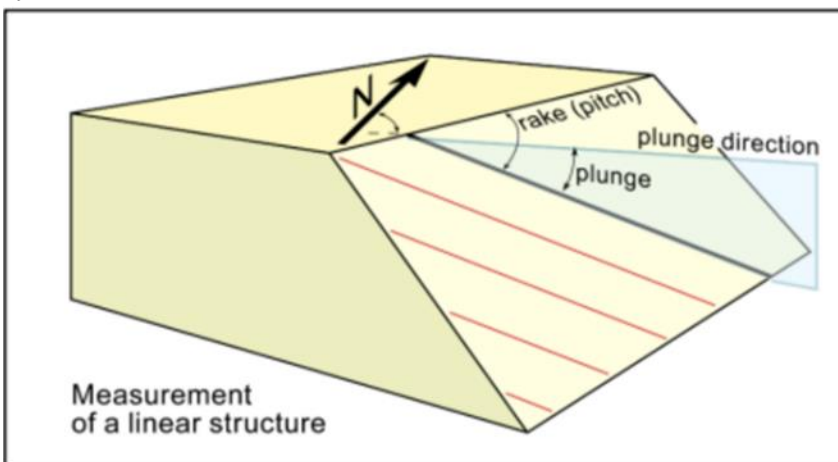


Figure 30: Lineations on a planar surface are specified either using rake or plunge direction along with strike and dip of the surface (Burg, 2020).

Apparent rake measurements from the study area were converted to true rake and then analyzed in terms of the slip characteristics of faults making up the KFS. Final rake values were imported into Stereonet v.11 (Allmendinger, 2020) to create radial histograms showing the distribution of slip directions and the relative contribution of dip-slip and strike-slip components of fault movement (Fig. 31). Radial histograms were constructed using bidirectional rake measurements so that rake varied from 0° for pure strike slip to 90° for pure dip slip. Therefore, rake values greater than 45° have a larger component of dip-slip movement, and those less than 45° have a larger component of strike-slip movement.

The resulting rake histogram for all measurements shows a spread of values that range from mostly strike slip to mostly dip slip, with an arithmetic average of 50°. Using all the data, an overall strike-to-dip slip ratio of 0.84:1 was calculated, which indicates that the collective action of all measured faults is almost as much strike-slip as dip-slip. The rake values are not evenly distributed between 0° and 90°, but instead are bimodal (Fig. 32) with one group having mostly strike slip (10°-20° mode) and the other having mostly dip slip (70°- 80° mode). The bimodal nature of the rake distribution suggests that strain partitioning has occurred, which is discussed later in the context of prior EdMap studies. By splitting the data near the minimum bin value of 50°, the two main modes in the data can be characterized as follows: a dominantly strike-slip mode with an average rake of 26° (Fig. 32, left) that is similar to previous EdMap results, and a dominantly dip-slip mode with an average rake of 70° (Fig. 32, right) that so far is unique to this area.

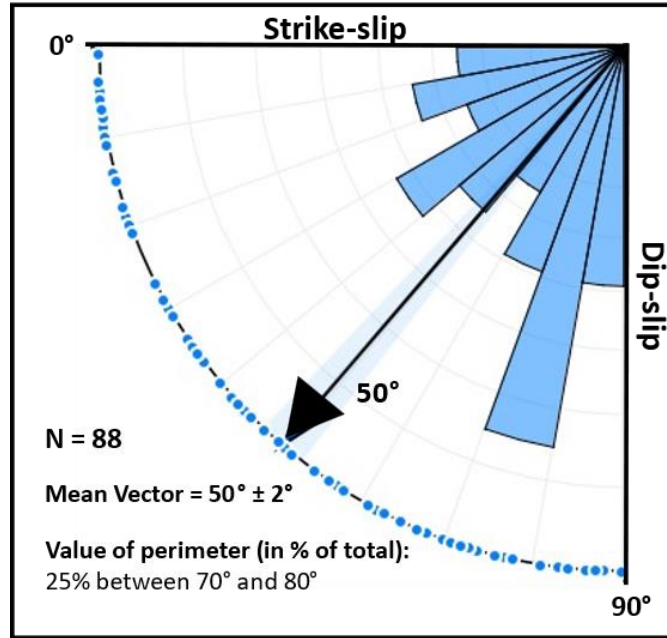


Figure 31: Radial histogram of site-averaged lineation rakes counted within 10° bins. Black arrow shows arithmetic mean. The largest wedge (70° to 80°) has 25% of data. Strike-slip corresponds to rake = 0°; dip-slip corresponds to rake = 90°. Blue dots on perimeter are input rake values.

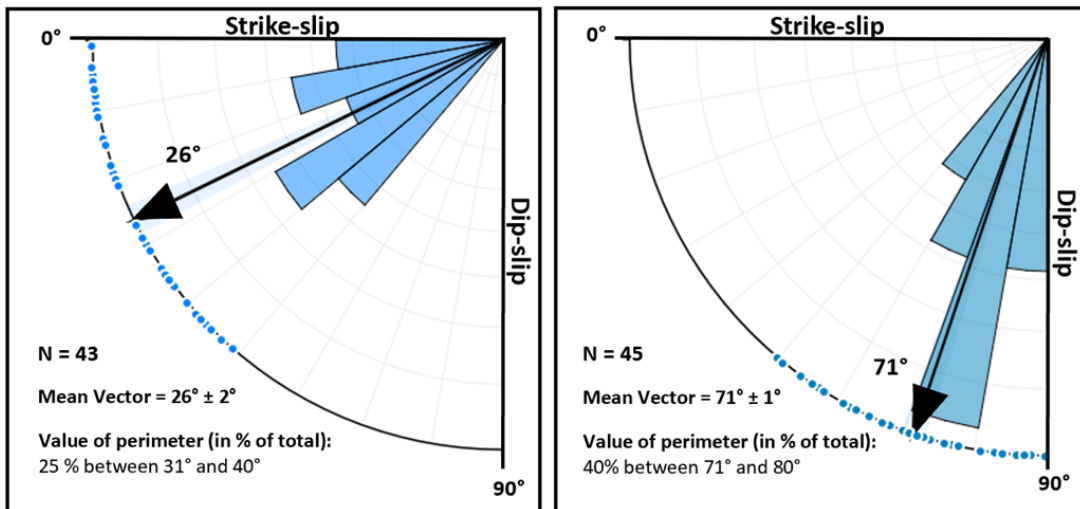


Figure 32: Radial histograms of fault lineation rakes counted into 10° bins. Black arrow denotes arithmetic mean of data. Composite dataset sub-divided into two groups: rake < 50° (left) and rake > 50° (right). The largest wedge (31°-40°) has 25% of data (left); largest wedge (71°-80°) has 40% of data (right). Strike-slip corresponds to rake = 0°; dip-slip corresponds to rake = 90°. Blue dots on perimeter are input rake values.

Fault-slip lineations coupled with asymmetric steps allow both the direction and sense of fault slip to be determined. With a robust dataset of such measurements, the regional principal axes of paleostrain can be estimated by using fault-slip inversion analysis (Marrett and Allmendinger, 1990). The principal strain axes represent the directions of maximum shortening (P-axis), maximum extension (T-axis), and an intermediate axis normal to the other two. Assuming that the regional strain through time was non-rotational relative to regional stress, the principal paleostrain axes coincide with the principal paleostress axes as inferred from patterns of fault slip.

Fault-slip inversion was performed on the processed field data using the FaultKin application (Fig. 33; Table 3). The calculated maximum shortening axis (P-axis) has a horizontal projection along the line 2°-182° and the calculated maximum extensional axis (T-axis) has a horizontal projection along the line 118°-298°. The calculated direction of the principal compressional strain in this area differs by nearly 90° from that determined by previous EdMap projects to the east, which is addressed in the Discussion section.

Table 3: Fault Plane Solutions

Principal Strain Axes	Trend	Plunge
P-axis; relative shortening	182°	42°
T-axis; relative extension	298°	26°
I-axis; intermediate	50°	37°

The moderate plunges of the calculated principal strain axes and the oblique orientation of P and T axes relative to mapped faults imply a complex fault-slip regime with a mix of slip modes (strike vs. dip slip) as well as slip senses within each mode. In this regard,

seventy faults with a determined sense of slip were tabulated by slip mode and slip sense (Fig. 34). The tabulation shows a fault sample with a similar amount of thrust and normal fault movement as well as right and left lateral movement, but the combinations of slip modes and senses is not uniform as shown by the asymmetry of table values. The complexity of fault slip characteristics shown by this tabulation is connected to the complexity in the estimated principal strain axes, given that both results are based on the same data. Further thoughts and possible explanations are given in the Discussion section.

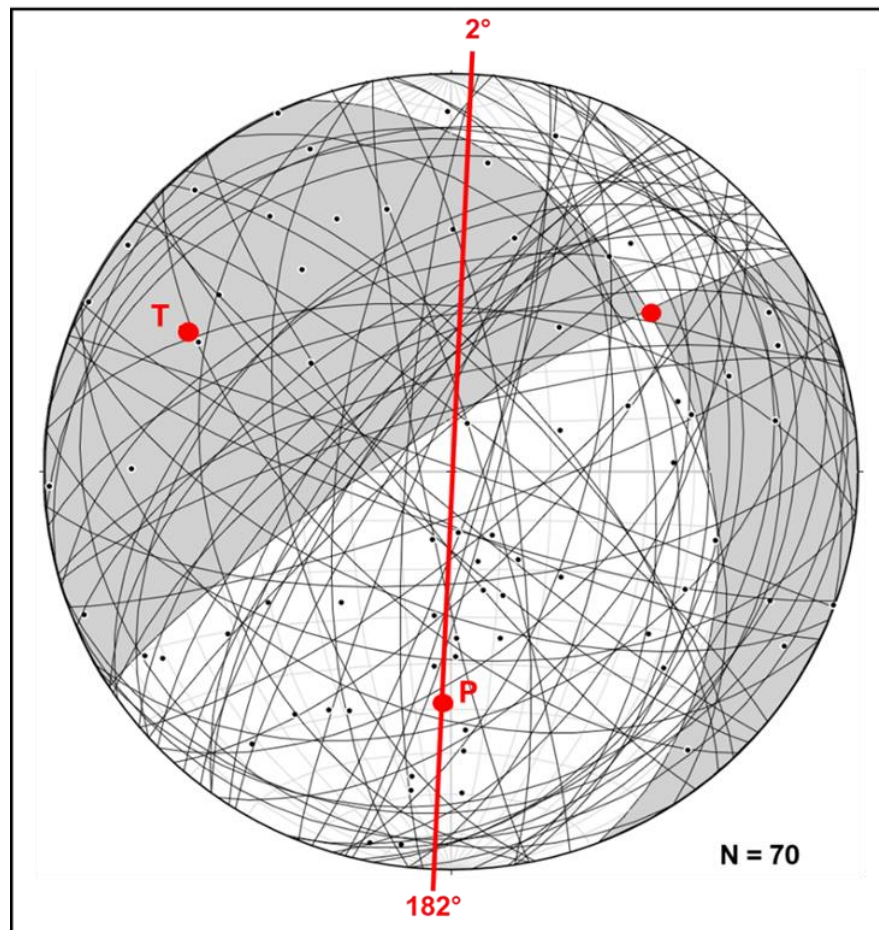


Figure 33: Linked Bingham, fault-plane solution showing inferred fault planes with maximum resolved shear (black arcs) and slip lineations on individual faults (black dots on arcs). Principal strain axes: P – relative shortening, T – relative extension, I – intermediate. Shortening direction in a horizontal plane is along an azimuth 002°-182°.

		Dip Slip		
		Thrust	Normal	
Strike Slip	Right	6	29	= 35
	Left	27	8	= 35
		 33	 37	70 Total

Figure 34: Tabulation of slip components and sense for fully determined fault surfaces. Values are number of sites with the specified components and senses of slip.

5.3 Cross-Section Construction and Interpretation

The new mapping results, fold and fault analyses, current concepts about fault systems, and modern cross-section construction methods were used to build cross-sections through four relatively well-known localities. Cross-sections were constructed perpendicular to the Keweenaw fault to better define downdip fault geometry and associated deformation in its hanging wall and foot wall (Fig. 35). The following cross-sections were selected at locations that represent the range of structural styles observed along the KFS: A-A' at Houghton-Douglass Falls crosses both the Keweenaw and Hancock faults southwest of their intersection; B-B' at the St. Louis ravine crosses the Keweenaw fault between the Hancock fault intersection and the Mayflower fault block; C-C' at the Mayflower fault block crosses the Keweenaw fault and the large footwall splay along the southeast side of the fault block; and D-D' near Copper City crosses the Keweenaw fault and the thickest part of the Copper City rhyolite complex.

Elevation profiles for the cross-sections were created in ArcGIS Pro and used to create templates, onto which unit contacts, stratal dips, faults and their dip, and fold axial surfaces were posted. Dip values of strata, fold axial surfaces, and faults were converted to apparent dip along the cross-sections. Diamond drillholes were also positioned along the cross-sections and drawn with their given inclination below horizontal adjusted as for apparent dip adjustments. Their available core log descriptions (Butler and Burbank, 1929; White, 1985) were used to constrain geologic contacts and thicknesses in the hanging wall of the KFS and within the MFB. PLV stratal dip in the footwall is not

constrained by observations, and so it was taken to be 15° NW based on published data for Silver Mountain ([Kulakov, 2013](#)).

A minimum thickness of JS section is inferred from a Mayflower diamond drillhole (MAY-41; see [Appendix A1](#)) and is used on all four cross-sections. The MAY-41 diamond drill hole along cross-section C-C' crosses the Keweenaw fault into JS at ~475 meters below sea level, which implies a minimum JS thickness of ~795 meters. The JS section could be as thick as 2,300 meters based on an early seismic experiment ([Bacon, 1966](#)), which value was used in a recent cross-section model ([DeGraff and Carter, 2023](#)). The cross-section work here did not attempt to tie into that cross-section work, and investigated a likely minimum case for JS section thickness instead. Evidence was previously cited for a basal JS unit that largely consists of poorly indurated, muddy to silty conglomerate at Natural Wall ravine, Lac La Belle, and Bête Grise Bay. Its thickness is uncertain but, based on sections examined at those locations, the thickness of the basal JS conglomerate was set to 50 m for the cross-sections presented here. The main protocols used to construct the sections were: 1) maintaining stratigraphic thicknesses of modeled sandstone layers in the footwall; 2) preserving the volume of the JS unit by adjusting the basal conglomerate thickness to accommodate folding of overlying sandstone layers; 3) integrating all available data from published maps and new mapping; and 4) using the dip-bisector method of cross section construction as much as possible. The resulting cross-sections are presented and discussed starting at Houghton-Douglas Falls in the southwest and proceeding towards the northeast.

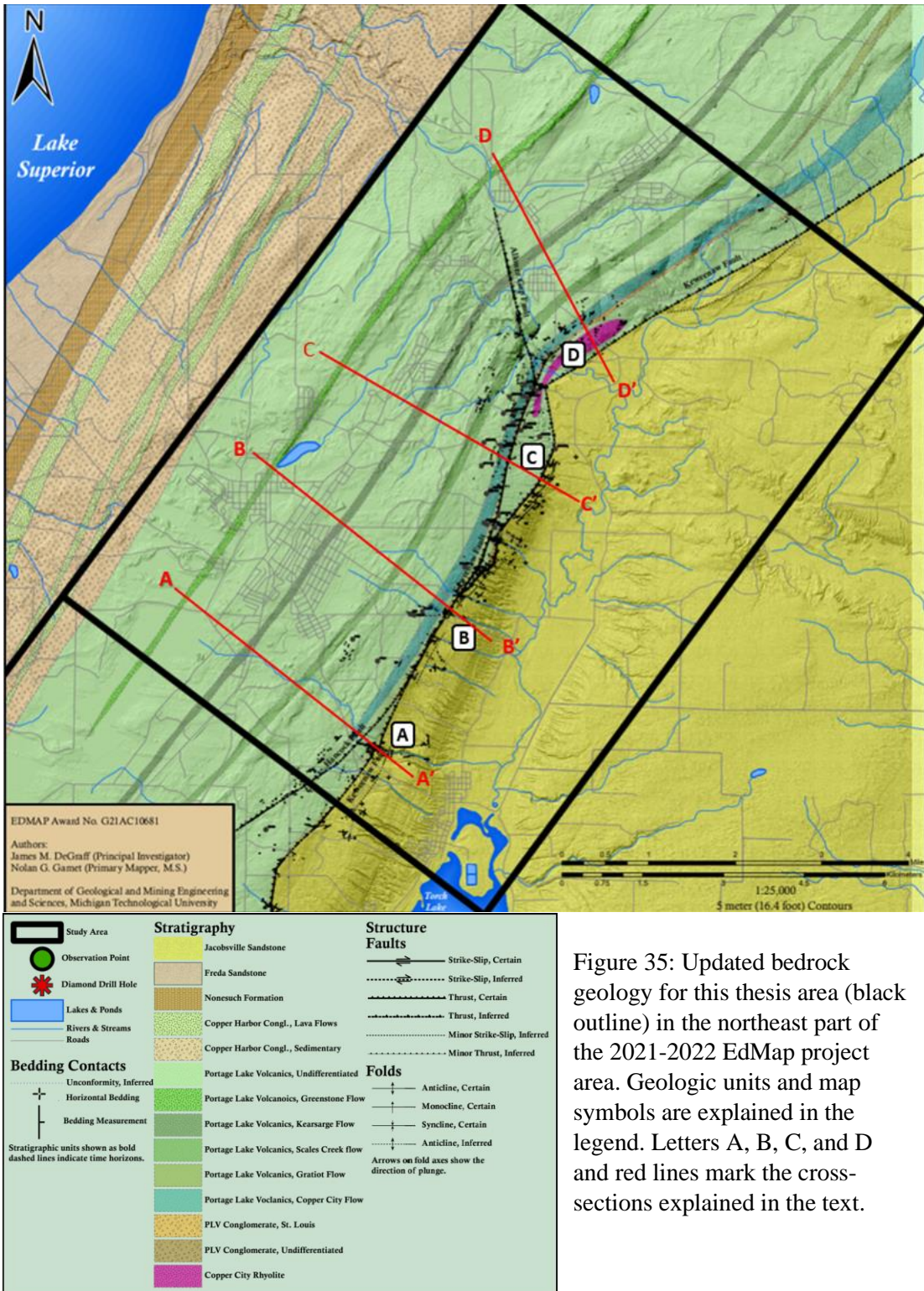


Figure 35: Updated bedrock geology for this thesis area (black outline) in the northeast part of the 2021-2022 EdMap project area. Geologic units and map symbols are explained in the legend. Letters A, B, C, and D and red lines mark the cross-sections explained in the text.

Excellent outcrop control along Hammell Creek above and below Houghton-Douglass Falls provides a rather clear picture of the surface geology and structural geometry for cross-section A-A' in the hanging wall and especially in the footwall of the Keweenaw fault (Fig. 36). First addressing the hanging wall in the cross-section, the Keweenaw fault is shown dipping 15°NW , adjusted for apparent dip, and parallel to overlying strata that have a similar measured dip. The position of the Hancock fault at the surface is based on the new map, and its dip of about 23°NW is constrained to be no shallower than measured dip of PLV strata from the USGS bedrock geology map. In fact, the Hancock fault must dip slightly steeper than the PLV strata in its hanging wall in order to duplicate the Copper City flow as indicated by the new map. The Hancock and Keweenaw faults must converge and intersect going downdip to the northwest, which is predicted to occur at ~ 300 meters beneath the surface. Given that the Keweenaw fault is the more significant fault because of its greater displacement and strike length, the model shows the Hancock fault terminating or merging into the Keweenaw fault. This fault model geometry creates a double-stacked pattern that repeats the St. Louis conglomerate and Copper City Flow.

Stratal geometry in the remainder of the KF hanging wall is constrained by outcrop measurements of layer orientation posted on USGS geology maps and the concept of the fault system here being largely detached on or near the St. Louis conglomerate (see DeGraff and Carter (2023) with a summary of detachments observed in mines). In such detached systems, hanging-wall stratal geometry largely mimics the shape of the underlying fault. Application of this concept along with the dip-bisector method of fold hinge construction allowed the downdip extrapolation of the merged KF and HF to the

bottom of the cross-section. A broad anticline in the hanging wall, defined by PLV stratal dips that increase going to the northwest, trends roughly parallel to the KF and HF and is similar to a recently published cross-section along Dover Creek about 4 kilometers to the southwest (DeGraff and Carter, 2023).

Next addressing the footwall, the broad anticlinal structure defined by measured stratal orientations in outcrop is the starting point for constructing this part of the cross-section. The basal contact of the JS is assumed to be nearly horizontal and resting on tilted PLV strata at a depth of 475 meters below sea level, based on the MAY-41 drill hole, which equates to a minimum JS thickness of 795 meters. In order to conserve volume within the JS section, layer thicknesses over most of the section, represented by construction form lines, were kept constant or nearly so. Adjustments to thickness were made in the lowermost 50 m of the JS section, where basal strata are inferred to be poorly indurated, relatively ductile, muddy conglomerate and silty layers, as mentioned earlier. The ductile basal unit was made thicker below the surface anticline to accommodate upward flexing of overlying JS strata. Similarly, the ductile unit was made thinner going northwest from the anticline into a broad flat-bottomed syncline that starts at the KF surface trace and is inferred to extend below the shallow-dipping thrust sheet. In the corner at the intersection of the KF with the footwall PLV-JS unconformity, the ductile unit was made much thicker to fill the volume opened by upward dragging of overlying JS strata along the underside of the thrust sheet. The various thickness adjustments in the basal ductile unit were made so that the volumes added by local thickening equaled the volumes subtracted by local thinning, thus conserving overall volume of the basal layer.

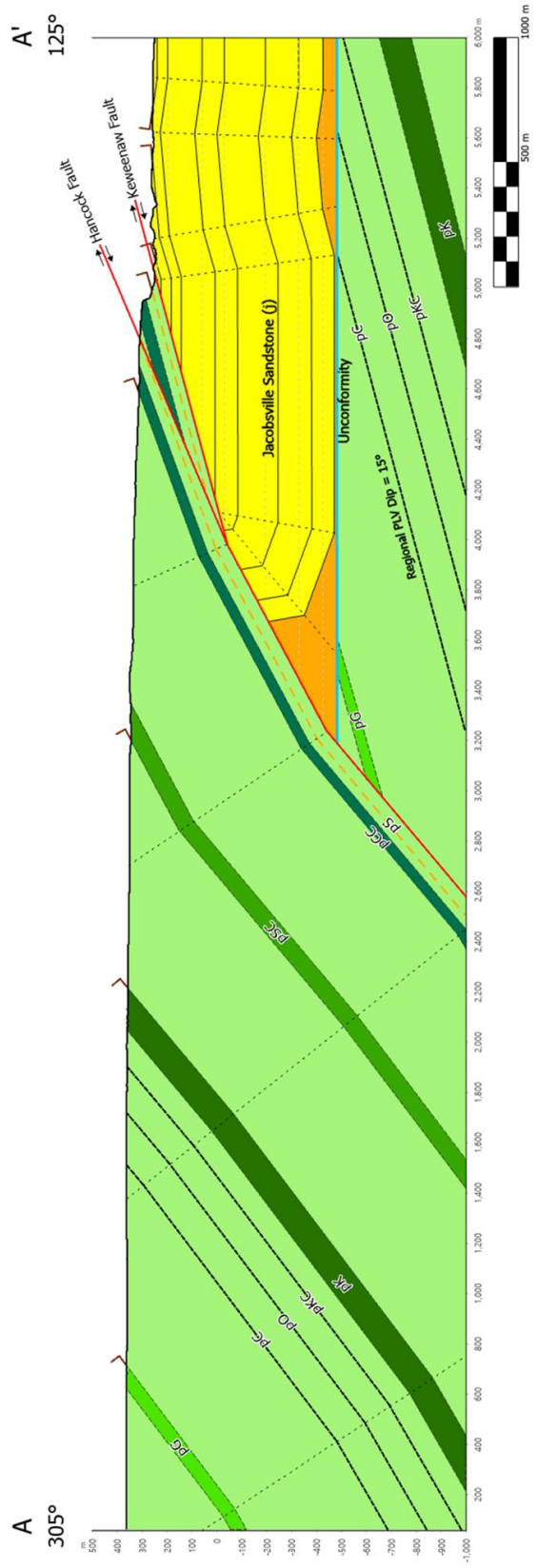


Figure 36: Cross-section A-A' at Houghton-Douglass Falls. Bedding dip markers on the topographic surface are at locations where new measurements were made or old ones were adapted from published maps. Strata and related folds are drawn to reflect apparent dips. Unit colors explained in Figure 34. Dashed lines indicate inferred contacts or unit horizons; bold red lines indicate faults. Letter codes as follows: pS – St. Louis conglomerate; pCC – Copper City flow; pSC – Scales Creek flow; pK – Kearsarge flow; pKC – Kingston conglomerate; pO – Osceola flow; pC – Calumet and Hecla conglomerate and pG – Greenstone flow.

Relatively good outcrop control along St. Louis ravine also provides a fairly clear picture of the surface geology and structural geometry in the hanging wall and footwall of the Keweenaw fault for cross-section B-B' (Fig. 37). The hanging-wall part of the cross-section is simple in comparison to cross-section A-A' because it lacks the repetition of PLV strata caused by the Hancock fault, which does not extend this far north. The downdip extension of the Keweenaw fault is again constrained by the stratal geometry of the hanging wall and the concept that it formed by detachment at or near the St. Louis conglomerate. Here, the fault dips more steeply at the surface (N35°W) than at Houghton-Douglass Falls (N15°W) based on HW stratal measurements. Moving northwest from the fault, the dip of PLV layers in the hanging wall changes in a way that suggests a broad anticlinal structure parallel to the KF, similar to what is seen in the Houghton-Douglass cross section but less prominent.

In the field, JS strata in the immediate footwall of the fault are vertical to overturned 74°NW, but they change orientation to 7°SE less than 100 m southeast of the fault. The observed geometry of footwall deformation at the surface is that of a tight asymmetric syncline with an overturned northwest limb, a nearly horizontal southeast limb, and an axial surface that dips moderately toward the fault. The deformation style seen at the surface is largely reflected in the subsurface stratal geometry of the footwall that is modeled in the cross-section.

To accommodate the sharp synclinal bend near the fault, the ductile basal JS unit was made thicker at the intersection between the KF and the PLV-JS unconformity in the footwall, comparable to cross-section A-A' at an analogous location. To conserve volume

within the ductile unit, a broad open syncline with a flat bottom was modeled as suggested by stratal dip at the surface. The broad synclinal geometry implies a broad anticline to the south, similar to the overall geometry at Houghton-Douglass Falls. However, a lack of JS exposures farther downstream along St. Louis Creek does not allow this modeled anticlinal geometry to be tested with currently available data.

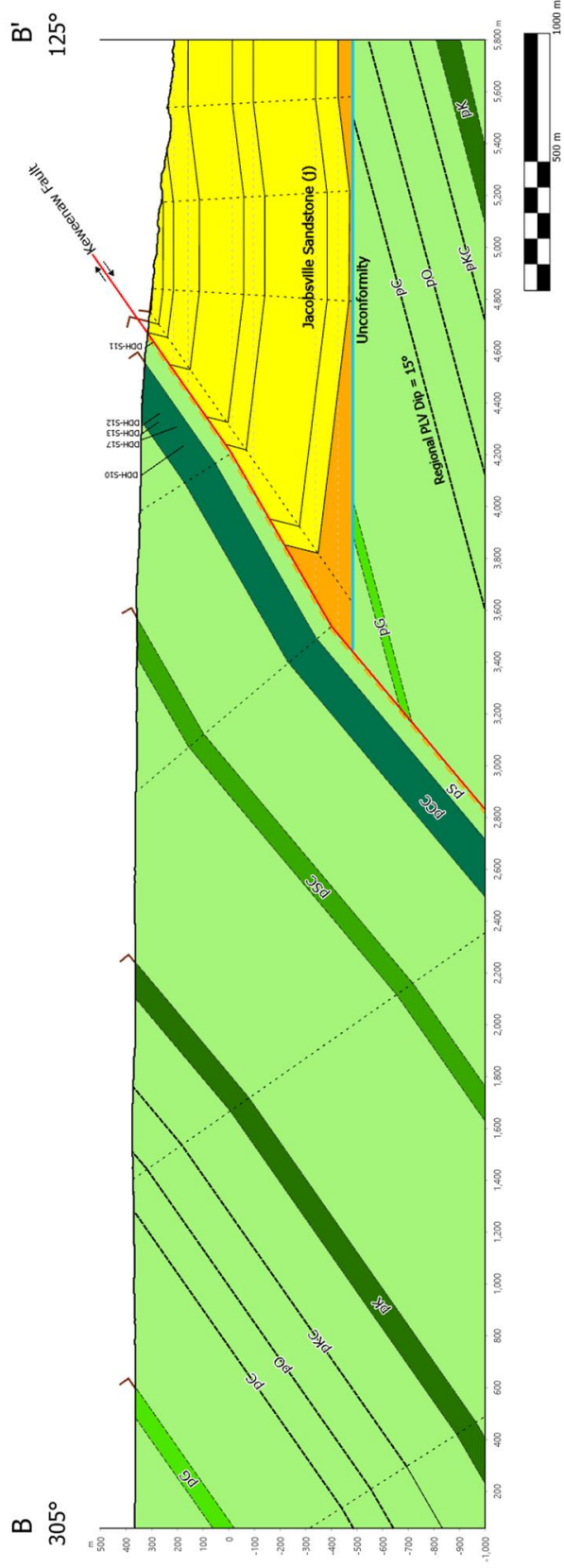


Figure 37: Geologic cross-section B-B' at St. Louis Ravine drawn normal to the main Set 1 fault trend. Bedding markers on the topographic surface represent the locations from which the measurements were taken in the field or adapted from published USGS maps of the area and used to create dip domains. Strata and related folds are drawn to reflect apparent dips. Unit colors explained in Figure 34. Dashed lines indicate inferred contacts or unit horizons; bold red lines indicate faults. Letter codes as follows: pS – St. Louis conglomerate; pCC – Copper City flow; pSC – Scales Creek flow; pK – Kearsarge flow; pK-C – Kingston conglomerate; pO – Osceola flow; pC – Calumet and Hecla conglomerate and pG – Greenstone flow.

Cross-section C-C' across the Mayflower fault block (Fig. 38) lacks the excellent surface control of the previous two cross-sections, but it has better subsurface control from numerous exploratory drill holes of the Mayflower and Old Colony series of holes. Here, the absence of deeply incised valleys required extensive use of the available core logs and the projection of surface observations and measurements from well off the line of section. The best constrained part of the cross-section is the hanging wall of the Keweenaw fault, which is reinterpreted to be what was previously called the Mayflower fault. The fault here is well constrained by drill hole data, mine workings, and to a lesser degree by outcrop relationships (White et al., 1953; this thesis). The fault on the west side of the Mayflower fault block strikes N15°E and dips 60°NW, which is parallel to PLV layers in its hanging wall, including the St. Louis conglomerate and the Copper City flow. Within the depth extent of the cross-section, the fault's dip changes only slightly based on the same methods and concepts explained for previous cross-sections. Other than the fault's steeper dip here relative to previous cross-sections, its stratigraphic position near the St. Louis conglomerate and subparallel relationship to hanging-wall stratigraphy is identical to the relationships documented for the Keweenaw fault on the other cross-sections. Therefore, this fault segment, formerly called the Mayflower fault, is now interpreted as the continuation of the main Keweenaw fault coming from the southwest.

In the footwall southeast of the Mayflower fault block, JS strata near the bounding fault are tilted into subvertical orientations with both northwesterly and southeasterly dips that appear to define a series of tight anticlines and synclines (Fig. 15). A fold analysis of stratal orientations from this area yields fold axes plunging ~01° to the NE, and subparallel axial surfaces trending ~46°. The fold axes generally conform to the natural

bend and trend of the faults bounding the southeast edge of the MFB (Fig. 15). Along the line of cross-section C-C', footwall JS strata near the main splay fault dip steeply in opposite directions within a relatively short horizontal distance, similar to what is observed along the St. Louis ravine (Fig. 37). Because of this and considerations of volume conservation, a small NE-trending splay fault is inferred to offset footwall JS strata in a reverse sense to explain the inferred overturned strata and to reduce the need to thicken the basal JS unit near the bottom of the Mayflower fault block. Other solutions to this complex region may be possible but have not yet been found. The modeled wedge of JS strata between the major footwall splay fault on the west and the inferred splay fault within JS on the east is probably not unique, but small fault blocks such as this postulated one are difficult to resolve with the available exposures. The footwall interpretation near the major footwall splay fault looks closest to what is shown on B-B' (Fig. 37), however with the complication of faulting within the JS section. Moving to the southeast, the broad synclinal structure modeled here is like those modeled in the previous cross sections but lacks the amount of outcrop control available along those transects. The presence of JS strata below the MFB is constrained by the MAY-41 drill hole, but its lithology is not described in much detail. Its geometry shown in the cross-section is not well constrained but is consistent with the other cross-section models as far as thickening of the unit in this complex region.

The internal geometry of the Mayflower fault block along the cross-section was interpreted using the map relationships and the following diamond drillholes from the Mayflower (MAY) and Old Colony (OC) mining companies: MAY-7.5, MAY-39, MAY-41, OC-14, OC-15, OC-19, OC-21, OC-22, and OC-28 (Appendices A1 and A2).

However, other drill holes off the line of section further constrained the block's internal geometry, especially along the reinterpreted Keweenaw fault. The Old Colony drill holes listed above constrain the positions of the main bounding faults and conglomerate layers within the fault block. Drill hole MAY-41 provides critical data because it cuts the Keweenaw fault and important hanging-wall stratigraphy, part of the Mayflower fault block, the basal thrust of the block, and underlying Jacobsville Sandstone at its deepest proven point in this area.

The overall stratal and fault geometry for the Mayflower fault block seems fairly clear from the exploratory core logs, but the details in some parts are difficult to resolve probably because of complications due to small-scale deformation. The general stratal geometry within the Mayflower fault block (MFB) is defined by two conglomerate layers penetrated by six to seven drill holes near the base of the PLV section in the block (Fig. 38). These conglomerate layers are easily correlated across the drill holes, and they define an open anticline-syncline pair along a northwest to southeast direction. The basal thrust of the MFB in the MAY-41 drill hole cuts about 120 meters below the lower conglomerate layer. Based on the concept of a mostly detached style of faulting here, the shape of the basal thrust is constrained by the geometry of the overlying PLV strata in the MFB and is modeled thusly in the cross-section. The lower conglomerate layer within the MFB is tentatively taken to be the St. Louis conglomerate based on its proximity to the fault, which implies that the Copper City flow should lie immediately above it as labeled with a question mark on the cross-section. Another possible interpretation is that the two conglomerate layers traced within the MFB correlate to conglomerate layers higher in the PLV section, such as the Kingston, Calumet and Hecla, Houghton, or Allouez

conglomerates. Such a correlation would increase the amount of reverse slip calculated on the Keweenaw fault at this location from a minimum of 1.5 kilometers using the St. Louis conglomerate correlation to more than twice that distance using the Kingston conglomerate correlation as an example.

The internal geometry of the Mayflower fault block as modeled in the new cross-section is similar to what is shown on the published Ahmeek bedrock geology map sheet ([White et al., 1953](#)), which is expected given the extensive drill hole control. The previous cross section only reaches a depth of ~490 meters below sea level, however, and does not include information from the MAY-41 drill hole. The new cross section extends to 1,000 meters below sea level and models a likely connection between the KF and the major splay fault at a depth of ~780 meters below sea level.

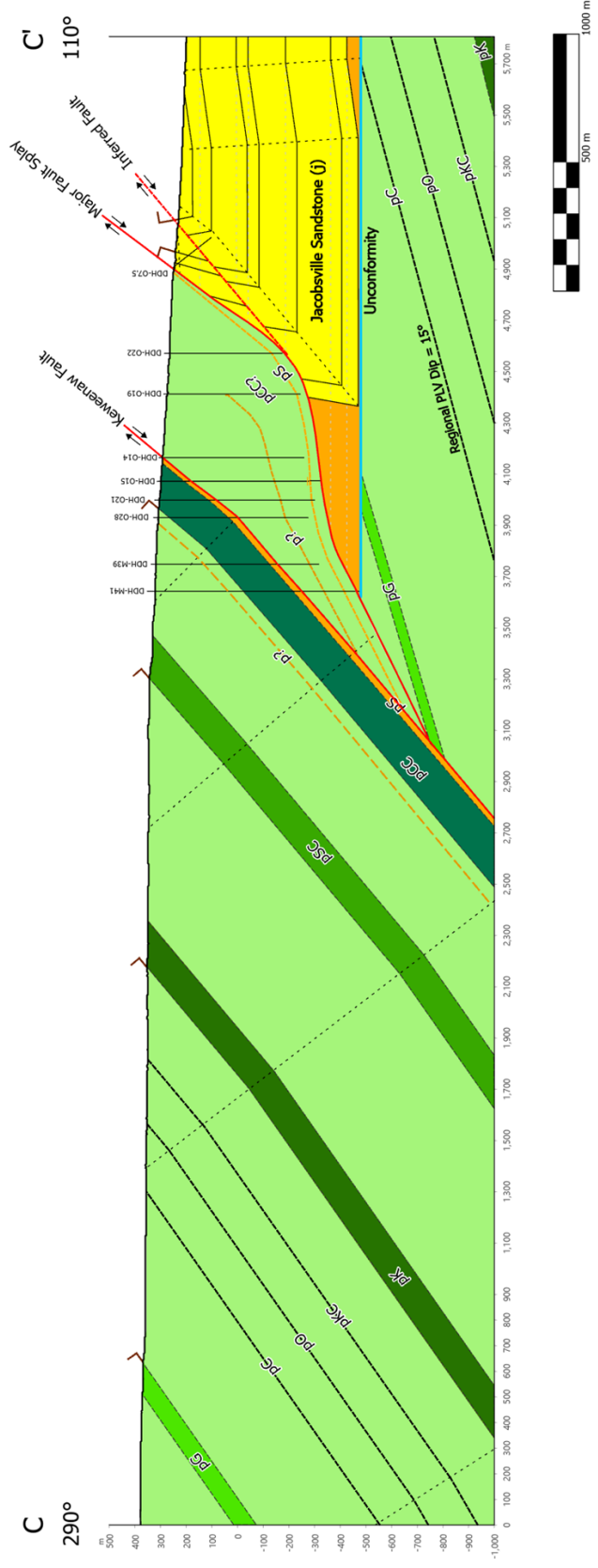


Figure 38: Geologic cross-section at the Mayflower fault block. Bedding markers on the topographic surface represent the locations from which the measurements were taken in the field or adapted from published USGS maps of the area and used to create dip domains. Unit colors explained in Figure 34. Dashed lines indicate inferred faults or unit horizons; bold red lines indicate faults. Letter codes as follows: pS – St. Louis conglomerate; pCC – Copper City flow; pSC – Scales Creek flow; pK – Kearsarge flow; pKC – Kingston conglomerate; pO – Osceola flow; pC – Calumet and Hecla conglomerate and pG – Greenstone flow.

Cross-section D-D' across the Copper City rhyolite complex and a new section of the Keweenaw fault system (KFS-3) lacks geologic control in the footwall of the Keweenaw fault and has very little subsurface control from drilling, such that it is the least constrained of the four cross-sections (Fig. 39). However, it does have moderately good surface control in the hanging wall from outcrops and two quarries, one in the Copper City rhyolite complex and the other in the Copper City flow (Fig. 16). The Keweenaw fault in this third main section of the fault system strikes N50°E and dips 35°NW based on outcrop mapping, but is nowhere exposed at the surface or cut by drill holes.

Again, beginning with the hanging-wall part of the cross-section and using the same construction methodology explained previously, the variation of PLV stratal dip along the line of section defines a broadly listric geometry of PLV strata with a slight shallowing of dip toward the KF. The shallowing of PLV stratal dip by ~14° toward the KF is documented by measurements at the Copper City flow and on conglomerate layers interbedded in the Copper City rhyolite complex. The rationale for continuing the rhyolite complex down dip in the cross-section is based on its new interpretation as an extrusive complex and therefore part of PLV stratigraphy. The rhyolite is modeled as becoming thinner down dip because of the thinning along strike that is apparent at the surface (Fig. 16).

The footwall geometry of Jacobsville Sandstone layers lacks any constraint, therefore, the general model shown on previous cross-sections was also implemented here but in a somewhat schematic way. Given the moderately steep dip of the KF, the general footwall geometry modeled on cross-section B-B' (Fig. 37) was adopted for D-D'. Vertical JS

strata shown on the cross-section along the underside of the Keweenaw fault are supported by observations of vertical strata in a small JS outcrop about 4 kilometers northeast of the cross-section along strike and just outside the current project area (Mueller, 2021). The part of the cross-section that lies in the corner between the KF and the footwall PLV-JS unconformity is probably more complex than shown and may be similar to JS folding observed near the fault intersection at the Natural Wall or at another fault intersection along Bruneau Creek west of Gratiot Lake (Mueller, 2021).

6 Discussion of Results and Significance

Important insights from the new geologic mapping and structural measurements have led to significant changes in map and cross-sectional geometry of strata and faults, an improved understanding of deformation related to movement along the KFS, and implications for causal tectonic events. Map changes include recognition and tracing of stratigraphic units along strike and across faults, improved definition of the fault network by adding new fault splays and reinterpreting previously recognized fault segments, and quantitative characterization of folding in footwall JS strata. The following paragraphs discuss the main changes in the new map relative to published USGS maps of the 1950s and a later compilation ([Cannon and Nicholson, 2001](#)). They also compare the structural style and analysis results for this section of the KFS with those of the previous EdMap projects conducted to the northeast where the fault system strikes more easterly.

Regarding stratigraphic changes, the Copper City rhyolite body shown on published bedrock geology maps had been previously interpreted as intrusive ([White et al., 1953](#)) or as either intrusive or extrusive ([Davidson et al., 1955](#)). It was recognized as being unique from all other rhyolite occurrences farther northeast along the Keweenaw Peninsula based on differences in mineralogy and geochemistry ([Nicholson, 1992](#)). The new quarry observations and mapping show that the Copper City rhyolite occurrence is a subaerial complex with felsic conglomerate (breccia) interbedded with rhyolite flows. This Copper City rhyolite complex can be traced along strike for at least 2.6 kilometers using the new quarry site, the sites to the southwest along the Calumet and Hecla railway, and core log

information, which more than doubles its previously mapped extent of ~1.2 kilometers. The shape of the complex in map view suggests that it has a broad domal geometry, similar to other rhyolitic occurrences farther to the northeast along the Keweenaw Peninsula and interpreted to be largely extrusive (Nicholson, 1992). Therefore, the Copper City rhyolite complex is interpreted to be a significant stratigraphic unit of the PLV that is older than the other rhyolites documented thus far along the Keweenaw Peninsula.

Other occurrences of rhyolite northeast and southwest of the Copper City rhyolite complex are judged to be part of the same stratigraphic unit, though they may not be continuous and connected to the main complex. Comparison of new geochemical data and thin-section observations with previous work by Nicholson and Shirley (1990) suggests that other rhyolite occurrences along strike of the main complex are more similar to those of the main complex than to Type I rhyolites found farther to the northeast. The other rhyolite occurrences in this project area are also near or below the level of the St. Louis conglomerate, like the Copper City rhyolite complex. Their inclusion as part of this rhyolitic stratigraphic unit would extend it ~3.8 kilometers northeast to just beyond the Mohawk-Gay Road and ~7.2 kilometers southwest to just beyond Highway M-26 between Lake Linden and Laurium.

Another important change in stratigraphic correlation involves the St. Louis conglomerate and Copper City flow, which are now traced along strike from the Allouez Gap fault southwest to beyond Houghton-Douglass falls in the hanging wall of the Keweenaw fault. The new correlation extends these PLV units across the Hancock fault

in the southern portion of the thesis area in a way that matches the apparent left-lateral offset of PLV layers mapped by the USGS elsewhere along that fault. The identification of these units at Houghton-Douglass Falls southeast of the Hancock fault fills a stratigraphic gap for the thrust sheet lying between the Keweenaw and Hancock faults, making further interpretation of that area more feasible. The extended correlation of these units along strike and recognition of the link between the St. Louis conglomerate and the Keweenaw fault also makes a strong case that the former Mayflower fault, previously considered to be a branch of the Keweenaw fault on the west side of the Mayflower fault block ([White et al., 1953](#)), is instead a continuation of the Keweenaw fault as defined to the southwest. The formerly designated Keweenaw fault along the southeast side of the Mayflower fault block is now interpreted to be a major footwall splay of the main Keweenaw fault.

The fault pattern and associated deformation within this project area appear to become more complex from southwest to northeast in the project area. The structural geometry is most complex and difficult to interpret near the Allouez Gap fault, where the main slip surface of the KFS abruptly changes direction and shifts downward to a lower stratigraphic level. The hanging-wall structural geometry generally changes less along the fault system than the footwall geometry, where deformation intensity appears to increase from near Houghton-Douglass Falls northeastward to the Mayflower fault block. This apparent northeastward change in deformation intensity within JS strata is manifested by tighter folds with vertical to overturned strata and a greater number of parallel folds, though the latter are not well defined by available outcrops. In general, the fold trends conform to the shape of the nearby fault contact with PLV, but locally they diverge from

the nearby fault trend as in the case of a corner formed by intersecting faults at Natural Wall ravine.

The orientations of faults and fold axes provide insight regarding the regional stresses and tectonic events that caused folding in the footwall portions of the KFS. The orientations of fold axes in footwall JS strata indicate local shortening along azimuths between 110° and 130° , which is based on the range of directions normal to the fold axes. If this local shortening direction reflects the regional principal shortening direction, then this result is similar to those obtained by previous EdMap projects based on fault-slip inversion analyses (Tyrell, 2019; Mueller, 2021; Lizzadro-McPherson, 2023). However, as discussed below, it differs from the results of fault-slip inversion analysis on data from this project area.

Fault-slip results for this thesis project have some similarities to those of previous EdMap projects, but also show important differences. The arithmetic means of rakes calculated for the previous EdMap projects were nearly the same and indicated a strike-to-dip slip ratio of about 1.8:1 for the composite effect of faults in the fault system where it trends roughly east-west (Fig. 39, A-C). The minor differences between these projects likely result from the number and sample of faults available to measure, but may reflect position along the Keweenaw Peninsula. Whereas the previous study areas exhibited low rake values indicative of dominant strike slip on the KFS, this project area exhibited a bimodal distribution of rake values. One of the modes in the bimodal distribution has an average rake of 26° , which matches the results of previous EdMap projects and indicates a set of faults in the sample that mostly have strike slip motion. The other mode,

however, has an average rake value of 71° , which indicates another set of faults in the sample that mostly have dip slip motion. The overall average rake value of 50° for this study, which combines the two modes, indicates that the KFS here collectively has roughly equal strike-slip and dip-slip components (Fig. 40, D). The difference between the rake histogram from this study and those from previous studies is expected considering how the curvature of the KFS would affect its orientation relative to applied far-field effects.

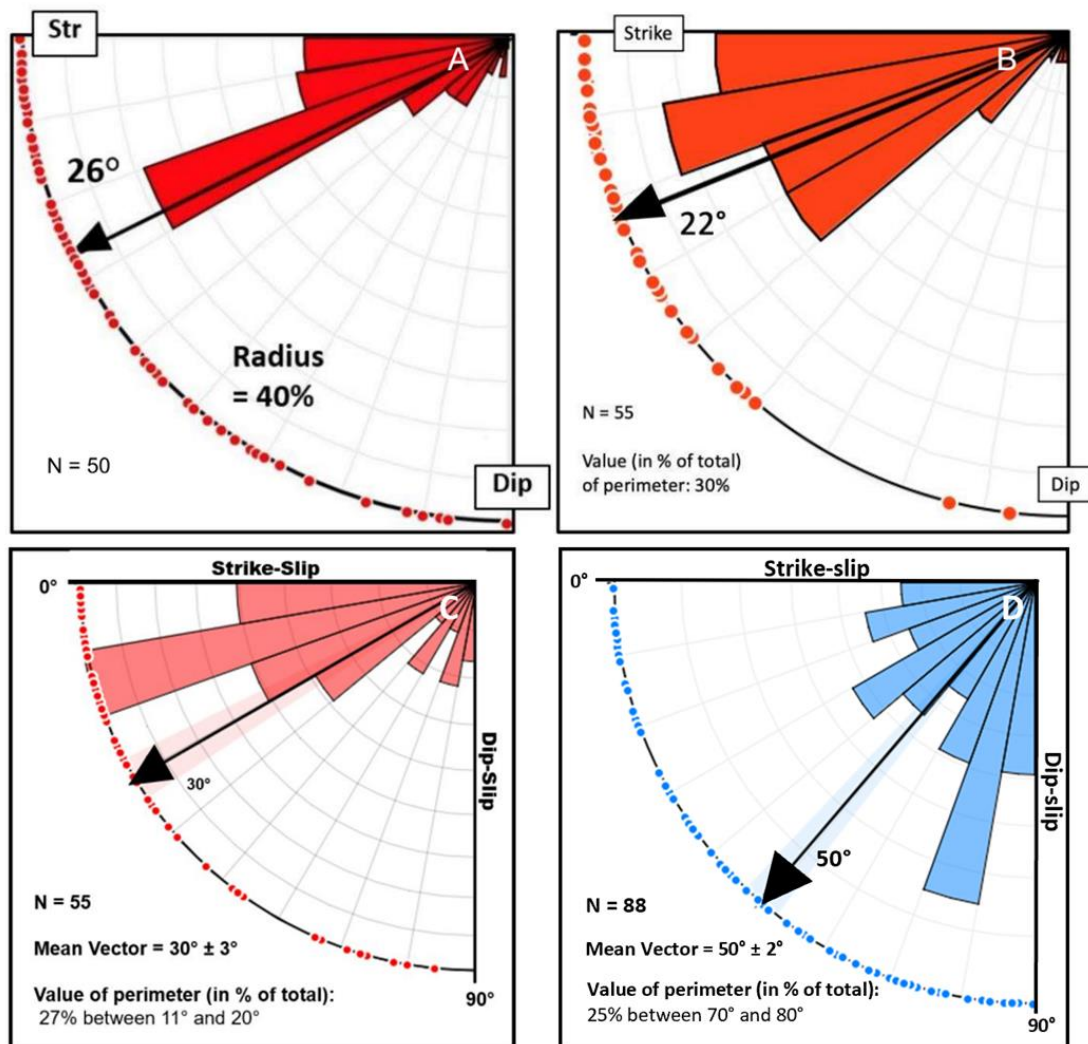


Figure 40: Comparison of radial rake histograms for three EdMap projects. A) Tyrrell (2018); B) Mueller (2020); C) Lizzadro-McPherson (2023); D) This thesis project.

Fault-slip inversion results for the three completed EdMap projects also suggest varying slip kinematics along the curved trajectory of the KFS (Fig. 41). Focusing on the P-axes in the plots, inferred principal shortening directions derived for the three previous projects range from nearly east-west to east-southeast and yield an average shortening direction of 282° - 102° . The principal shortening direction calculated for the current project area is 002° - 182° , which is roughly normal to the average of previous results. In one sense, it makes sense that the current result would differ from previous results given where this project area lies along the curvature of the fault system relative to others. However, the nearly north-south shortening direction inferred for the current project area is counter-intuitive based on the previous results. This unexpected difference could be due to variations in timing and number of episodes of faulting along the KFS, local lithologic or structural complications not resolved by the mapping, the relatively small sample size and possibility of non-representative measurements, other reasons or all of the above.

Considering all available data, fault-slip kinematics and fold orientations indicate regional shortening along an east-southeast to west-northwest line, which satisfies all the data except for the fault-slip inversion results for this project. This shortening direction is consistent with the likely direction of structural transport expected for the Grenville Orogeny and the north-northeast trend of the Grenville Front in the area of Lake Huron (Fig. 4). Based on this shortening direction, the most likely slip characteristics can be inferred for the major fault segments making up the KFS. NNE-trending Set 1 faults are inferred to have mostly west-side-up reverse slip, with minor right-lateral strike slip if any. NE-trending Set 2 faults that branch off the main slip surface of the KFS are inferred

to have the same reverse slip component as Set 1 faults but combined with a right-lateral strike-slip component. NNW-trending Set 3 faults are inferred to have mostly reverse slip but combined with a left-lateral strike-slip component. The Hancock fault may be an exception to this model because it has an apparent left-lateral sense of slip in map view. Ongoing work on that fault in the Quincy Mine adit may help to resolve this inconsistency.

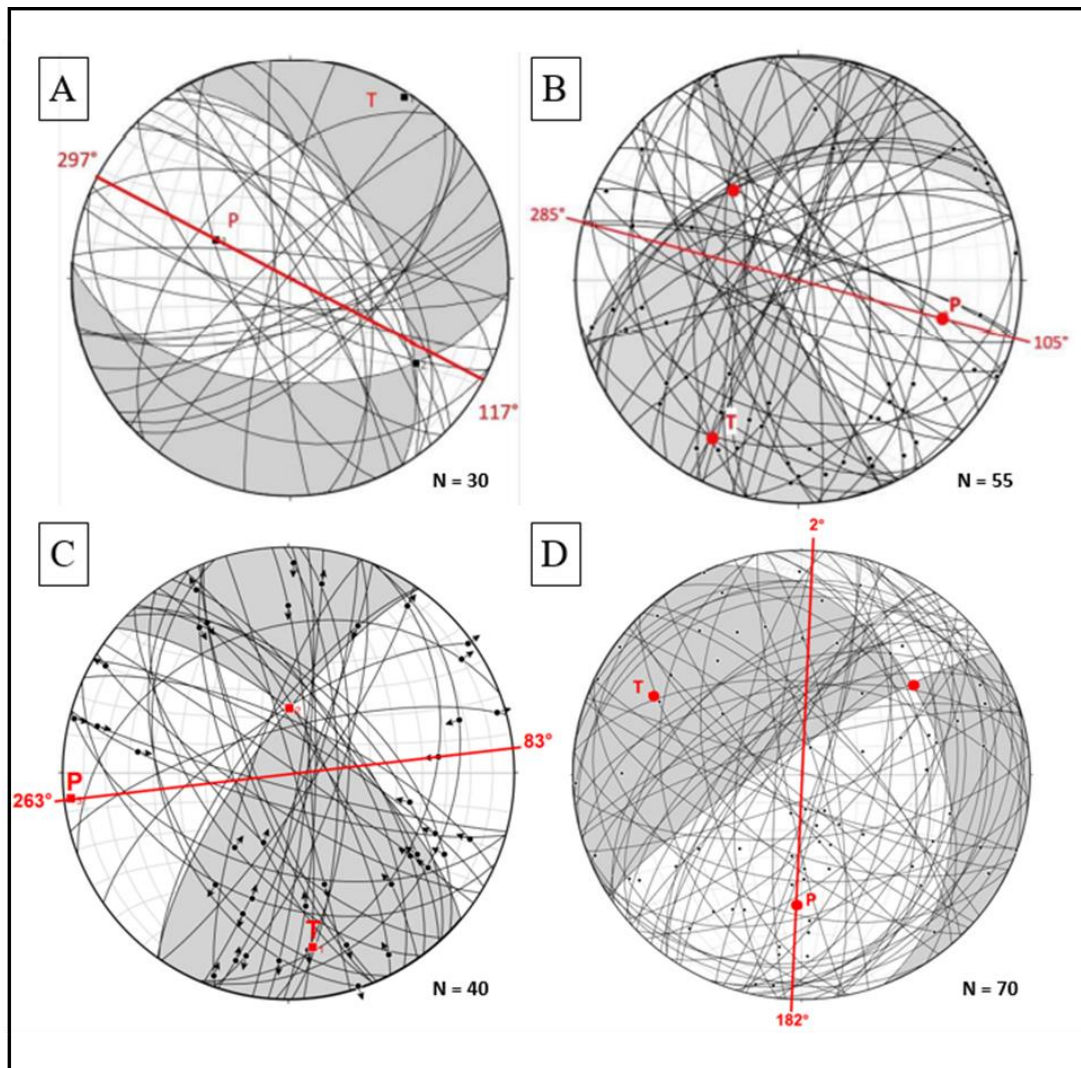


Figure 41: Fault-slip inversion plots: (A) Tyrrell (2019), (B) Mueller (2021), (C) Lizzadro-McPherson (2023); (D) This thesis project. P-axes are principal shortening directions; T-axes are principal extension directions; unlabeled red dots are the intermediate strain directions.

Uncertainties in the map and cross-sections, and contradictions in some analytical results, are probably due to a lack of outcrops and drill holes in geologically complex areas. They may also result from an incomplete three-dimensional vision of the stratal and structural geometries, which could benefit from additional cross-sectional modeling with other available drill hole data. Examples of complex areas with remaining uncertainties include the Natural Wall ravine, the Mayflower fault block, and the intersection of four faults west of the Copper City rhyolite complex. Alternative cross-section models are possible, especially for footwall JS strata where assumptions remain to be tested and JS stratigraphy and overall thickness is not well constrained. Results of the fault-slip inversion analysis for this area raise more questions about regional deformation and stress, and how local stress and deformation vary along the fault system (Fig. 34). Explaining the contradiction in principal strain directions between this project and previous EdMap projects is a challenge at this time.

To try to resolve the uncertainties and any contradictions, I would start by pooling map data and structural measurements from all three EdMap projects along Keweenaw Peninsula. The four slip combinations (Fig. 33) could be tabulated for the other areas to see if there are systematic changes along strike in terms of the ratio of strike-to-dip slip, left- versus right-lateral strike slip, and thrust versus normal dip slip. With regards to the fault-plane solution and paleostain axes, more fault-slip measurements could be obtained to increase data set size in an attempt to remove site-specific biases. Pooled fault orientation and rake values could be grouped by ranges of strike that are nearly parallel to nearby major faults to restrict the rake analysis to small faults that may more closely reflect the behavior of their larger neighbors.

Additional fieldwork could be conducted to search for other outcrops and more completely describe existing exposures, which would likely provide more fault-slip data. This work would benefit greatly by interpreting landform patterns in the new LiDAR images for Houghton and Keweenaw counties that are just now becoming available. Geophysical surveys, such as electrical resistivity, ground magnetics, and seismic transects may help to reveal and locate alternate fault geometries where outcrops are sparse and to reveal true JS thicknesses. Existing water well information available through the Michigan GeoWebFace site and additional exploratory core descriptions can also be used to supplement the surface and subsurface data set used in this project. All the above work and the new data it provides could be used to update the cross-sections presented here and to construct new cross-sections to create a regional scale fault model of the KFS using the 3D Move application.

Regarding the timing of fault movement in the context of the Grenville Orogeny, mentioned above but not the primary focus of this thesis, additional dating work could be attempted on calcite samples from fault zones and detrital zircon grains from deformed JS to look for evidence of multiple slip events ([Hodgin et al., 2022](#)). Lastly, further investigations focusing on locations where in situ native copper was found near faults may provide support to the idea that the KFS was, in part, responsible for bringing Cu-bearing solutions to the surface. This would entail the integration of mining data, cross-section models, fault geometries, updated geospatial locations of faults, and fault-slip data.

7 Conclusion

The fault-slip kinematics and geometry of the Keweenaw fault in this project area reveals that the previous idea of the fault system being a simple thrust is not an accurate characterization. Results of this mapping project have furthered our understanding of the Keweenaw fault system by better defining fault network geometry, quantifying fault-slip kinematics, and characterizing deformation style in adjacent strata. Since near the beginning of the copper mining period, the Keweenaw fault has been interpreted as a single, continuous thrust fault or as a normal fault that later became inverted to a thrust fault during a compressional tectonic event. This thesis project contributes to the understanding that the Keweenaw fault of published maps is a complex fault system consisting of fault segments that display a range of dip-slip and strike-slip behavior, rather than a simple thrust fault as commonly described.

The results of this project are generally similar to the findings of previous EdMap projects, but with important differences that probably result from the change in strike of the fault system relative to Grenville compression that likely produced the fault system. Future structural analyses and integration of all orientation measurements, rake values, and updated cross sections will help to characterize the Keweenaw fault system at a regional scale. Completing a regional-scale analysis should help to explain the documented changes in fault and fold geometry, as well as fault slip characteristics, when moving from southwest to northeast along the Keweenaw Peninsula. It may also help to resolve the slip history along the fault during multiple phases of the Grenville Orogeny.

The implications of this and future work on the KFS for other major faults in the Lake Superior basin may lead to a better understanding of the widespread distribution of copper throughout the area.

8 Reference List

- Allison, D.T., 2020, Lecture 8: Faults, Structural Geology: University of Alabama: https://www.southalabama.edu/geography/allison/GY403/GY403_Faulting.pdf (accessed October 2022).
- Allmendinger, R.W., Siron, C.R., Scott, C.P., 2017, Structural data collection with mobile devices: accuracy, redundancy, and best practices. *Journal of Structural Geology* v. 102, p. 98-112.
- Bacon, L.O., 1966, Geological structure east and south of the Keweenaw fault on the basis of geophysical evidence: in Steinhart, J.S. and Smith, T.J. (eds), *The Earth Beneath the Continents: Am. Geophys. Union, Geophysical Monograph 10*, p. 38-39.
- Billings, M.P., and Billings, M., 1972, *Structural geology*, Prentice-Hall Englewood Cliffs, New Jersey, v. 551.1 B5.
- Bodwell, W.A., 1972, Geologic compilation and nonferrous minerals potential, Precambrian section, northern Michigan: Houghton, Mich., Michigan Technological University, unpublished M.S. thesis. 106 p.
- Bornhorst, T.J., and Barron, R.J., 2011, Copper deposits of the western Upper Peninsula of Michigan, Archean to Anthropocene: Field guides to the geology of the Midcontinent of North America, [https://doi.org/10.1130/2011.0024\(05\)](https://doi.org/10.1130/2011.0024(05)).
- Bornhorst, T.J., Paces, J.B., Grant N.K., Obradovich, J.D., and Huber, N.K., 1988, Age of native copper mineralization, Keweenaw Peninsula, Michigan: *Economic Geology*, v. 83, no. 3, p. 619-625.
- Brojanigo, A., 1984, Keweenaw fault; structures and sedimentology [M.S. thesis]: Houghton, Michigan, Michigan Technological University, 124 p.
- Brown, A.C., 2008, District-scale concentration of native copper lodes from a tectonically induced thermal plume of ore fluids on the Keweenaw Peninsula, Northern Michigan. *Econ. Geology*, v. 103, p. 1691–1694.
- Butler, B.S., and Burbank, W.S., 1929, *The copper deposits of Michigan*: Washington, D.C., U.S. Geological Survey, Professional Paper 144, 238 p.
- Cannon, W.F., 1994, Closing of the Midcontinent rift-A far-field effect of Grenvillian compression. *Geology*, 22 (2): 155–158. [https://doi.org/10.1130/0091-7613\(1994\)022<0155:COTMRA>2.3.CO;2](https://doi.org/10.1130/0091-7613(1994)022<0155:COTMRA>2.3.CO;2).
- Cannon, W.F., Green, A.G., Hutchinson, D.R., Lee, M., Milkereit, B., Behrendt, J.C.,

- Halls, H.C., Green, J.C., Dickas, A.B., Morey, G.B., Sutcliffe, R., Spencer, C., 1989, The North American Midcontinent Rift beneath Lake Superior from GLIMPCE seismic reflection profiling. *Tectonics* v. 8, p. 305–332.
- Cannon, W.F., and Nicholson, S.W., 2000, Geologic Map of the Keweenaw Peninsula and Adjacent Area, Michigan: U.S. Geological Survey, pamphlet to accompany IMAP 2696, 7 p., <https://doi.org/10.3133/i2696>.
- Cannon, W.F., and Nicholson, S.W., 2001, Geologic map of the Keweenaw Peninsula and adjacent area, Michigan. U.S Geological Survey: To Accompany Map I-2696. p. 1-5.
- Cannon, W.F., McRae, M.E., and Nicholson, S.W., 1999, Geology and Mineral Deposits of the Keweenaw Peninsula and Vicinity, Michigan: U.S. Geological Survey Open-File Report 99-0149.
- Cannon, W.F., Peterman, Z.E., and Sims, P.K., 1993, Crustal scale thrusting and origin of the Montreal River monocline: A 35-km-thick cross section of the Midcontinent Rift in northern Michigan and Wisconsin: *Tectonics*, v.12, p. 728-744, <https://doi.org/10.1029/93TC00204>.
- Cornwall, H.R. and Wright, J.C., 1956a, Geologic map of the Hancock Quadrangle, Michigan: U.S. Geological Survey, Washington, D.C., Mineral Investigations Field Studies Map MF-46, scale 1:24,000.
- Cornwall, H.R. and Wright, J.C., 1956b, Geologic map of the Laurium Quadrangle, Michigan: U.S. Geological Survey, Washington, D.C., Mineral Investigations Field Studies Map MF-47, scale 1:24,000.
- Dallmeyer, R. D., Wright, J.E., SECOR JR, D.T., and Snoke, A. W., 1986, Character of the Alleghenian orogeny in the southern Appalachians: Part II. Geochronological constraints on the tectonothermal evolution of the eastern Piedmont in South Carolina: *Geological Society of American Bulletin*, v. 97, no. 11, p. 1329-1344.
- Davidson, E.S., Espenshade, G.H., White, W.S., and Wright, J.C., 1955, Bedrock geology of the Mohawk Quadrangle, Michigan: U.S. Geological Survey, Washington, D.C., Geologic Quadrangle Map GQ-54, scale 1:24,000.
- Davis, D.W., Paces, J.B., 1990, Time resolution of geologic events on the Keweenaw Peninsula and implications for development of the Midcontinent Rift system, *Earth Planet, Science Letter* 97, 54–64 p.
- DeGraff, J.M. and Carter, B.T., 2023, Detached structural model of the Keweenaw fault

system, Lake Superior region, North America: Implications for its origin and relationship to the Midcontinent Rift system: Geological Society of America Bulletin, v. 51, no. 1, p. 449-466.

DeGraff, J.M., Tyrrell, C.W., and Hubbell, G.E., 2018, Keweenaw fault geometry, secondary structures, and slip kinematics along the Bête Gris Bay shoreline: U.S.G.S EDMAP Program, Award No. G17AC00115, Final Technical Report.

DeGraff, J.M., Lizzadro-McPherson, D.J., and Mueller, S.A., 2020, Keweenaw fault geometry, related structures, and slip kinematics along the Lac La Belle-Mohawk segment, Michigan: U.S.G.S EDMAP Program, Award No. G19AC00140, Final Technical Report.

DeGraff, J.M., Gamet, N.G., and Langfield, K.M., 2022, Keweenaw fault geometry, related structures, and slip kinematics along the Mohawk-Hancock segment, Michigan: U.S.G.S. EDMAP Program, Award No. G21AC10681, Final Technical Report.

Green, J. C., 1989, Physical volcanology of mid-Proterozoic plateau lavas: The Keweenawan North Shore Volcanic Group, Minnesota. Geological Society of America Bulletin, 101(4), 486-500. doi:10.1130/0016-7606(1989)101<0486:PVOMPP>2.3.CO;2.

Hamblin, W.K., 1958, The Cambrian Sandstones of Northern Michigan: Lansing, Michigan, USA, Michigan Department of Conservation, Geological Survey Division, Publication 51, 146 p.

Hinze, W. J., Braile, L.W., and Chandler, V.W., 1990, A geophysical profile of the southern margin of the Midcontinent Rift System in western Lake Superior: Tectonics, v. 9, no. 2, p. 303-310, <https://doi.org/10.1029/TC009i002p00303>.

Hodgin, E.B., Swanson-Hysell, N.L., DeGraff, J.M., Kylander-Clark, A.R.C., Schmitz, M.D., Turner, A.C., Zhang, Y., and Stolper, D.A., 2022, Final inversion of the Midcontinent Rift during the Rigolet Phase of the Grenvillian orogeny: Geology, <https://doi.org/10.1130.G49439.1>.

Hubbard, L.L., 1898, Keweenaw Point with particular reference to the felsites and their associated rocks: Lansing, Geological Survey of Michigan, v. 6, part 2, 155 p.

Hubbard, H., 1975, Lower Keweenawan volcanic rocks of Michigan and Wisconsin. Journal of Research U.S. Geological Survey, v. 3(5), p. 529-541.

Huber, N., 1973, The Portage Lake volcanics (Middle Keweenawan) on Isle Royale, Michigan. U.S. Geological Survey Professional Paper, 754-C p.

- Hynes, A., and Rivers, T., 2010, Protracted continental collision: Evidence from the Grenville Orogen: *Canadian Journal of Earth Sciences*, v. 47, p. 591-620, <https://doi.org/10.1139/E10-003>.
- Irving, R.D., and Chamberlin, T.C., 1885, Observations of the junction between the Eastern sandstone and the Keweenaw series on Keweenaw Point, Lake Superior: Washington D.C., U.S. Geological Survey, Bulletin v. 23, 142 p.
- Kalliokoski, J., 1982, Jacobsville sandstone. *in* Wold, R.J., and Hinze, W.J., eds., *The Geology and Tectonics of the Lake Superior Basin*: Geological Society of America, Memoir v. 156, p. 147-155.
- Kulakov, E.V., 2013, Field trip 3 geology of Silver Mountain, Houghton County, Michigan, *Institute on Lake Superior Geology*, v. 59, part 2, 59-67 p.
- Lizzadro-McPherson, D.J., 2023, Structural analysis and slip kinematics of the Keweenaw fault system between Bête Grise Bay and Gratiot Lake, Keweenaw County, Michigan [M.S Thesis]: Michigan Technological University, 140 p.
- Marrett, J. and Allmendinger, R.W., 1990, Kinematic analysis of fault-slip data: *Journal of structural geology*, v. 12, no. 8, p. 973-986.
- Malone, D.H., Stein, C.A., Craddock, J. P., Stein, S., and Malone, J. E., 2020, Neoproterozoic sedimentation and tectonics of the Laurentian midcontinent: Detrital zircon provenance of the Jacobsville sandstone, Lake Superior Basin, USA, and Canada. *Terra Nova* (Oxford, England), v. 32, no. 6, p. 442–449. <https://doi.org/10.1111/ter.12481>.
- Mueller, S.A., 2021, Structural analysis and interpretation of deformation along the Keweenaw Fault System West of Lake Gratiot, Keweenaw County, Michigan [M.S Thesis]: Michigan Technological University, 69 p.
- Nicholson, S.W., 1992, Geochemistry, petrography, and volcanology of rhyolites of the Portage Lake volcanics, Keweenaw Peninsula, Michigan: U.S.G.S. Bulletin 1970.
- Nicholson, S., Shirley, S., Schulz, K., and Green, J., 1997, Rift-wide Correlation of 1.1 Ga Midcontinent Rift system basalts: Implications for multiple Mantle Sources During Rift Development. *Canadian Journal of Earth Sciences*, v. 34, p. 504-520.
- Nicholson, SW. and Shirley, S., 1990, Midcontinent Rift volcanism in the Lake Superior region: Sr, Nd, and Pb isotopic evidence for a mantle plume origin. *Journal of Geophysical Research*, v. 95, no. 7, p. 10851-10868.
- Rose, W.I., 2020, Keweenawan Geoheritage, Michigan Technological University:

<https://www.geo.mtu.edu/KeweenawGeoheritage/KeweenawGeoheritage/Welcome.html> (accessed August 2022).

Rose, W.I., 2015, Keweenaw fault lecture: Michigan Technological University: https://pages.mtu.edu/~raman/SilverI/KeweenawGeoheritage/Fault_Lecture.html (accessed February 2023).

Spencer, C.J., Cawood, P.A., Hawkesworth, C.J., Prave, A.R., Roberts, N.M., Horstwood, M.S., and Whitehouse, M.J., 2015, Generation and preservation of continental crust in the Grenville Orogeny: *Geoscience Frontiers*, v.6, no. 3, p. 357-372.

Stein, S., 2011, Learning from failure: The SPREE Mid-Continent rift experiment. *GSA Today*, v. 21, p. 5-7. 10.1130/G120A.1.

Stein, S., Stein, C.A., Elling, R., Kley, J., Keller, G.R., Wysession, M., Rooney, T., Frederiksen, A., and Moucha, R., 2018, Insights from North America's failed Midcontinent Rift into the evolution of continental rifts and passive continental margins: *Tectonophysics*, v. 744, p. 403-421.

Stevens, H.J., 1909, *The Copper Handbook*. v. 8, Houghton, MI: Horace Stevens. 1466 p.

Stewart, E.K., Grauch, V.J.S., Woodruff, L.G., 2018, Seismic stratigraphy of the 1.1 Ga Midcontinent Rift beneath western Lake Superior Part II: Evolution of rift-fill through time. *Geological Society of America. Abs. Prog.* 50, no. 6. <https://doi.org/10.1130/abs/2018AM323536>.

Strekeisen, A., 2020, Embayed Texture: <https://www.alexstrekeisen.it> (accessed January 2023).

Swanson-Hysell, N.L., Ramezani, J., Fairchild, L.M., Rose, I.R., 2019, Failed rifting and fast drifting: Midcontinent Rift development, Laurentia's rapid motion and the driver of Grenvillian orogenesis. *GSA Bulletin*; v. 131 (5-6), p. 913-940. <https://doi.org/10.1130/B31944.1>.

Trimble geo 7x handheld user guide, 2013, Trimble Navigation Limited, Version 1, revision A, 91-98 p.

Tyrrell, C.W., 2019, Keweenaw fault geometry and slip kinematics – Bête Gris Bay, Keweenaw Peninsula, Michigan [M.S Thesis]: Michigan Technological University, 38 p.

White, W.S., Cornwall, H.R., and Swanson, R.W., 1953, *Bedrock geology of the*

Ahmeek Quadrangle, Michigan: U.S. Geological Survey, Washington, D.C.,
Geologic Quadrangle Map GQ-27, scale 1:24,000.

White, W.S., 1968, The native copper deposits of northern Michigan, in Ridge, J.D., Ore Deposits of the United States 1933-1967, Vol. 1: New York, USA, American Institute of Mining, Metallurgical, and Petroleum Engineers, Rocky Mountain Series, Graton-Sales Volume, p. 301-325.

White, W.S., 1972b, The base of the Upper Keweenawan, Michigan and Wisconsin. U.S. Geological Survey Bulletin, v. 1354-F, p. 23.

White, W.S., 1985, Unpublished diamond drillhole core logs: U.S. Geological Survey, Field Records Collection, Boxes 282, p. 287-290.

Woodruff, L.G., Schulz, K.J., Nicholson, S.W., Dicken, C.L., 2020, Mineral deposits of the Mesoproterozoic Midcontinent Rift system in the Lake Superior region – A space and time classification, Ore Geology Reviews, v. 126, p. 103716, ISSN 0169-1368, <https://doi.org/10.1016/j.oregeorev.2020.103716>.

A Diamond Drill Holes

A.1 Mayflower Diamond Drill Holes

Mayflower D.D. Hole No. 7-1/2. Depth 580 feet. Overburden 40 feet.
Pitch 82°. Bearing S 85°-35' E. Lat. +5762.86. Dep. 16635.16.
Elev. +179.11 feet.

Depth
in feet

	No overburden.
0-580	Eastern Sandstone. Bedding about 45° to core. At 329, angle 30°. At 350-360, 10° and nearly parallel to core. At 400-500 angle 10-15°. Took specimen: 450 feet.
580	Bottom of Hole (10 boxes.)

Mayflower D.D. Hole No. 41. Elevation 460.03 feet.

Depth in feet		Depth in feet	
0-13	Overburden.	611-623	Amygdaloid, cellular, poorly oxidized.
13-15	Trap, mel. fel.	623-630	Trap, glomo.
15-18	Amygdaloid, cellular, poorly oxidized.	630-633	Amygdaloid, cellular, poorly oxidized.
18-25	Trap, mel. glomo.	633-664	Trap, glomo.
25-27	Amygdaloid, cellular, poorly oxidized.	664-676	Amygdaloid, cellular, poorly oxidized.
27-34	Trap, mel. glomo.	676-696	Trap, glomo.
34-36	Amygdaloid, cellular, poorly oxidized.	695-703	Amygdaloid, cellular, poorly oxidized.
36-58	Trap, mel. glomo.	703-745	Trap, glomo.
58-60	Amygdaloid, cellular, poorly oxidized.	745-750	Amygdaloid, cellular, poorly oxidized.
60-73	Trap, mel. fel. glomo.	750-774	Trap, mel. fel.
73-74	Amygdaloid, cellular, poorly oxidized.	774-780	Amygdaloid, cellular, poorly oxidized.
74-119	At 74 hard epidotized sand. Trap, mel. fel. glomo.	780-810	Trap, mel. fel.
119-124	Amygdaloid, cellular, poorly oxidized.	810-815	Amygdaloid, cellular, poorly oxidized.
124-146	Trap, mel. fel.	815-861	Trap, melaphyre.
146-149	Amygdaloid, cellular, poorly oxidized.	861-865	Amygdaloid, cellular, poorly oxidized.
149-168	Trap, mel. fel.	865-879	Trap, mel.
168-170	Amygdaloid, cellular, poorly oxidized.	879-882	Amygdaloid, cellular, poorly oxidized.
170-175	Trap, glomo.	882-910	Trap, mel.
175-176	Amygdaloid, cellular, poorly oxidized.	910-914	Amygdaloid, cellular, poorly oxidized.
176-208	Trap, mel. fel. glomo.	914-925	Trap, mel.
208-216	Amygdaloid, cellular, poorly oxidized.	925-930	Amygdaloid, cellular, poorly oxidized.
216-238	Trap, glomo.	930-945	Trap, mel.
238-240	Amygdaloid, cellular, poorly oxidized.	945-948	Amygdaloid, cellular, poorly oxidized.
240-246	Trap, glomo.	948-959	Trap, mel.
246-249	Amygdaloid, cellular, poorly oxidized.	959-968	Amygdaloid, cellular, poorly oxidized.
249-259	Trap, glomo.	968-989	Trap, melaphyre.
		989-992	Amygdaloid, cellular, poorly oxidized.
		992-996	Trap, mel.
		996-1006	Amygdaloid, cellular, poorly oxidized.
		1006-1101	Trap, mel. dark.
		1101-1105	Amygdaloid, slightly fragmental, cellular.
		1105-1116	Trap, mel. fel.
259-262	Amygdaloid, cellular, poorly oxidized.	1116-1119	Amygdaloid, cellular, poorly oxidized.
262-284	Trap, glomo.	1119-1127	Trap, mel. fel.
284-287	Amygdaloid, cellular, poorly oxidized.	1127-1130	Amygdaloid, cellular, poorly oxidized.
287-290	Trap, glomo.	1130-1152	Trap, mel. fel.
290-292	Amygdaloid, cellular, poorly oxidized.		
292-351	Trap, glomo.	Depth in feet	
351-355	Amygdaloid, cellular, poorly oxidized.	1152-1155	Amygdaloid, cellular, poorly oxidized.
355-377	Trap, glomo.	1155-1697	Trap, mel. fel. glomo - doleritic. Coarse ophitic. Great Trap.
377-383	Amygdaloid, cellular, poorly oxidized.	1697-1701	Amygdaloid, cellular, poorly oxidized.
383-394	Trap, glomo.	1701-1824	Trap, mel. fel. ophitic.
394-399	Amygdaloid, cellular, poorly oxidized.	1824-1855	Conglomerate. Took specimen.
	Butler, Burbank 5/30/24	1855-1873	Gouge, brecciated trap.
399-428	Trap, glomo.	1873-1874	Amygdaloid, cellular, poorly oxidized.
428-430	Amygdaloid, cellular, poorly oxidized.	1874-2380	Trap, mel. Much broken trap and amygdaloid with poor core recovery, about 200 feet to the box.
430-433	Trap, glomo.	2380-2418	Trap, mel. fel.
433-436	Amygdaloid, cellular, poorly oxidized.	2418-2423	Felsitic, possibly conglomerate.
436-450	Trap, glomo.	2423-2440	Trap, mel. with gouge zone E432-E439.
450-453	Amygdaloid, cellular, poorly oxidized.		
453-464	Trap, glomo.	2440-2569	Box 78, missing.
464-473	Amygdaloid, cellular, poorly oxidized.		
473-486	Trap, glomo.		
486-489	Amygdaloid, cellular, poorly oxidized.	2569-2587	Trap, broken.
489-493	Trap, glomo.	2587-2635	Sandstone, quartzose, probably Eastern sandstone.
493-499	Amygdaloid, cellular, poorly oxidized.		
499-515	Trap, glomo.		
515-520	Amygdaloid, cellular, poorly oxidized.		
520-526	Trap, glomo.	2635	Bottom of Hole.
526-528	Amygdaloid, cellular, poorly oxidized.		
528-547	Trap, glomo.		
547-551	Amygdaloid, cellular, poorly oxidized.		
551-567	Trap, glomo.		
567-570	Amygdaloid, cellular, poorly oxidized.		
570-584	Trap, glomo.		
584-588	Amygdaloid, cellular, poorly oxidized.		
588-611	Trap, glomo.		

Old Colony D.D. Hole No. 21.

Depth 1975 feet. Overburden 14 feet. Pitch 90°. Elev. +403.29. Lat. +5814.51. Dep. +13448.98.

Depth in Feet		Depth in Feet	
	Box 1 missing.	1374-1375 1375-1387	Amygdaloid, cellular, poorly oxidized. Trap, melaphyre.
		1387-1393 1393-1429	Amygdaloid, cellular, poorly oxidized. Melaphyre, finely glomeroporphyrite.
	Box 2 begins 55 feet.	1429-1462 1462-1477	Amygdaloid, probably several flows. Trap, melaphyre, glomeroporphyrite.
55-98	Trap, pegmatitic (doleritic.)	1477-1480	Amygdaloid, cellular, poorly oxidized.
98-113	Ophitic.	1480-1510	Trap, melaphyre.
113-126	Glomeroporphyrite.		
126-140	Pegmatitic.	1510-1517	Amygdaloid.
140-280	Somewhat mottled Glomeroporphyrite.	1517-1532	Trap, feldspathic melaphyre.
280-310?	Coarsely mottled.	1532-1535	Amygdaloid, cellular, poorly oxidized.
310-330	Melaphyre, glomeroporphyrite.	1535-1538	Trap, melaphyre, glomeroporphyrite.
330-370	Coarsely mottled.	1538-1541	Amygdaloid, cellular, moderately oxidized.
370-389	Repetition of mottled and unmottled zones continues.	1541-1559	Trap, melaphyre, glomeroporphyrite.
-465		1559-1564 1564-1589	Amygdaloid, cellular, poorly oxidized. Trap, melaphyre, glomeroporphyrite.
465-471	Amygdaloid, cellular, poorly oxidized. Possibly basal amygdaloid.	1589-1590 1590-1611	Amygdaloid, cellular, moderately oxidized. Trap, feldspathic melaphyre.
471-477	1 foot core recovery. Probably epidotized conglomerate.	1611-1621 1621-1628	Amygdaloid, cellular, poorly oxidized. Trap, melaphyre.
477-627	Trap, feldspathic melaphyre, slight mottling.	1628-1629 1629-1642	Amygdaloid, cellular, poorly oxidized. Trap, melaphyre.
627-653	No core recovery.	1642-1644 1644-1663	Amygdaloid, cellular, poorly oxidized. Trap, melaphyre, fine chloritic.
653-723	Conglomerate, probably starting at 627.	1663-	Breccia and gouge zone.
723-735	Badly crushed, probably trap.	1663-1692	Feldspathic ophite. Some mottling.
735-757	Melaphyre, ophitic.	1692-1700 1700-1708	Amygdaloid, cellular, moderately oxidized. Trap, melaphyre.
757-758	Amygdaloid, cellular, tight.	1708-1717	Amygdaloid, cellular, poorly oxidized. Fine copper at 1715.
758-873	Glomeroporphyrite. 807 amygdaloidal. 837 crushed zone 841. 843 ophitic.	1717-1725	Trap, melaphyre. (Fissure with copper at 1725.)
		1725-1727 1727-1752	Amygdaloid, cellular, poorly oxidized. Trap, melaphyre.
		1752-1754 1754-1766	Amygdaloid, cellular, poorly oxidized. Trap, melaphyre.
		Depth in feet	
		1766-1772 1772-1791	Amygdaloid, cellular, poorly oxidized. Trap, melaphyre. 1775 breccia (possibly conglomerate).
		1791-1792 1792-1826	Amygdaloid, cellular, poorly oxidized. Trap, melaphyre.
		1826	Conglomerate, felsite, few fragments.
		1826-1912	Trap, melaphyre.
		1912-1913 1913-1924	Amygdaloid, moderately oxidized. Trap, melaphyre.
		1924-	Conglomerate, much basic material, pebbles to 2".
		1975	Bottom of hole.
873-875	Amygdaloid, cellular, poorly oxidized.		
875-900	Feldspathic melaphyre, glomeroporphyrite. Phenocrysts.		
900-918	Amygdaloid, cellular, poorly oxidized.		
918-930	Feldspathic melaphyre, glomeroporphyrite. Phenocrysts.		
930-927	Amygdaloid, cellular, poorly oxidized.		
927-1010	Trap, feldspathic melaphyre, amygdaloidal. 940-950 much brecciated, vein with copper at 941. 1005-1010 less amygdaloidal.		
1010-1013	Amygdaloid, cellular, poorly oxidized.		
1013-1027	Trap, melaphyre, glomeroporphyrite, some phenocrysts.		
1027-1064	Amygdaloid, cellular, poorly oxidized.		
1064-1086	Trap, amygdaloidal.		
1086-1129	Trap, feldspathic melaphyre, glomeroporphyrite		
1129-1139	Amygdaloid, cellular, poorly oxidized.		
1139-1155	Trap, feldspathic melaphyre.		
1155-1164	Amygdaloid, cellular, poorly oxidized.		
1164-1171	Trap, feldspathic melaphyre.		
1171-1178	Amygdaloid, cellular, zoned.		
1178-1206	Trap, feldspathic melaphyre, glomeroporphyrite		
1206-1215	Amygdaloid, cellular, poorly oxidized.		
1215-1255	Trap, feldspathic melaphyre, glomeroporphyrite		
1255-1256	Amygdaloid, cellular, poorly oxidized.		
1256-1265	Trap, melaphyre.		
1265-1269	Amygdaloid, cellular, poorly oxidized.		
1269-1294	Trap, amygdaloidal.		
1294-1296	Crushed zone.		
1296-1305	Melaphyre.		
1305-1312	Amygdaloid, cellular, poorly oxidized.		
1312-1329	Feldspathic melaphyre, glomeroporphyrite.		
1329-1333	Amygdaloid, cellular, poorly oxidized.		
1333-1337	Melaphyre, glomeroporphyrite.		
1337-1346	Amygdaloid, cellular, poorly oxidized.		
1346-1364	Trap, brecciated.		
1364-1374	Melaphyre.		

Old Colony D.^U. Hole No. 22. Depth 1430 feet. Overburden 8 feet.
 Pitch 90°. Elev. +888.12. Lat. +8238.09. Dep. +15219.25

Depth in feet		Depth in feet	
8-9 9-157	Amygdaloid, cellular, poorly oxidized. Trap, mel. fel., amygdaloidal, becoming glom. Probably a number of flows.	1071-1073 1073-1106	Amygdaloid, cellular, poorly oxidized. Trap, ophitic.
157-160 160-200	Amygdaloid, cellular, poorly oxidized. Trap, melaphyre, glomo.	1106-1113 1113-1129	Amygdaloid, cellular, poorly oxidized. Trap, mel.
200-202 202-215	Amygdaloid, cellular, poorly oxidized. Trap, glomo.	1129-1131 1131-1150	Amygdaloid, cellular, poorly oxidized. Trap, mel. fel.
215-220 220-226	Amygdaloid, cellular. Trap, glomo.	1150-1153 1153-1160	Amygdaloid, cellular, poorly oxidized. Trap, mel.
226-226 226-228	Amygdaloid, cellular. Trap, glomo. Amygdaloidal. Number small flows. Little copper at 226 and 227.	1160-1175 1175-1190	Amygdaloid, slightly fragmental, fairly oxidized. Little copper. Trap, melaphyre, fine grained.
228-258	Trap, glomo.	1190-1200 1200-1219	Amygdaloid, cellular, poorly oxidized. Trap, mel. fine grained.
258-260 260-270	Amygdaloid, cellular. Trap, glomo.	1219-1230 1230-1248	Amygdaloid, brecciated. Possibly frag- mental. Little fine copper. Trap, mel., fine grained.
270-272 272-287	Amygdaloid, cellular. Trap, glomo.	1248-1255 1255-1280	Amygdaloid, cellular, poorly oxidized. Trap, mel. finely glomo. Mottled.
287-295 295-426	Amygdaloid, cellular. Trap, glomo.	1280-1285 1285-1298	Amygdaloid, cellular, poorly oxidized. Trap, mel.
426-428 428-448	Amygdaloid, cellular. Trap, glomo.	1298-1310 1310-1335	Agglomerate, felsite. Trap, mel.
448-452 452-460	Amygdaloid, cellular, poorly oxidized. Fine copper at 448. Trap, glomo.	1335-1364	Breccia, basic, possibly partly conglom- erate.
460-467 467-476	Amygdaloid, cellular. TRAP, glomo.	1364-1380	Trap, melaphyre.
476-486 486-498	Amygdaloid, cellular. Trap, glomo.	1380-1405 1405-1430	Amygdaloid, cellular. Trap, mel.
		1430	Bottom of hole.
<u>Depth in feet</u>			
498-502 502-505	Amygdaloid, cellular, poorly oxidized. Trap, glomo.		
505-506 506-512	Amygdaloid, cellular, poorly oxidized. Trap, glomo.		
512-518 518-554	Amygdaloid, cellular, poorly oxidized. Trap, glomo.		
554-562 562-580	Amygdaloid, cellular, poorly oxidized. Trap, glomo.		
580-582 582-678	Amygdaloid, cellular, poorly oxidized. Trap, glomo. Possibly several flows.		
678-682 682-714	Amygdaloid, cellular, poorly oxidized. Trap, glomo.		
714-718 718-729	Amygdaloid, cellular, poorly oxidized. Trap, glomo.		
729-731 731-792	Amygdaloid, cellular, poorly oxidized. Trap, glomo.		
792-795 795-801	Amygdaloid, cellular, poorly oxidized. Trap, glomo.		
801-808 808-871	Amygdaloid, cellular, poorly oxidized. Trap, mel. fel. ophitic.		
871-877 877-881	Amygdaloid, cellular, poorly oxidized. Trap, mel.		
881-886 886-896	Amygdaloid, cellular, poorly oxidized. Trap, mel.		
896-901 901-911	Amygdaloid, cellular, poorly oxidized. Trap, mel. Amygdaloidal.		
911-929 929-950	Amygdaloid, cellular, poorly oxidized. Trap, mel. Ophitic.		
950-959 959-991	Amygdaloid, cellular, poorly oxidized. Trap, mel. fel.		
991-994 994-1019	Amygdaloid, moderately oxidized, cellular. Trap, mel. fel.		
1019-1021 1021-1027	Amygdaloid, cellular, poorly oxidized. Trap, mel. fel.		
1027-1029 1029-1071	Amygdaloid, cellular, poorly oxidized. Trap, mel. fel.		

Old Colony D.D. Hole No. 28. Depth 1904 feet. Overburden 5 feet.
 Pitch 90°. Elev. +410.67. Lat. +6889.70. Dep. +13235.79.

Depth in feet	
5-54	Trap, mel. fine grained.
54-60	Amygdaloid, cellular, poorly oxidized.
60-729	Trap, mel. changing to glomo, 200 feet. mottled, 400 feet. Took sample. Pegmatite (dolomite) at 625 feet.
739-740	Amygdaloid, cellular, poorly oxidized.
740-749	Trap, mel.
749-751	Amygdaloid, cellular, poorly oxidized.
751-875	Trap, mel. ophitic.
875-915	Conglomerate.
915-923	Trap, mel.
923-999	Sandstone and trap.
999-1006	Amygdaloid, cellular, poorly oxidized.
1006-1088	Trap, mel. Little copper 1014. Brecciated 1053-1062.
1088-1092	Amygdaloid, cellular, poorly oxidized.
1092-1104	Trap, mel.
1104-1124	Amygdaloid, cellular, poorly oxidized.
1124-1199	Trap, mel.
1199-1207	Amygdaloid, cellular, poorly oxidized.
1207-1234	Trap, mel. fel.
1234-1236	Amygdaloid, cellular, poorly oxidized.
1236-1246	Trap, mel.
1246-1247	Amygdaloid, cellular, poorly oxidized.
1247-1264	Trap, mel.
1264-1267	Amygdaloid, cellular, poorly oxidized.
1267-1304	Trap, mel.
Depth in feet	
1304-1310	Amygdaloid, cellular, poorly oxidized.
1310-1316	Trap, melaphyre, brecciated 1316-1316.
1316-1320	Amygdaloid, cellular, poorly oxidized.
1320-1324	Trap, brecciated.
1324-1326	Amygdaloid, cellular, poorly oxidized.
1326-1350	Trap, mel. brecciated.
1350-1351	Amygdaloid, cellular, poorly oxidized.
1351-1390	Trap, mel. dark, fine grained.
1390-1395	Amygdaloid, cellular, well oxidized.
1395-1427	1395 hard quartz, possibly vein copper. Trap, mel.
1427-1442	Amygdaloid, cellular, poorly oxidized.
1442-1482	Trap, mel.
1482-1509	Amygdaloid, cellular, fairly oxidized.
1509-1614	Some copper 1509. Trap, mel. fine grained, dark.
1614-1618	Conglomerate, felsite.
1618-1621	Amygdaloid, foety, cellular, poorly oxidized.
1621-1676	Trap, mel.
1676-1685	Amygdaloid, cellular, poorly oxidized.
1685-1742	Fine copper. Trap, mel. Amygdaloidal 1702-1704 with copper. Altered and silicified, 1729-1742. Possibly conglomerate.
1742-1870	Trap, melaphyre.
1870-1904	Conglomerate.
1904	Bottom of hole.

A.3 St. Louis Diamond Drill Holes

D.D. Hole No. 11. Located 6150 ft. S 56° - 30' E. of collar of No. 20 shaft. Angle of hole 55°. Direction of hole S 56° - 30' E.

0-8	Surface
8-13	Broken ledge, trap.
13-36	Trap, brown, sandy.
36-87	Amalg., brown, sandy.
87-101	Trap.
101-112	Amalg., brown, sandy.
112-120	Trap.
120-131	Amalg., brown, sandy.
131-177	Trap.
177-226	Sandstone. <u>Eastern Sandstone.</u> End of hole.

Assay of sludge samples -

13-33	0.09% copper in sludge.
33-53	0.11% " " "
53-77	0.23% " " "
77-89	0.22% " " "
89-109	0.23% " " "
109-120	0.15% " " "
120-131	0.15% " " "
131-173	0.14% " " "
173-199	0.07% " " "
199-226	? " " "

D.D. Hole No. 18. Located 2350 ft. S 33° - 30' E. from No. 8 hole. Angle of hole 55°. Direction of hole S 56° - 30' E.

0-9	Surface
9-27	Amalg. 9413 broken ledge.
27-46	Trap
46-58	Amalg.
58-76	Trap
76-82	Amalg.
82-103	Trap. Copper pellet at 86.
103-128	Amalg. <u>St. Louis.</u> No copper. Brown Am. 103-116. Green Am. 116-128.
128-139	Trap.
139-159	Amalg., hard.
159-200	Trap, fine grain.
200-207	Amalg.
207-243	Trap. " <u>Big Trap</u> ". End of hole.

Assay of sludge samples -

0-243	No copper in sludge.
-------	----------------------

ST. LOUIS

D. D. Hole No. 37

Located in the SW¹/₄ of the SW¹/₄ of Section 19, 55-32, about 50 feet north and 400 feet west of the south & corner of the section. The hole is vertical. The hole is intended to explore the St. Louis conglomerate at a depth of about 1000 feet. It will also cut the St. Louis amygdaloid.

Drilled May, 1943, by the E. J. Langyear Co. Size of bit 1/2". Size of core 1 3/16".

Pipe left in hole: 11 feet of 3 inch drive pipe, 5 feet of 1/2 inch flush joint casing and 9 feet of 2 inch common pipe.

Note: Unless otherwise stated angles are from the axis of the core.

Depth	Description	Notes
0-11	Overburden.	
11-14	Trap, glomeroporphyrite.	11-14 Drilled with casing bit.
14-15	Amygdaloid, cellular, poorly oxidized.	
15-37	Trap, glomeroporphyrite.	34 1/2" quartz vein? at 15". There may be a flow top at 31. The flows are difficult to separate.
37-40	Amygdaloid, cellular, poorly oxidized.	
40-49	Trap, glomeroporphyrite.	
49-54	Amygdaloid, cellular, poorly oxidized, ash.	
54-75	Trap, glomeroporphyrite.	
75-77	Amygdaloid, cellular, poorly oxidized.	
77-127	Trap, glomeroporphyrite.	35 1/2" calcite, laumontite vein at 15". There may be a flow top at 102. Considerable alteration throughout the flow.
127-136	Amygdaloid, cellular, moderately oxidized.	
136-229	Trap, glomeroporphyrite, porphyrite.	Many feldspar phenocrysts. Occasional laumontite veinlets at 30 to 45". 171 5" of breccia cemented by laumontite. 180 1" laumontite, calcite vein at 56". 184 1/2" laumontite vein at 48". 192 3" calcite vein zone at 45".

ST. LOUIS

D. D. Hole No. 37

229-236	Amygdaloid, cellular, moderately oxidized, a little ash.
236-240	Trap, glomeroporphyrite, porphyrite.
240-243	Amygdaloid, cellular, slightly coalescing, well oxidized.
243-246	Trap, glomeroporphyrite, porphyrite.
246-254	Amygdaloid, cellular, well oxidized.
254-258	Trap, feldspathic melaphyre, glomeroporphyrite.
258-258	Amygdaloid, cellular, coalescing, moderately oxidized.
258-258	Trap, feldspathic melaphyre, glomeroporphyrite.
258-293	Amygdaloid, cellular, slightly coalescing, moderately oxidized.
293-331	Trap, feldspathic melaphyre, glomeroporphyrite, slightly ophitic.
331-346	Amygdaloid, cellular, poorly oxidized.
346-355	Trap, feldspathic melaphyre, glomeroporphyrite.
355-355	Amygdaloid, cellular, well oxidized.
355-375	Trap, glomeroporphyrite.
375-390	Amygdaloid, cellular, poorly oxidized.

ST. LOUIS

D. D. Hole No. 37

386-392	Trap, glomeroporphyrite.
392-394	Amygdaloid, cellular, moderately oxidized.
394-413	Trap, glomeroporphyrite, porphyrite.
413-420	Amygdaloid, cellular, fragmental in upper part. The entire amygdaloid is bleached to a grayish tan color.
429-464	Trap, glomeroporphyrite, porphyrite.
464-475	Amygdaloid, cellular, slightly coalescing, moderately oxidized.
475-512	Trap, melaphyre fine grained, porphyrite, a few small feldspar phenocrysts.
512-524	Amygdaloid, fragmental, moderately oxidized.
524-559	Trap, melaphyre fine grained, porphyrite, a few small phenocrysts.

ST. LOUIS

D. D. Hole No. 37

559-565	Amygdaloid, cellular, moderately oxidized.
565-567	Trap, melaphyre fine grained, porphyrite.
567-572	Amygdaloid, cellular, moderately oxidized.
572-611	Trap, melaphyre fine grained, porphyrite.
611-618	Amygdaloid, cellular, a little ash, unoxidized.
618-692	Trap, glomeroporphyrite.
692-694	Amygdaloid, cellular, somewhat coalescing, poorly oxidized.
694-698	Trap, feldspathic melaphyre.
698-700	Amygdaloid, cellular, moderately oxidized.
700-703	Trap, feldspathic melaphyre.
703-709	Amygdaloid, cellular, moderately oxidized.
709-723	Trap, feldspathic melaphyre.
723-728	Amygdaloid, cellular, slightly coalescing, moderately oxidized.
728-733	Trap, feldspathic melaphyre.
733-736	Amygdaloid, cellular, slightly coalescing, poorly oxidized.
736-738	Trap, feldspathic melaphyre.
738-743	Amygdaloid, cellular, moderately oxidized.

ST. LOUIS

D. D. Hole No. 27

743-1051

Trap, glomeroporphyrite, dolerite, slightly
ophitic.
The entire bed is much broken and in places
considerably altered. There are many
laumontite, chlorite ranging from 30 to 90°.
The broken core extends above this trap to
890 and above.
772 2" calcite vein at 65°.
772 5/8" coarsely crystallized calcite
vein at 45°.
791-791a Intensely altered breccia ce-
mented by calcite and laumontite.
865 1" laumontite vein at 60°.
869 1/2" coarse calcite vein at 35°.
898 1/2" laumontite vein at 25°.
899 4" breccia cemented by laumontite
and calcite.
In places the rock is faintly and coarsely
mottled, elsewhere coarsely doleritic.
832 1" laumontite, calcite vein at 60°.
940 1" laumontite vein at 65°.
953 1" " " " 45°.
959-961 Considerable laumontite, calcite
veining ranging from 0° to 45°.
974 1/2" calcite, laumontite vein at 35°.
976 1/2" laumontite vein at 45°.
977 1" laumontite, chlorite vein at 75°.
986 2" laumontite vein zone at 75°.
986 3" laumontite, calcite vein zone at
45°.
993 1/2" laumontite, chlorite vein at 30°.
1002 3" of core with very irregular
laumontite, calcite veining, ranging from
35° to 80°.
1005-1006 Four laumontite veinlets at
from 35 to 85°.
1014 1" laumontite breccia at 80°.
1015 4" of breccia at 25° cemented by
laumontite and chlorite.
Between 1016 and the bottom of the flow
there are many laumontite veinlets and core
is considerably broken and in places con-
siderably altered.
1016 1/2" laumontite, calcite vein at
30°.
1020 1" epidote, calcite vein at 85°.

1061-1063

Amygdales, cellular, poorly oxidized.
Calcite, chlorite.

1063-1066

Trap, feldspathic melaphyre.

ST. LOUIS

D. D. Hole No. 27

1068-1069

Amygdales, cellular, poorly oxidized.
Epidote, chlorite.
Trap, feldspathic melaphyre.

1069-1068

Trap, feldspathic melaphyre.

1062-1066

Amygdales, cellular, tight.
Several trappy layers.
Epidote, calcite, chlorite.

1066-1136

Trap, feldspathic melaphyre.
1067 1" calcite, laumontite vein at
60°.
The upper part of the flow has numerous
closely spaced feldspar individuals.
These feldspars are from 1/16" to 3/32"
long and very slender.
There are occasional laumontite veinlets.
1137 1" laumontite vein at 80°.
1138 1/2" of laumontite breccia at 30°.

1136-1138

Amygdales, cellular, poorly oxidized.

1138-1141

Calcite, quartz, chlorite, epidote.
Trap, feldspathic melaphyre.

1141-1142

Amygdales, cellular, moderately oxidized.

1142-1144

Epidote, calcite, chlorite.
Trap, feldspathic melaphyre.

1144-1145

Amygdales, cellular, tight, moderately oxi-
dized.
quartz, chlorite, epidote.
Several pipe-like amygdules just above
1145g.

1145-1149

St. Louis Conglomerate.
Dark felsitic and basic amygdaloidal peb-
bles up to 2" long. A few small red
felsite grains. A little very fine copper.

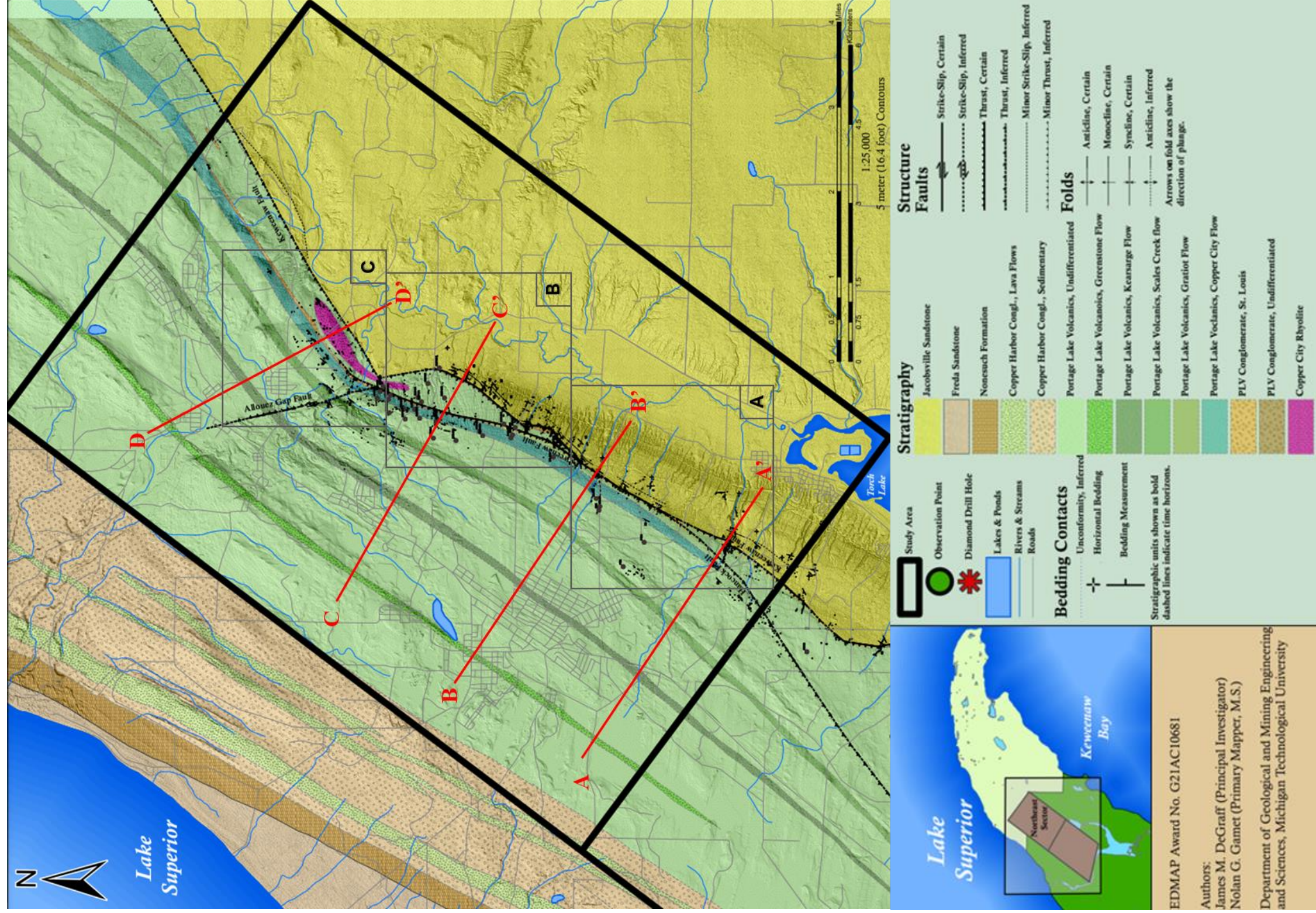
1149-1150

Amygdales, cellular, trappy, tight.
Epidote, calcite, laumontite, chlorite.

1150-

Trap, feldspathic melaphyre.

Stopped 5/22/43 at 1161 feet by H.N.K.



D Copywrite Documentation

All images in this document are public domain, or licensed for reuse under Creative Commons license 4.0.